Vol. 74, Part II, 2004

ISSN 0369-8211

Proceedings of the National Academy of Sciences India

SECTION A — PHYSICAL SCIENCES

The National Academy of Sciences, India, Allahabad
राष्ट्रीय विज्ञान अकादमी, भारत, इलाहाबाद

The National Academy of Sciences, India

(Registered under Act XXI of 1860)

Founded 1930

COUNCIL FOR 2004

President

1 Prof Jai Pal Mittal, Ph D (Notre Dame), F N A , F A Sc , F N A Sc , F T W A S , Mumbai

Two Past Presidents (including the Immediate Past President)

2 Prof S K Joshi, D Phil , D Sc (h c), F N A , F A Sc , F N A Sc , F T W A S , New Delhi

3. Dr V P Sharma, D Phil ,D Sc ,F.A M S ,F E S I , F I S C D , F N A , F A Sc , F N A Sc , F R A S , New Delhi

Vice-Presidents

4. Dr P K Seth, Ph D , F N A , F N A Sc , Lucknow

5. Prof M Vijayan, Ph D , F N A , F A Sc , F N A Sc , F T W A S , Bangalore

Treasurer

6 Prof S L Srivastava, D Phil ,F I E T E , F N A Sc , Allahabad

Foreign Secretary

7 Dr S E Hasnain, Ph D , F N A , F A Sc , F N A Sc , F T W A S , Hyderabad

General Secretaries

8 Dr V P Kamboj, Ph D , D Sc , F N A , F.N A Sc , Allahabad

9 Prof Pramod Tandon, Ph D , F N A Sc , Shillong

Members

10 Dr Samir Bhattacharya, Ph D , F N A , F A Sc , F N A Sc , Kolkata

11 Prof Suresh Chandra, D Phil , Grad Brit I R E , F N A Sc , Varanasi

12. Prof Virander Singh Chauhan, Ph D , D Phil (Oxford), F N A , F N A Sc , New Delhi

13 Prof Asis Datta, Ph D , D Sc , F N A , F A.Sc , F N A Sc , F T W A S ,New Delhi

14 Prof Kasturi Datta, Ph D , F.N A , F A Sc , F N A Sc , F T W A S , New Delhi

15 Prof Sushanta Dattagupta, Ph D , F N A , F A Sc , F N A Sc , F T W A S , Kolkata

16 Dr Amit Ghosh, Ph D , F N A , F A Sc , F N A Sc , Chandigarh

17 Prof H S Mani, Ph D (Columbia), F A Sc , F N A Sc , Chennai

18 Prof G K Mehta, Ph.D , F N A Sc , Allahabad

19. Dr. G C Mishra, Ph D , F N A Sc , Pune

20 Dr Ashok Misra, M S (Chem Engg), M S (Polymer Sc), Ph D , F N A Sc ,Mumbai

21 Prof Kambadur Muralidhar, Ph D , F N A , F A Sc , F.N A Sc.,Delhi

22 Dr Vijayalakshmi Ravindranath, Ph D ,F N A Sc , F T W A S , Manesar

23 Prof Ajay Kumar Sood, Ph D , F N A , F A Sc , F N A Sc , F T W A S , Bangalore

Special Invitees

1 Prof M G K Menon, Ph D (Bristol), D Sc (h c), F N A , F A Sc , Hon F N A Sc , F T W A S , F R S Mem Pontifical Acad Sc , New Delhi

2 Dr (Mrs) Manju Sharma, Ph D , F N A A S , F A M I , F I S A B , F N A Sc , F T W A S , New Delhi

3 Prof P N Tandon, M S , D Sc(h c), F R C S , F A M S , F N A , F A Sc , F N A Sc , F T W A S Delhi

4 Prof Girjesh Govil, Ph D , F N A , F A Sc , F T W A S , Mumbai

The *Proceedings of the National Academy of Sciences, India*, is published in two Sections Section A (Physical Sciences) and Section B (Biological Sciences) Four parts of each section are published annually (since 1960)

The Editorial Board in its work of examining papers received for publication is assisted, in an honorary capacity by a large number of distinguished scientists The Academy assumes no responsibility for the statements and opinions advanced by the authors The papers must conform strictly to the rules for publication of papers in the *Proceedings* A total 25 reprints is supplied free of cost to the author or authors The authors may ask for a reasonable number of additional reprints at cost price, provided they give prior intimation while returning the proof.

Communication regarding contributions for publications in the *Proceedings*, books for review, subscriptions etc should be sent to the Managing Editor, The National Academy of Sciences, India, 5, Lajpatrai Road, Allahabad - 211002 (India)

Annual Subscription for both Sections : Rs. 500.00; for each Section Rs. 250.00; Single Copy . Rs. 100.00. Foreign Subscription : (a) for one Section : US $100, (b) for both Sections US $200.

(Air-Mail charges included in foreign subscription)

Co-Sponsored by C S T U P (Lucknow)

PROCEEDINGS

OF THE

NATIONAL ACADEMY OF SCIENCES, INDIA

2004

VOL LXXIV SECTION–A PART II

Some new biscoumarinyl ethers as analogues of Lasiocephalin

RUDRESH S. SHEELAVANTAR, GANESH N. ALAWANDI and MANOHAR V. KULKARNI*

Department of Chemistry, Karnatak Univesity, Dharwad – 580 003, India.

Received November 8, 2002, Revised April 6, 2003, Accepted September 18, 2003

Abstract

4-Bromomethyl coumarins (II) have been reacted with different hydroxy coumarins to obtain biscoumarinyl ethers as analogues of Lasiocephalin. All the compounds have been characterized by spectral data and anti-microbial activity of some of them has been reported.

(**Keywords** . spectral data/bis coumarinyl ethers/hydroxy coumarins/lasiocephalin).

Introduction

Compounds containing two coumarin moieties have been found to be extremely useful as anticoagulants[1], antimicrobials[2] and triplet sensitizers[3]. Further Bhattacharya and Das[4] have isolated a biscoumarinyl ether Lasiocephalin[5] (I) from the roots of "*Lasiocephon eriocephalus*" the structure of which was deduced by Vishwanathan and Balakrishnan[6]. An Important feature of this compound is the presence of an aryl ether linkage between C_7 and C_6 position of the two coumarin moieties. In the present paper 6-hydroxy-4-methyl coumarin[7], 4-hydroxy coumarin[8] and 7, 8-dihydroxy-4-methyl coumarin[9], have been used as a nucleophiles and the ether linkage has been established by substituting the bromine situated at the allylic position with respect to

the biogenetically important C_3–C_4 double bond[10] in various 4-bromomethyl coumarins[11, 12].

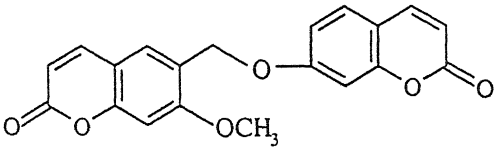

(I)

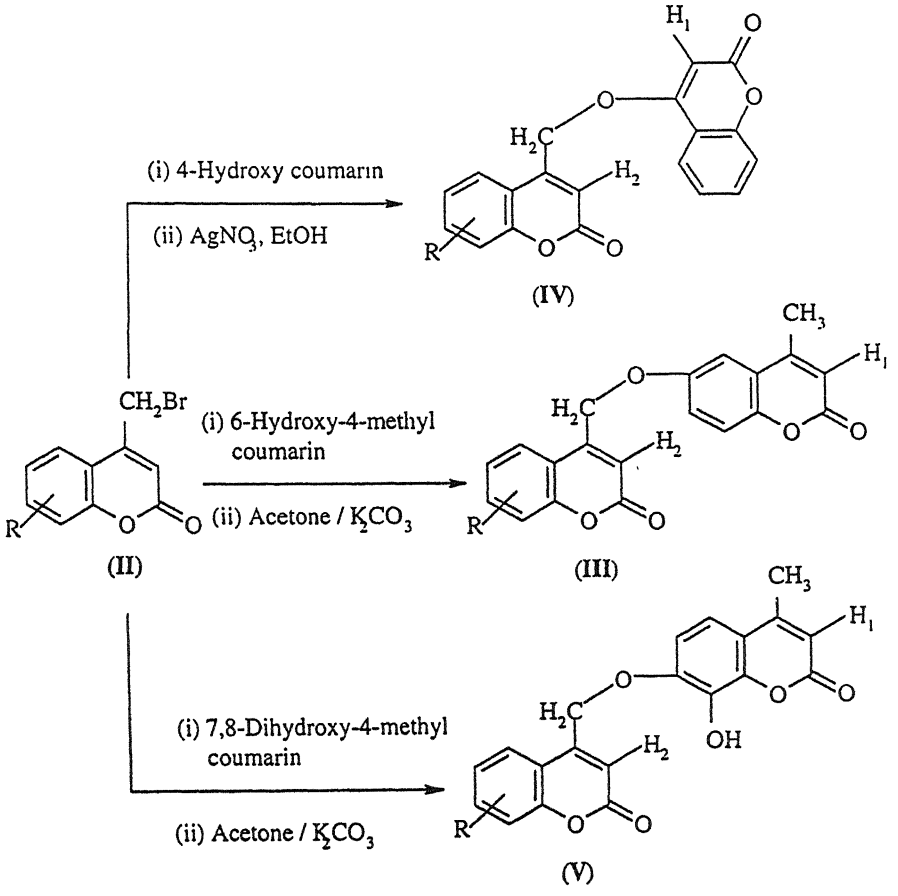

R = -6-CH_3, -7-CH_3, -5,6-Benzo, -7,8-Benzo, -7-OCH_3, -6-OCH_3, 6-Cl

Scheme - 1

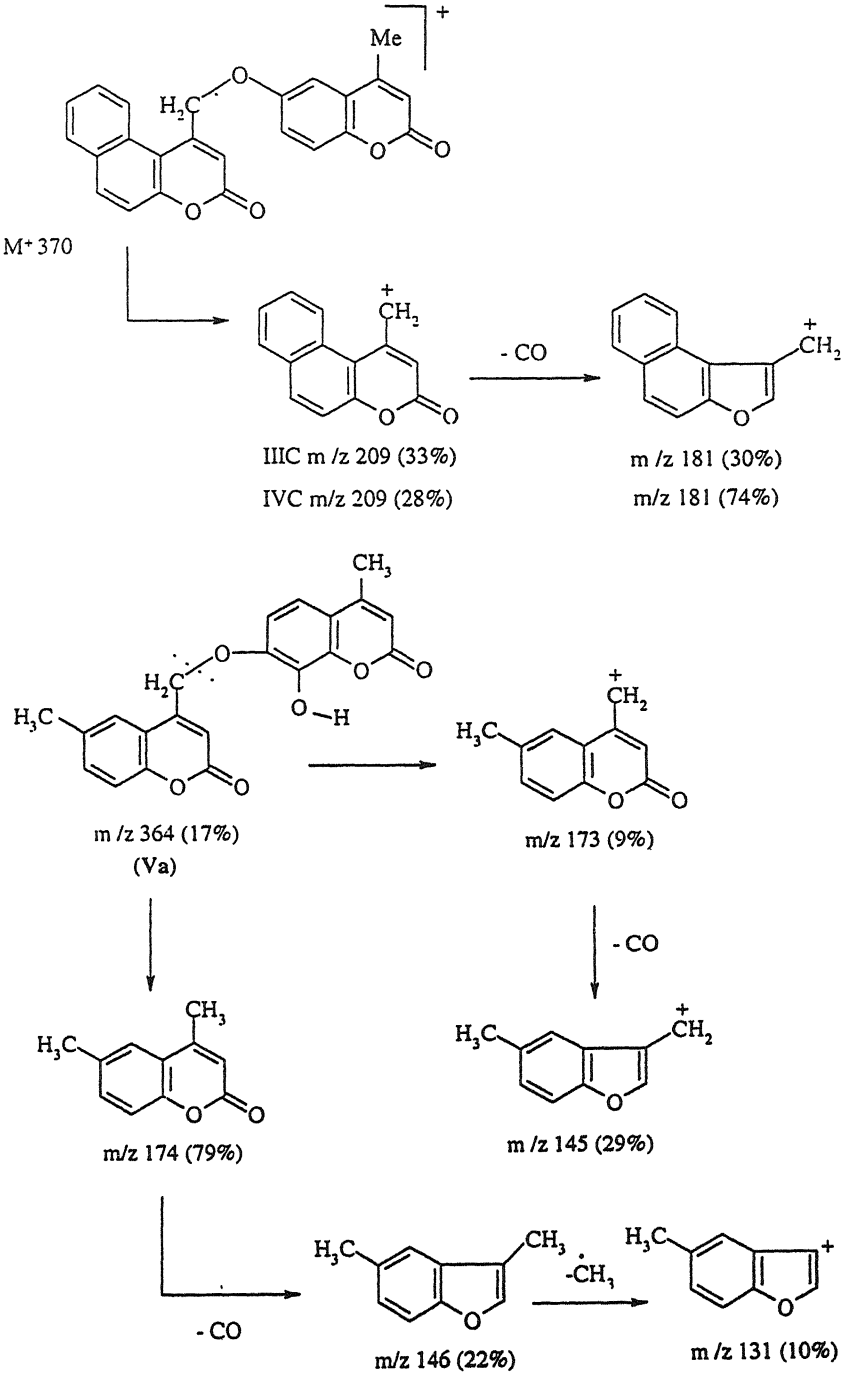
Me
M+ 370
- CO
IIIC m /z 209 (33%)
IVC m/z 209 (28%)
m /z 181 (30%)
m/z 181 (74%)
m /z 364 (17%)
(Va)
m/z 173 (9%)
- CO
m/z 174 (79%)
m /z 145 (29%)
- CO
m/z 146 (22%)
m /z 131 (10%)

Scheme – 2

Materials and Method

The methodology adopted for the synthesis of the title compounds is outlined in Scheme-1. 4-Bromomethyl coumarins[13] (II) which are the required synthons have been synthesised by the Pechmann cyclisation of various phenols with 4-bromoethylacetoacetate[14] The reaction of 6-hydroxy-4-methyl coumarin with (II), resulted in the formation of ethers (III). However, in the reaction of 4-hydroxy coumarin with (II) an equimolar quantity of $AgNO_3$ was used to bring about the ether formation. The reaction probably proceeds *via* the formation of the silver salt of 4-hydroxy coumarin, which is evidenced by the formation of silver bromide which precipitates in the reaction mixture.

Out of the two phenolic hydroxyls in 4-methyl daphnetin the C_7-OH is more nucleophilic than C_8-OH and is also less sterically hindered. The reaction of (II) with this substrate has shown that the ether linkage is established with the C_7-OH and the resulting ethers have the structure (V) with a free C_8-OH group. This is further supported by the formation of 7-benzyloxy-8-hydroxy-4-methyl coumarin in the reaction of benzyl chloride with 7,8-dihydroxy-4-methyl coumarin. Spectral and physical data (m.p. 180-81°) of this compound agrees with the literature report[15].

Melting points reported are uncorrected. IR spectra (ν_{max} in cm^{-1}) were recorded in KBr on Nicolet. Impact-410. FT-IR spectrometer. PMR spectra were recorded on Brucker-Varian-300 MHz FT-NMR using TMS as internal standard. The elemental analyses was recorded on Thermo Quest EA 1110 CHN rapid analyser.

4-Bromoethylacetoacetate was prepared according to the method of Burger and Ullyot[14] and substituted 4-bromomethyl coumarins (II) were synthesised by the Pechmann cyclisation of various phenols with 4-bromoethylacetoacetate according to the literature methods.[13] Amongst the hydroxy coumarins, 4-hydroxy coumarin was a commercial sample and 6-hydroxy-4-methyl and 7,8-dihydroxy-4-methyl coumarins were prepared by the reaction of hydroquinone and pyrogallol with ethyl acetoacetate using 70% sulfuric acid.

I. Synthesis of 6-(O-4'-coumarino methyl)-4-methyl-coumarins (III)

General method :

A mixture of 6-hydroxy-4-methyl coumarin (0.01 mol), anhydrous potassium carbonate (0.01 mol.) was stirred for 30 min. in dry acetone (30 ml). To this, 4-

bromomethyl coumarin (II) (0.01 mol) was added and the stirring was continued for 24 h. The separated solid, was filtered, and washed with 1:1 HCl (30 ml) and with water and recrystallised from dioxane. The compounds prepared are listed in Table 1.

Table 1– Physical and analytical data for biscoumarinyl ethers

No	Compound		M P°c	Yield %	Mol. formula	Analysis(%) Req (found)	
	R	No				C	H
1	6-CH_3	IIIa	272-73	72	$C_{21}H_{16}O_5$	72 40 (72 20)	4 63 (4 50)
2.	7-CH_3	IIIb	282-84	64	$C_{21}H_{16}O_5$	72 40 (72 16)	4 63 (4 38)
3	5,6-Benzo	IIIc	266	78	$C_{24}H_{16}O_5$	75 00 (74 80)	4 16 (4 08)
4.	7,8-Benzo	IIId	286-88	80	$C_{24}H_{16}O_5$	75 00 (74 78)	4 16 (4 02)
5	6-OCH_3	IIIe	270	76	$C_{21}H_{16}O_6$	69 23 (69 02)	4 39 (4.08)
6	7-OCH_3	IIIf	292-94	70	$C_{21}H_{16}O_6$	69 23 (68 98)	4 39 (4 18)
7.	6-Cl	IIIg	275	72	$C_{20}H_{13}O5Cl$	65 13 (64 96)	3 53 (3 41)
8.	6-CH_3	IVa	110	70	$C_{20}H_{14}O_5$	71 85 (71 50)	4 19 (4.10)
9.	5,6-Benzo	Ivb	160	75	$C_{23}H_{14}O_5$	74 59 (74 21)	3.78 (3.56)
10.	7,8-Benzo	Ivc	154-55	72	$C_{23}H_{14}O_5$	74.59 (73.80)	3 78 (3.60)
11.	6-OCH_3	Ivd	138	75	$C_{20}H_{14}O_6$	71.85 (71 50)	4.19 (4 10)

Table Contd..

Table 1 Contd.

12	6-Cl	IVe	104	70	$C_{19}H_{11}O_5Cl$	64 32 (64 10)	3 10 (3 02)
13	6-CH_3	Va	250°	80	$C_{21}H_{16}O_6$	69 23 (69 10)	4 40 (4 30)
14.	7-CH_3	Vb	258	78	$C_{21}H_{16}O_6$	69 23 (69 05)	4 40 (4 20)
15.	5,6-Benzo	Vc	265	80	$C_{24}H_{16}O_6$	72 00 (71 80)	4.00 (3.90)
16	7,8-Benzo	Vd	278	75	$C_{24}H_{16}O_6$	72.00 (71 75)	4 00 (3 88)
17	6-OCH_3	Ve	232	80	$C_{21}H_{16}O_7$	66 32 (66 10)	4.21 (4 10)
18.	7-OCH_3	Vf	246	70	$C_{21}H_{16}O_7$	66 32 (66 20)	4 21 (4 15)
19.	6-Cl	Vg	262	75	$C_{20}H_{13}O_6Cl$	62 42 (62 25)	3 38 (3 18)

Ethers III & V were recrystallised from dioxane and IV were recrystallised from ethanol/aq ethanol

II. Synthesis of 4-(O-4'-coumarino methyl)-coumarins (IV)

General method :

A mixture of 4-hydroxy coumarin (0.01 mol), and silver nitrate (0.01 mol) in rectified spirit (30 ml) was heated on water bath for half an hour using a reflux condenser. To this was added, 4-bromomethyl coumarin (II) (0.01 mol) and heated on a water bath for 3 h. The pale yellow precipitate of silver bromide separates out. From the hot solution AgBr is separated by filtration. The filtrate was added to ice cold water. The separated solid was washed with water, alcohol, and was recrystallised from ethanol or aqueous ethanol. The compounds prepared are listed in Table 1.

III. Synthesis of 7-(O-4'-coumarino methyl)-8-hydroxy-4-methyl-coumarins (V)

General method:

A mixture of 7,8-dihydroxy-4-methyl coumarin (0.01 mol) and anhydrous potassium carbonate (0.01 mol) in dry acetone (30 ml) was stirred for 1 h. To this was added 4-bromomethyl coumarin (II) (0.01 mol) and the stirring was continued for 24 h. The separated solid was filtered and washed with 1:1 HCl and water. It was then dried and recrystallised from dioxane. The compounds prepared are listed in Table 1.

Results and Discussion

The biscoumarinyl ether (IIIa, R=6-CH_3) obtained by the reaction of 4-bromomethyl coumarins and 6-hydroxy-4-methyl coumarin exhibited C=C–H vibrations at 2919 cm^{-1} and the characteristic band at 1702 cm^{-1} due to the C=O, stretching vibrations of coumarin. The C=C and C–O–C vibrations were observed at 1579 cm^{-1} and 1171 cm^{-1} respectively (Table 2). In the PMR spectra the, methyl and methylene protons appeared as singlets at 2.46 δ ppm and 5.29 δ ppm respectively. The aromatic multiplet was observed in the region of 6.95-7.5 δ ppm. The two C_3 protons appeared as singlets, at 6.69 and 6.36 δ ppm. The C_3-H_2 proton which is in close spatial proximity with the ether oxygen appears down field when compared with the other C_3-H_1 (Table 2) which is in agreement with an earlier observation on 4-aryloxymethyl coumarins[16].

Ether (IVa, R = 6-CH_3) exhibited C=C–H vibrations at 2919 cm^{-1} and the characteristic band at 1715 cm^{-1} due to C=O stretching vibration of coumarin. The C=C and C–O–C vibrations were observed at 1574 cm^{-1} and 1196 cm^{-1} respectively. (Table 2). In the PMR spectra, the methyl and methylene protons appeared as singlets at 2.46 δ ppm and 4.68 δ ppm respectively. The aromatic multiplet was observed in the region of 7.28-7.43 δ ppm. The two C_3 protons appeared as singlets at 6.57 δ ppm and 5.62 δ ppm. The C_3-H_2 proton which is in close spatial proximity with the ether oxygen appears down field when compared with the other C_3–H_1 (Table 2) which is in agreement with our earlier observations, on 4-aryloxymethyl coumarins[16].

Ether (Va, R = 6-CH_3) exhibited a broad band at 3413 cm^{-1} due to –OH stretching, C=C–H vibrations at 2919 cm^{-1} and characteristic band at 1721 cm^{-1} due to C=O stretching vibrations of coumarin. The C=C and C–O–C observed at 1572 cm^{-1} and

1110 cm^{-1}, and respectively (Table 2). In the PMR spectra, the methyl and methylene protons appeared as singlets at 2.38 and 2.45 δ ppm and 5.20 δ ppm respectively. The aromatic multiplet was observed in the region of 6.90 - 7.50 δ ppm, where as the phenolic –OH appeared at 5.40 δ ppm (Table 2).

Mass Spectra : The mass spectra by electron ionisation (EI) have been recorded for ethers IIIc, IVc and Va. The molecular ion peaks of moderate intensities have been observed for Va and IVc at *m/z* values 364 (17%) and 384 (81%) respectively. However, in the case of IIIc the M^+ ion at *m/z* (370) is not observed. The main fragmentation pattern appears to be the α cleavage of ethers resulting in the formation of even electron ions which further follow the established fragmentation pathway of coumarins and benzofurans[17]. A plausible fragmentation pattern is out lined for the benzo ether (IIIc) in Scheme 2.

In the case of the hydroxy ether Va the low intensity molecular ion at *m/z* 364 17% is observed. Though the expected α-cleavage is observed in this compound, another predominant path way is the transfer of the phenolic hydrogen to the methylene group *via* a cyclic six membered ring leading to the formation of 4,6-dimethyl coumarin fragment at m/z 174 in high intensity. This odd electron ion can easily expel a molecule of carbon monoxide and a methyl radical leading to the formation of benzofuran fragments.

Antimicrobial studies · Biscoumarinyl ethers III, IV and V synthesized during the present investigation have been subjected to a preliminary antimicrobial screening. The compounds were chosen at random by selecting two compounds from each III, IV and V and have been screened against one bacterial and one fungal species at a dose of 100 μg in 10 ml of DMF as a solvent. The methodology adopted for the evaluation is described as follows.

Antibacterial activity : Antibacterial activity of test compounds were evaluated against *Pseudomonas chlororaphis* bacteria by cup plate method[18]. The bacteria were subcultured in a medium containing peptone (0.5%), yeast extract (0.15%), beef extract (0.15%), sodium chloride (0.35%), potassium dihydrogen phosphate (0.13%). Nutrient agar which served as the basal medium was prepared by dissolving bacteriological peptone (0.61%), yeast extract (0.3%), beef extract (0.13%) and agar (2.1%) in distilled water. The solution was sterilised for 20 min. at 15 lbs pressure in an autoclave.

Table 2– IR and PMR spectral data of biscoumarinyl ethers

Sl No.	Compound		$\nu_{C=O}$ cm^{-1} lactone	Chemical shift in ppm (δ)
	R	No.		
1	6-CH_3	IIIa	1702	2.46 (s, 6H, - CH_3), 5 29 (s, 2H, -CH_2O), 6.36 (s, 1H, C_3-H_1), 6.69 (s, 1H, C_3-H_2), 6.95-7 50 (m, 6H, Ar-H).
2	7-CH_3	IIIb	1704, 1727	2.49 (s, 3H, - CH_3), 2.45 (s, 3H, -CH_3), 5.28 (s, 2H, -CH_2-O), 6 20 (s, 1H, C_3-H_1) 6.50 (s, 1H, C_3-H_2), 7.10-7 50 (m, 6H, Ar-H)
3	5,6-Benzo	IIIc	1709	2.48 (s, 3H, - CH_3), 5.60 (s, 2H, -CH_2-O), 6 30 (s, 1H, C_3-H_1) 6 90 (s, 1H, C_3-H_2), 7.21-8.06 (m, 9H, Ar-H).
4	7,8-Benzo	IIId	1714	2.33 (s, 3H, - CH_3), 5.40 (s, 2H, -CH_2-O), 6 20 (s, 1H, C_3-H_1) 6.80 (s, 1H, C_3-H_2), 7.00-7.90 (m, 9H, Ar-H)
5	7-OCH_3	IIIe	1702	2 44 (s, 3H, - CH_3), 3.90 (s, 3H, OCH_3), 5.26 (s, 2H, -CH_2-O) 6.30 (s, 1H, C_3-H_1), 6.60 (s, 1H, C_3-H_2).
6	6-Cl	IIIf	1721	2 47 (s, 3H, - CH_3), 5.25 (s, 2H, -CH_2-O-), 6.30 (s, 2H, C_3H), 6.70 (s, 1H, C_3-H_2), 7 20-7 50 (m, 6H, Ar-H).
7	6-CH_3	IVa	1715	2.46 (s, 3H, - CH_3), 4.68 (s, 2H, -CH_2O), 5.62 (s, 1H, C_3-H_1), 6 57 (s, 2H, C_3-H_2) 7.28-7 43 (m, Ar-H).
8	5,6-Benzo	IVb	1727	5.07 (s, 2H, - CH_2-O), 6 06 (s, 1H, -C_3-H_2), 6.90 (s, 1H, -C_3H_1), 7.28-8.60 (m, 10H, Ar-H).
9	7,8-Benzo	IVc	1721	4.79 (s, 2H, - CH_2-O), 5.70 (s, 1H, -C_3-H_1), 6.62 (s, 1H, C_3-H_2), 7.28-8.60 (m, 10H, Ar-H).
10	-6–Cl	IVe	1713	4.65 (s, 2H, - CH_2-O), 5 60 (s, 1H, -C_3-H_1), 6.65 (s, 2H, C_3-H_2) 7.28-7.56 (m, 9H, Ar-H).

Table 2 Contd. .

Table 2 Contd. .

11	6-CH_3	Va	1721	*3413	2.38 (s, 3H, - CH_3), 2 45 (s, 3H, CH_3), 5.20 (s, 2H, -CH_2-O-), phenolic – OH 5.46, 6.20 (s, 1H, C_3-H_1), 6.65 (s, 1H, C_3-H_2), 6 90-7.50 (m, 5H, Ar-H).
12	7-CH_3	Vb	1726	*3419	2.44 (s, 3H, - CH_3), 2.47 (s, 3H, CH_3), 5.26 (s, 2H, -CH_2-O-), 5 45 (s, 1H, OH) 6 36 (s, 1H, C_3-H_1), 6 59 (s, 1H, C_3-H_2), 6.93-7.60 (m, 5H, Ar-H).
13	7,8-Benzo	Vd	1725	*3444	2 45 (s, 3H, - CH_3), 5.30 (s, 2H, -CH_2-O), 5.45 (s, 1H, OH), 6.25 (s, C_5-H), 3.96-7.75 (m, Ar-H).
14	-6–Cl	Ve	1727	*3419	2.46 (s, 3H, - CH_3), 5 28 (s, 2H, -CH_2-O), 5.30 (s, 1H, OH), 6.30 (s, 1H, C_3-H_1), 6 30 (s, 1H, C_3-H), 6.70 (s, 1H, C_3-H_2), 6.90-7 50 (m, 5H, Ar-H).
15	7-OCH_3	Vf	1720	*3410	2 44 (s, 3H, CH_3), 3 89 (s, 3H, -OCH_3), 5.20 (s, 2H, CH_2O), 5.46 (s, 1H, OH), 6.27 (s, C_3-H_1), 6.46 (s, C_3-H_2), 6.80-7.30 (m, Ar-H) A.

* $\gamma_{\text{-OH}}$ cm^{-1}

The basal medium 25-30 ml with glucose solution [(0.1 ml, 10%) to hasten the bacterial growth] with bacterial culture was poured in sterile petridishes. After the solidification of the medium holes of 9 mm diameter were bored to form cups with the help of a sterile cork borer. To this cup 0.025 ml of the solution as the test compound was added by sterilised pipettes. The petridishes were kept in a cold room to facilitate the diffusion of the solvent for about 2 h. The plates were then incubated at 37°C for 24 h. The extent inhibition was measured by the width of the zone in mm. Norfloxacin was used as a positive control and solvent control was also used to know the activity of the solvent (DMF). The results of the antibacterial testings have been summarised in Table 3.

Table 3– Antibacterial and antifungal activity of biscoumarinyl ethers

Compound	Zone of inhibition in mm after 24 h	
	Bacteria *Psedomonas clororaphis*	Fungi *Aspergillus niger*
IIIe	18 (+ +)	22 (+ + +)
IIIf	18 (+ +)	14 (+)
IVa	14 (+)	14 (+)
IVb	14 (+)	14 (+)
Vd	18 (+ +)	18 (+ +)
Ve	14 (+)	14 (+)

Antifungal Activity : Fungicidal activity of test compounds were evaluated against *Aspergillus niger* species by cup plate method[19]. The fungi were sub-cultured in the medium containing peptone (1%), yeast extract (0.6%), sodium chloride (0.5%), potassium dihydrogen phosphate (0.3%) and glucose (1%) in distilled water. The pH of the medium was adjusted to 6.0 and sterilised at 15 lbs for 20 min. The method of testing for antifungal activity was the same as followed for evaluating antibacterial activity. Griseofulvin was used as a positive control and solvent control (DMF) was also used to know its activity. The results of fungicidal activities are summarised in Table 3.

Amongst the various biscoumarinyl ethers (III) having R = 5, 6-Benzo and R = 6-Cl substitution in coumarin enhanced the antibacterial activity against *Pseodomonas chlororaphis.* Similarly in compound (V) having R=7,8-benzo substitution enhanced

the antibacterial activity. These compounds also reflected comparative anti-fungal potency.

Acknowledgements

The authors thank USIC, KUD for the IR and NMR data. One of the authors (RSS) thanks the UGC for the M. Phil. Fellowship.

References

1. Groth, A. (1945) *Science* **101** : 383.
2. Bachman, G. L. (1970) *Chem Abstr* **73** · 130889.
3. Specht, D P., Peter, A., Martic, R & Farid, S. (1982) *Tetrahedron* **38** : 1203
4. Bhattacharya, A. K. & Das, S C. (1971) *Chem Ind. (London)* **31** : 885
5. Bandopadhyay, M., Pardeshi, N. P. & Seshadri, T. R. (1974) *Ind J Chem.* **12** : 295
6. Viswanathan, N. & Balakrishnana, V (1974) *Ind J Chem.* **12** · 450.
7. Borsche, W. (1907) Ber **40** · 2732.
8. Shah, V.R., Bose J. L. & Sha, R. C. (1960) *J Org Chem* **25** 677
9. Zorip, Z. (1939) *J Pharm Soc Japan* **59** : 201.
10. Feuer, G. (1974) in "*Progress in Medicinal Chemistry*", ed Ellis, G F and West, G B , North Holland (New York), Vol. 10, p. 86.
11. Dey, B. B. & Radhabai, K. (1934) *J Ind Chem. Soc* **11** 635
12. Kulkarni, M. V., Pujar, B. G. & Patil, V. D. (1983) *Arch Pharm (Weinheim)* **316** 15.
13. Siddappa, S. & Agasimunddin, Y. S. (1970) *J Kar Univ Sci* , **15** 1
14. Burger, A. & Ullyot, G E. (1947) *J Org Chem.* **12** 346
15. Ahluwalia, V. K., Sachdev, G. P & Sheshadri T R. (1969) *Ind J. Chem.* 7(1) . 59.
16. Kulkarni, M. V., Pujar, B G & Patil, V. D (1981) *Arch Pharm (Weineim)* **316** . 15
17. Barnes, C S. & Occolowitz, J. L. (1964) *Austral J Chem.* **17** 975
18 Seeley, H. W & Van Demark, P. J. (1972) "*Microbes in action*" A laboratory manual of microbiology 2nd ed , Taraporewala Sons & Co. Pvt. Ltd., Bombay p 35.
19. Kavanagh, F. (1963) "*Analytical microbiology*" Academic press, New York, p 125

PROC. NAT. ACAD. SCI. INDIA, 74 (A), II, 2004

On the molecular interactions of L-amino acids and iodine in 50% aqueous ethanol solvent : Conductometric and electronic absorption spectroscopic studies

H S RANDHAWA, POONAM PATYAR and B S SEKHON

Department of Biochemistry and Chemistry, Punjab Agricultural University, Ludhiana-141 004, India.

Received January 16, 2003, Revised May 1, 2003, Accepted September 15, 2003

Abstract

The conductometric and electronic absorption spectroscopic studies of L-amino acids with iodine in 50% aqueous ethanol medium have been reported It is shown that the amino acids exhibit 1:2 (amino acid iodine) stoichiometry while 1 1 in excess of donor The band around 212 nm has been assigned to I^+ moiety while the bands near 293 and 355 nm are attributed to I^-_3 moiety The interaction of I^-_3 and 1^+ to donors is discussed

(**Keywords** molecular interaction/charge transfer complexes/amino acids/iodine)

Introduction

Electronic absorption spectra of solutions of proteins namely fibrinogen, γ-globin, trypsin, bovine plasma albumin, amino acids *viz*, glycine, tryptophan, hydroxyproline, tyrosine, α-alanine, β-alanine, isoleucine, leucine, phenyalanine, arginine, and amines namely ethyl-, diethyl- and triethylamine with iodine which is essential constituent of thyroid hormone have been reported in the literature[1]. It has been demonstrated that the effect of amino acids and proteins in aqueous solutions of iodine can be reproduced by increasing the polarity of the solvent. The amino acids and the proteins exist as polar molecules in aqueous solution and the spectral changes observed on mixing in iodine has been attributed to the increase of the polarity of the solvent. However, aminobenzoic acids being non-polar molecules would not be expected to have such an effect unless the aminobenzoic acid-iodine interaction product is polar. No firm evidence has been produced that charge transfer occurs between the amino acids or proteins and iodine but in view of the results with the non-polar

aminobenzoic acids and chloranil[1] and the earlier evidence[2-4] that the amino acids and proteins are good n-electron donors, it is likely that complexes of the form, (amino acids/or proteins, 1^+) are initially present in these solutions. Moreover, the equilibrium constant K which reflects on the stability of the complex and the enthalpy which is a true measure of the strength of interaction, however, has not been determined with any of the electron donors so far studied.

We report in this paper the conductomertic and electronic absorption studies on the interaction of iodine with ten L-amino acid donors namely glycine, leucine, isoleucine, phenylalanine, tryptophan, valine, asparagine, threonine, histidine monohydrochloride and lysinemonohydrochloride. These studies are aimed at (i) establishing the stoichiometry and nature of CT complexes; (ii) determining the stability constants and thermodynamic parameters of the complexes; (iii) correlating the parameters characterizing the CT complexes with those of D and A, and (iv) substantiating or contradicting the earlier studies.

Materials and Method

The conductometric[5-7] (Table 1) and thermodynamic parameters[8] (Table 2) were determined by experimental procedures and methodology reported earlier[9]. For composition determination, the equimolar stock solution (5×10^{-4} M) of D and A were prepared in 50 per cent aqueous ethanol whereas for thermodynamic paramerters, the stock solution of amino acids with concentration 5×10^{-2} M and acceptor with 5×10^{-4} M except in case of tryptophan –iodine system were prepared in 50 per cent aqueous ethanol. In case of tryptophan-iodine system, the concentration of D and A were 5×10^{-3} M and 5×10^{-5} M, respectively Electronic absorption spectra of solutions of L-amino acids with iodine in 50% aqueous ethanol were measured on Backmann DU7 Spectrophotometer.

Results and Discussion

The presence of a well developed maxima at a stoichiometric ratio of 1:2 (amino acid : iodine) (Fig. 1) in the conductivity concentration plots observed in all the systems studied are indicative of the fact that in the various amino acids-iodine systems, molecular complexes of ionic CT type are formed. Inspection of data in Table 1 reveal that there exists no definite relationship between the values of σ_P, σ_M and $E^{\#}$ among themselves as well as with pK_1 of amino acids as expected due to small variation of pK_1 (± 0.34) and pK_2 (± 0.74) values of amino acids[10].

Table 1– Conductance (σ) data for CT complexes of L-amino acid donors with iodine acceptor in 50% aqueous ethanol at 293K

Donor	pK_1 (amino acid) (a)	Stoichiometry	Conductance (μS)			$E^{\#}$ (kJ mol^{-1})
			σ_p	σ_0	σ_M	
Isoleucine	6 04	(1.2)	52 9	41 3	8025	13 28
Leucine	6 03	(1 2)	62 5	46 5	1725	8.85
Phenylalanine	5 67	(1 2)	52 6	42 4	8019	7.29
Tryptophan	5 93	(1 2)	57 5	45 5	7535	6 16
Valine	6.01	(1:2)	55.5	44.0	7468	6 64
Asparagine	10.84	(1:2)	58.5	42 5	10756	8 45
Glycine	6 06	(1·2)	55 0	44 6	6662	9.96
Threonine	5.59	(1 2)	57.5	43 5	9726	8.12
Histidinemonohydrochloride	7 76	(1 2)	59.1	45.0	8952	9 96
Lysinemonohydrochloride	9 70	(1 2)	53 6	43.0	8217	9 30

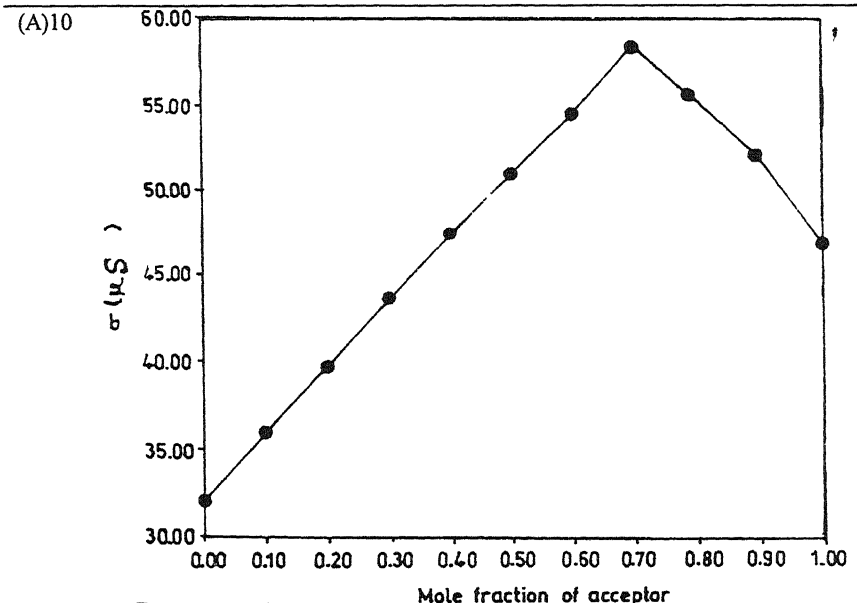

Fig 1–Plot of conductance (σ) vs concentration for iodine-asparagine system in 50% aqueous ethanol solution at 293K

Table 2– Thermodynamic functions for CT complexes of L-amino acid-iodine systems

Amino acid	K_{293}	K_{303}	K_{313}	$-\Delta H$	$-\Delta G$	ΔS	$\rho_d \times 10^{-5}$ (μmhos dm^3 mol^{-1})		
		(dm^3 mol^{-1})		(kJmol^{-1})	(kJmol^{-1})	(Jmol^{-1}K^{-1})	293 K	303 K	313 K
Isolcucine	93.34	71.18	63.05	14.63	11 05	-12 22	2 44	3 05	3 91
Leucine	82 97	63.05	50.13	18.62	10.76	-26 89	2 14	2 68	3.48
Phenylalanine	130 37	104 49	82.60	18.45	11.86	-22 49	2 52	3 17	4 33
Tryptophan	118.96	96.85	65.44	31.76	11.64	-68 67	43.41	54 64	78 81
Valine	88.50	79.97	70.24	8.06	10 92	+9 76	1.96	2.38	3 20
Asparagine	42 18	37.54	33.95	8.31	9 12	+2 46	2.06	2 38	2 76
Glycine	133.27	120.10	103.60	9.14	11 92	+9 49	2 16	3 15	5.30
Thrconine	158 0	130.61	107 82	15.04	12 33	-9 25	2.13	2 30	2 50
Histidinemonohydro chloride	535.72	499 04	466.69	5.40	15.31	+33 82	85 06	90 0	95 50
Lysincmonohydroch loride	184.43	173.90	163.35	4 37	12.71	+28 46	3 66	4 53	6 01

The equilibrium constants of the complexes recorded in Table 2 have been determined on the assumption that in large excess of the donor $C_D^0 >> C_A^0$), the composition of the complex is 1: 1. The correctness of the assumption has been verified from the consistency of the results obtained from model[8] based on 1:1 complex formation. The absence of any definite relationship between the parameters of Tables 2 i.e. K and ρ_d with those of Table 1 i.e. σ_p, $E^{\#}$ and pK_1 may also be due to the reason cited earlier. The order of stability of the complexes (i.e. K value) is: histidinemonohydrochloride > lysinemonohydrochloride > threonine > glycine > phenylalanine > tryptophan > isoleucine > valine > leucine > asparagine. On the other hand the enthalpy ($-\Delta H$) which is a measure of the molecular interaction follows the trend: tryptophan > leucine ≈ phenylalanine > theronine > isoleucine > glycine > asparagine valine > histidinemonohydrochloride > lysinemonohydrochloride. The low stability (K) and strong interaction ($-\Delta H$) of tryptophan as compared to that of phenylalanine is because of imidazole N in the former.

Further, the inspection of Table 2 (columns 8-10) shows that ρ_d the depolarization constant grows with the growth of temperature which is reverse to the behaviour of K values with temperature as expected[8].

The absorption spectra (Table 3) of dark brown colored old solution of iodine in de-ionized water exhibits bands at 287, 353, and 465 nm, the first two bands being characterized of the tri-iodide negative ion (I_3^-) formed according to the following reactions[11].

$$I_2 \rightleftharpoons I^+ + I^-$$

$$I_2 + I^- \rightleftharpoons I_3^-$$

The 465 nm band arises from solvated iodine. The iodine absorption band in inert solvent is 540 nm[12]. The absorption spectra of iodine in potassium iodide solution (freshly prepared) in water exhibit bands at 230, 285.5 and 352.5 nm (Table 3). The later two bands may be attributed to the tri-iodine ion (I_3^-) as expected. The band at 230 nm may be because of iodide (I^-) as expected[13]. When iodine is directly dissolved in neat alcohols the conductance increases with time and reaches the maximum value in about 24 h[14]. It is reported that the intensity of CT band at 225 nm due to I^- in iodine-ethanol system decreases with time and also progressive intensification of I_3^- ion absorption at 297 and 363 nm have been observed[15]. Thus, it can be inferred that

time dependence of electrical conductivity is due to the transformation of initially formed 1:1 outer charge transfer complexes followed by very fast reaction of the inner charge transfer complexes with iodine to form the tri-iodide ion [14-15].

Table 3– Electronic absorption spectra of L-amino acids-iodine systems in 50% aqueous ethanol solution

System	λ_{max} (Absorbance)
Iodine in deionised water	287, 353, 465
Iodine in 50% aqueous ethanol	213, 226, 290 5, 259 5
KI+Iodine in 50% aqueous ethanol	230, 285 5, 352 5
L-Amino acids+ Iodine (I_2) in 50% aqueous ethanol	
Isoleucine	212 5 (0 5672), 297 (.2482), 356.0 (0 2498)
Leucine	212 0(6301), 297 0(3699), 359.0 (3695)
Phenylalanine	212 0(4957), 294 0(2338), 357.0 (2325)
Tryptophan	212 5(1 0345), 293 0 (0835), 347 0 (8040)
Valine	212 0 (9917), 291 0 (1760), 358 5 (1011)
Asparagine	212 5(1 0192), 295 5 (2514), 358 5 (1387)
Glycine	212.5(7072), 293 0(.1698), 359 0 (1037)
Threonine	212.5 (1 0981), 291 0 (3345), 358 5 (1918)
Histidinemonohydrochloride	212 0 (2 0152), 288 5(0 2425), 359 0 (0 1308)
Lysinemonohydrochloride	212.0 (2 0131), 299 5 (4181), 356.5 (.4191)

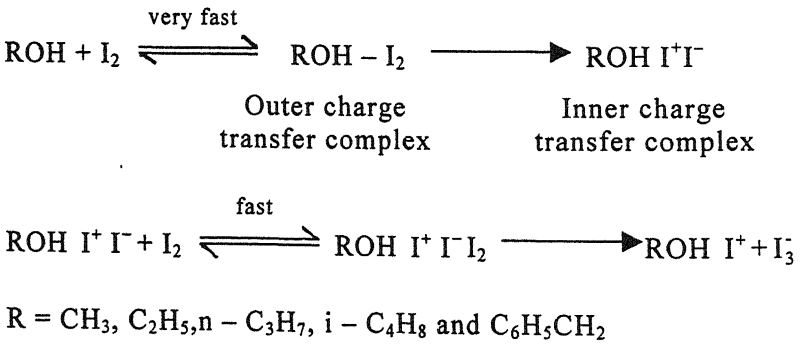

R = CH_3, C_2H_5,n – C_3H_7, i – C_4H_8 and $C_6H_5CH_2$

In case of amino acids-iodine systems in 50% aqueous ethanol (Table 3) the last two peaks (291-299, 347-354 nm) are assigned to I_3^- whereas the peak around 212 nm may be attributed to I^- since the conductometric studies give rise to a complex having stoichiometry 1:2 (D:A). The tentative structure of the molecular complex may be thus written as:

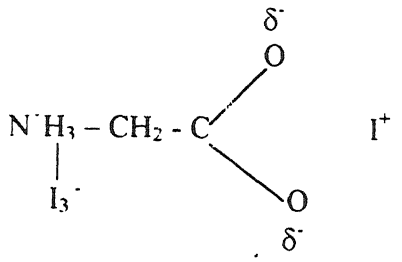

The interaction of I_3^- to protonated N in the present studies finds support from earlier spectroscopic observations that the band at 226 nm in the absorption spectra of iodine with amines, amino acids and protein in aqueous solution is due to binding of I^- with protonated nitrogen.

References

1. Slifkin, M A. (1964) *Spectrochim Acta* **20A** · 1543
2. Slifkin, M A (1962) *Nature* **193** . 464
3 Birks, J B & Slifkin, M A. (1963) *Nature* **197** 42
4 Slifkin, M A (1963) *Nature* **197** . 275
5 Gutmann, F & Keyzer, H. (1966) *Electrochim Acta* **11** 555, 11 1163
6 Gutmann, F & Keyzer, H. (1967) *Electrochim Acta* **12** 1255
7 Gutmann, F (1967) *J Sci Ind Res* **26** 19
8 Randhawa, H S & Lakhani, R. (1993) *Colln Czech Chem Commun* **58** 783
9 Randhawa, H S , Patyar P & Sekhon, B S., *Proc Natl Acad Sci , India* (Section A) (Revised communicated)
10 Murray, R K., Granner, D.K , Moyes, P.A. & Rodwell, V W (1996) *Harper's Biochemistry*', Prentice Hall, London
11. Katzin, L I (1953) *J Chem Phy* **21** . 490
12. Tsubomura. H & Lang, R.P. (1961) *J Am Chem Soc* **83** . 3085
13 Awtrey, A,D. & Connick, R.E. (1951) *J Am Chem Soc* **73** · 4546
14. Randhawa, H S., Sachdeva, R. & Brar, C K (1989) *Z Phys Chemie* **270** : 199.
15. Rao, C.N.R., Kalyanaraman, V. & George, M V. (1970) *Spectros Rev* **3** : 153

PROC. NAT. ACAD. SCI. INDIA, 74 (A), II, 2004

Thermodynamic parameters of complexes of bivalent transition metal ions with 3-(4-methoxyphenyl)-1-(2'-hydroxynaphthyl)-2-propen-1-one

K.G. MALLIKARJUN

Department of Chemistry, Jawahar Navodaya Vidyalaya, Peddapuram – 533 437, India.

Received December 17, 2002, Revised May 6, 2003, Accepted September 15, 2003

Abstract

The stability constants of UO_2^{2+}, Cu^{2+}, Zn^{2+}, Co^{2+}, Ni^{2+} and Mn^{2+} complexes of 3-(4-methoxyphenyl)-1-(2'-hydroxynaphthyl)-2-propen-1-one (HMPHPO) have been determined in 75% (v/v) dioxane-water, acetone-water and 2-ethoxyethanol-water mixtures using the Bjerrum-Calvin pH titration technique as developed by Irving and Rossotti. The stability constants are in fair agreement with Irving-Williams order The results obtained are compared with the data available in the literature Abnormal behaviour of the chelates was observed in acetone-water medium. The thermodynamic parameters such as free energy, enthalpy and entropy change involved in complexation have been calculated

(Keywords 2-hydroxy-1-acetonaphthone / p-methoxybenzaldehyde/free energy/stability constants/ enthalpy/entropy/Calvin-Bjerrum technique)

Introduction

Very few systems have been reported[1] showing the relationship between thermal stability of metal chelates and structure of the chelating agent. Wendlandt and co-workers[2-5] and Hill and co-workers [6, 7] studied the thermal properties of metal chelates with different types of complexing ligands. Lense *et al.*[8] reported that o-hydroxychalcones are much more reactive with metal ions than the ketones and aldehydes from which they are synthesized. Holm and O'Connor[9] have reviewed structural studies on several metal chelates of β-diketones and 2-hydroxycarbonyl compounds. The metal chelates of divalent transition metals with some o-hydroxychalcones standout as a distinct class of o-hydroxycarbonyl compounds with low spin square-planar configuration, which do not easily form adducts. Extensive conjugation was found to be responsible for the strong field nature of the ligand[10]. Chalcones were found to be physiologically and pharmacologically active. They were

also found to have germicidal[11], bactericidal[12], fungicidal[13] and carcinogenic activity[14]. Several of the chalcones have been employed as useful analytical reagents.

The present investigation deals with the determination of stability constants and the thermodynamic parameters of the complexes of UO_2^{2+}, Cu^{2+}, Zn^{2+}, Co^{2+}, Ni^{2+} and Mn^{2+} with 3-(4-methoxyphenyl)-1-(2'-hydroxynaphthyl)-2-propen-1-one(HMPHPO, Fig. 1) at different temperatures employing Calvin-Bjerrum pH titration technique[15-17] as modified by Irving and Rossotti[18].

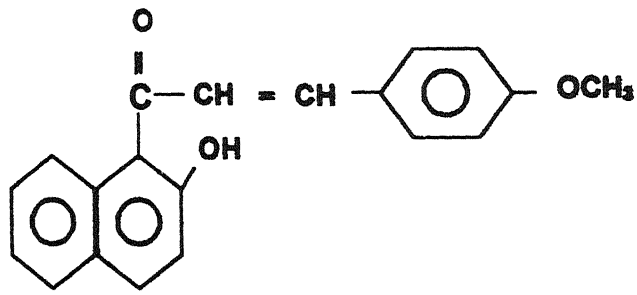

Fig 1–Structure of HMPHPO

Materials and Method

The ligand 3-(4-methoxyphenyl)-1-(2'-hydroxynaphthyl)-2-propen-1-one (HMPHPO) was prepared by the condensation of 2-hydroxy-1-acetonaphthone with p-methoxy benzaldehyde employing the Claisen-Schmidt condensation reported earlier[19]. The purity of the sample was checked by elemental analysis and melting point determination. The solution of the ligand was prepared using dioxane, acetone and 2-ethoxyethanol as solvent. The metal nitrate solutions were prepared in CO_2 free doubly distilled water and were standardized by standard methods. Dioxane, acetone and 2-ethoxyethanol were purified before use. An ELICO (< 1-120) digital pH meter was used for pH measurements.

The experimental method consists of pH titration of the following carbonate free solutions of 50 ml at the desired temperatures against standard sodium hydroxide.

(a) 5 ml 0.1 M KNO_3 + 37.5 ml organic solvent + 5 ml 0.01 M HNO_3 + 2.5 ml water.

(b) 5 ml of 0.1 M KNO_3 + 1 ml of 0.1 M ligand in pure organic solvent + 36.5 ml organic solvent + 5 ml 0.01 M HNO_3 + 2.5 ml water.

(c) 5 ml of 0.1 M KNO_3 + 1 ml of 0.1 M ligand solution + 36.5 ml organic solvent + 5 ml 0.01 M HNO_3 + 0.5 ml of (0.01 M) metal solution + 2 ml water.

The pH values (B) were corrected in all the aqua-organic mixture by the method of Van Uitert and Hass[20] (- log $[H^+]$ = B + log U_H) and others[21] under the present condition the following logU_H values were obtained in different media under consideration : 0.36 (75% aq. Dioxane), 0.29 (75% aq. acetone) and 0.24 (75% aq. 2-ethoxyethanol).

Results and Discussion

In our earlier work[22], calculation of proton ligand formation constants of the ligand was explained, the same method is applied for this ligand (HMPHPO) and calculated proton ligand formation constant in 75% aq. dioxane at 30°C, 35°C and 40°C are 12.80, 12.54, and 12.41 respectively. In 75% aq. acetone and 75% aq. 2-ethoxyethanol at 30°C are 12.36, 11.77 respectively.

From the titration curve of solution of (b) and (c), n and p_L values were calculated[15, 16, 19]. The stepwise formation constants were corrected by least squares method[19] and are presented in Table 1.

Table 1– Stability constants of bivalent transition metal complexes with HMPHPO at different temperatures and different solvent media (Ionic strength 0 1M)

		75% Dioxane			75% Acetone	75% 2-Ethoxyethanol
		30°C	35°C	40 °C	30°C	30°C
	log k_1	10.98	10.74	10 56	10 73	10.38
UO_2^{2+}	log k_2	10.36	10.17	9.78	10 34	10 10
	log β_2	21 34	20 91	20 34	21.07	20.48

Table 1 Contd...

Table 1 Contd...

	log k_1	9 86	9 64	9 48	9 61	9.52
Cu^{2+}	log k_2	9 43	9 32	9 15	9 35	8 85
	log β_2	19.29	18.96	18 63	18 96	18 37
	log k_1	9 08	8 83	8 55	8 74	8 55
Zn^{2+}	log k_2	8 36	8 12	7 94	8 42	7 96
	log β_2	17 44	16 95	16 49	17 16	16 5
	log k_1	8 35	8 01	7 88	8 02	7 82
Co^{2+}	log k_2	7 64	7 58	7 45	7 48	7 01
	log β_2	15 99	15 59	15 33	15 50	14 83
	log k_1	8 05	7 78	7 55	7 94	7 72
Ni^{2+}	log k_2	7 48	7.35	7 24	7 38	6 84
	log β_2	15 53	15 13	14 79	15 32	14 56
	log k_1	7 82	7 66	7 48	7 62	7 34
Mn^{2+}	log k_2	7 04	6 82	6 64	7 08	6 61
	log β_2	14 86	14 48	14 12	14 70	13 95

The formation of metal chelates takes place by replacement of hydrogen of the 2-hydroxynaphthyl groups and coordination occurs through the oxygen of the ketonic group. The acid dissociation constant of the ligand is found to decrease in different media in the order dioxane > acetone > 2-ethoxyethanol. A plot of pk_L against $1/D$ is linear. However in acetone-water solvent the dissociation constant of the ligand is less than the expected value and it may be attributed to the non-ideal behaviour of acetone-water solvent. The order of stability of the metal chelates, observed and studied in all the three mixed solvents is $UO^{2+} > Cu^{2+} > Zn^{2+} > Co^{2+} > Ni^{2+} > Mn^{2+}$ This order of stability follows the Irving – Williams[23] natural order expect cobalt (II) leading to the conclusion that the ligand used in the present investigation is weak field one. The greater stability of cobalt (II) chelate when compared to nickel (II) chelate may be attributed to the additional stabilization due to John – Teller distortion present in the former case. The order cobalt (II) > nickel (II) has been reported for some other ligands also *viz.* 4-nitro-2-aminophenol[24], 8-hydroxy-2-methylquinolinol[25], 2-hydroxychalcone[26] and 3-(4-chlorophenyl)-1-(2'-hydroxynaphthyl)-2-propen-1-one[22]. The values of log β for zinc (II) chelates are greater than those of nickel (II). The

order zinc (II) > nickel (II) has been observed earlier also[27, 28, 22] where the relative low value for nickel (II) has been attributed to the presence of a square planar structure. Further the hydrolysis constant of zinc (II) chelate is greater than that for nickel (II) indicates a greater affinity of zinc (II) for - OH ions. This factor seems to be accurate for the order zinc (II) > nickel (II). The order of stability of complexes with respect to the solvent in dioxane > acetone > 2-ethoxyethanol. The dielectric constants for the pure as well as mixed solvent are in the order acetone > 2-ethoxyethanol > dioxane. This also shows the abnormal behaviour of acetone-water mixture, similar abnormality was reported in the literature[27,22]. A plot of log β vs. ionization potential shows that the stability of the complexes can be better correlated with the second ionization potential rather than the first.

The data presented in Table 1 shows that the difference in log k_1 and log k_2 values are small and the ratio of log k_1 / log k_2 is positive in all cases indicating that there is little (or) no steric hindrance to the addition of the second ligand molecule[29]. It is also evident from the values of log k_1 and log k_2 that there is a almost equal tendency for the formation of neutral complex species ML_2 as for the species M_L^+.

The stability constant values decrease with increase in temperature (Table 1) that is in agreement with the conclusion reached by Pitzer[28]. The thermodynamic parameters free energy (ΔG), enthalpy (ΔH) and entropy (ΔS) change have been calculated[30] from the stability constants of the metal complexes determined at three different temperature (30^0 C, 35^0 C and 40^0 C) in 75% dioxane and are given in Table 2.

Table 2– Thermodynamic parameters of transition metal complexes with HMPHPO in 75% dioxane

Metal	$-\Delta G$ (K J.mole^{-1})	$-\Delta H$ (K J mole^{-1})	$+\Delta S$ (J deg^{-1}mole^{-1})
UO^2	123 79	113 02	35.54
Cu^{2+}	111 90	107.62	14 13
Zn^{2+}	101 17	94 19	23.12
Co^{2+}	92 76	91 88	2.11
Ni^2	90 09	80 71	30 96
Mn^{2+}	86 20	70.66	51 28

ΔG values at 30^{0}C

Error limits are ± 0.01 for ΔG and ΔH and ± 0.1 for ΔS

The ΔG values are all-negative and suggest that complexation is a spontaneous process. These values become less negative at higher temperatures indicating that low temperature favours complexation. The negative ΔH values for complex formation indicate the release of energy during the interaction of metal ions with ligand. The ΔH values of the metal complexes (HMPHPO with different metal ions) follow the order $UO^{2+} > Cu^{2+} > Zn^{2+} > Co^{2+} > Ni^{2+} > Mn^{2+}$, in agreement with the natural order of the stability constants. The values of ΔS are positive for all the system indicating that entropy is favourable for the complex formation.

Acknowledgements

The author thanks Dr. R. Seshadri Naidu, Director, Academic Staff College, S.V.University, Tirupathi and Dr. N.S. Reddi, Principal, JNV, East Godavari for their valuable suggestions.

References

1. Wendlandt, W.W. (1957) *Anal Chim Acta* **17** : 428.
2. Ascenzo, G.D. & Wendlandt, W.W (1969) *J Therm Anal* **1** : 423
3 Ascenzo, G.D & Wendlandt, W.W. (1970) *Anal Chim Acta* **50** 79
4 Chang, F.C & Wendlandt, W.W (1971) *Thermochem Acta* **2** 293
5. Perry, D.L, Vaz, C & Wendlandt W.W (1974) *Thermochim Acta* **9** 76
6. Scency, C G , Hill, J O. & Magee, R.J. (1975) *Thermochim Acta* **11** 301
7. Scency, C G , Smith, F , Hill, J.O. & Magee, R J (1976) *J Therm Anal* **9** 415
8. Lense, F.T , Glover, C A. & Markham, E.C. (1942) *Virginia J Sci* **3** 14
9. Holm, R H. & O'Connor, M J., (1971) *Prog Inorg Chem* **14** . 241.
10. Palaniandavar, M. & Natarajan, C (1980) *Aust J Chem* **33** 737
11 Russel, J & Clarke, H (1939) *J. Am Chem Soc* **61** : 3651
12. Devitt, P F., Timony, A & Vickars, M.A., (1961) *J Org Chem* **26** : 4941
13. Buu-Hoi, N P. & Xuong, N D. (1958) *J Org Chem* **23** 39.
14 Kushwaha, S C., Dinakar & Lal, J.B. (1967), Ind J Chem **5** . 82.
15. Calvin, M. & Wilson, K W. (1945) *J Am Chem Soc.* **67** · 2003.
16. Calvin, M. & Melchior, N C. (1948) *J. Am Chem Soc.* **70** : 3270
17. Bjerrum, J. (1941)\ *Metal ammine formation in aqueous solution*, P. House and Sons, Copenhagen,
18. Irving, H.M. & Rossotti, H.S. (1953\), (1954) *J. Chem Soc* 3397, 2904.

19. Mistra, S.S. & Dinakar (1972) *J Indian. Chem Soc* **6** 49.
20. Van Vitert, L G. & Hass, C A (1953), (1954) *J Am Chem Soc* **75** 451, 458, **76** 375
21. Chawla, I D. & Spittert, C R (1968) *J Inorg Nucl Chem* **30** 2127
22. Mallikarjun, K G. & Seshadri Naidu, R (1992) *Asian J Chem* **4(1)** . 135.
23. Irving, H.M. & Williams, R J.P (1948) *Nature* **162** 746
24 Vartak, D G. & Menon, N.G (1966) *J Inorg Nucl Chem* **28** · 2911
25. Irving, H M & Rossotti, H S (1954) *J Am Chem Soc* **76** 2910
26. Khadikar, P V., Kakkar, S N & Berge, D D (1975) *Indian J Chem* , **13** 844
27 Seshagiri, V & Brahmaji Rao, S. (1967) *Aust J Chem* **20** 2783
28 Pitzer, K S (1937) *J Am Chem Soc* **59** . 2365.
29. Cotton.F A & Wilkinson, G. (1980) *Advanced-Inorganic Chemistry*, 9th ed , Inter Science and New York.
30 Yatsimirskii, K.B & Vasilev, V P. (1960) *Instability constants of complex compounds,* Pergamon, London, p. 63.

PROC. NAT. ACAD. SCI. INDIA, 74 (A), II, 2004

Quantitative structure activity relationship studies on 1,3diaryl-4,5,6,7-2H-isoindole derivatives acting as potent and selective Cox-2 anti inflammatory agents

ARUN K. SRIVASTAVA, ARBAB A. KHAN, M. SHAKIL and ARCHANA

Department of Chemistry, University of Allahabad, Allahabad-211002, India.

Received August 7, 2002 Accepted October 7, 2002

Abstract

QSAR studies of anti inflammatory(1-10) novel tetrahydro 2H-isoindoles have been discussed The inhibitory potency of these compound is found to be dominantly controlled by steric factor $^1\chi^b$ Significant correlation have been obtained between inhibitory potency and molecular connectivity $^1\chi^b$.

(**Keywords** QSAR/1,3 diaryl-4,5,6, 7 -2 H-isoindole/Cox-2)

Introduction

Kujubu *et al.*[2] suggested that an inflammatory or mitogenic stimulus might result in gene expression responsible for the synthesis of a second inducible cyclo oxygenase isoenzyme called Cox-1 Cox-2[2] rapidly emerged as an invaluable target for developing anti inflammatory agents with reduced gastrointestinal *or* renal secondary effect .Nonsteroidal anti inflammatory drugs (NSAIDS)are widely used to treat pain, fever and inflammatory condition including Osteoarthritis. Recently ,it has been postulated that Cox-2 inhibitor may effectively relieve symptoms in diseases such as Osteoarthritis, while exhibiting a considerably safer toxicity profile than classical NSAIDS especially with respect to gastric complications[3]. It has been recently demonstrated that IL-1-stimulated chondrocytes from normal cartilage expressed the cox-2 gene and produced the cox-2 protein followed by PGE2 release[4], Cox-2 protein over expression has been detected in chondrocytes from Osteoarthritis patients as compared with normal subjects whereas cox-1 was not detected in either normal or Osteoarthritic chondrocytes[5]. PGE2 over induced in Osteoarthritic cartilage has been shown to coincide with cox-2 impregnation hence suggesting that PGE2 may be differentially regulated in normal and Osteoarthritic cartilage[6].In this field only Nimesulide[7], its analogues NS 398[8] and structural flosulide analogues[9,10] are described

as preferential cox-2 inhibition[11]. Pyrazole derivatives by Searle are serious candidates for potent and selective inhibitors which were structurally related to the class of cyclopentenyl lactones[12,13] Celeocoxib (1)[14,15] and rofecoxib(vioxx, 2) have been recently marketed.

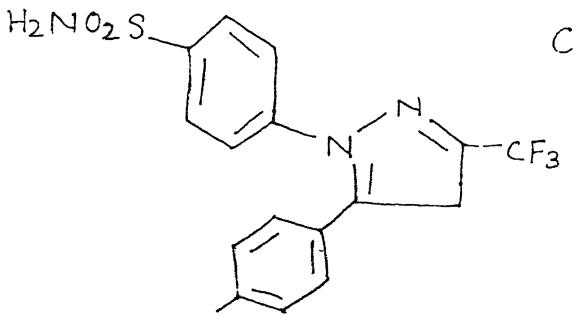

(1)

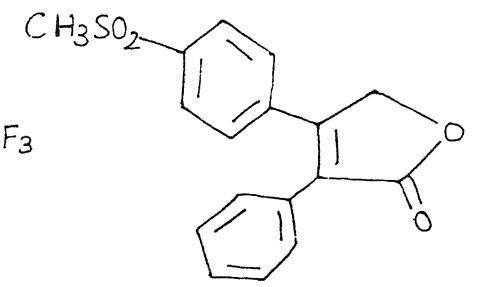

(2)

After several modification in structure in order to enhance the cox-2 inhibition potency a lead and a compound (3) had been reported

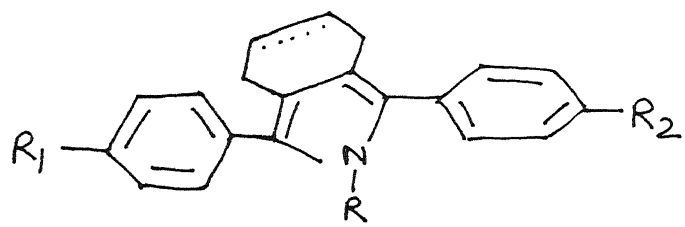

Method

In present work steric parameter $^{1}\chi^{b}$ i.e. molecular connectivity widely has been used to assess the role of molecular size, with a view to provide a better rational

approach for the design of potent drugs .The $^1\chi^b$ (first order of molecular connectivity index) was calculated as suggested by Kupchiik[16-18].

The regression analysis was performed with the help of statistical package SPSS.

The data listed in Table 1 has been used for QSAR study. IC_{50}, Cox-2 refer to concentration of compounds required to achieve 50% inhibition against Cox-2 from mouse resident macrophages

Table 1– Physio-chemical parameters and biological activity of Tetrahydro-2H isoindole.

S. No.	Structure			Physio-chemical parameters			Activity-log $1/IC_{50}$		
	R	R_1	R_2	*X*eq	*Id*	$^1\chi^b$	Obs	cal eqn (1)	cal eqn (6)
1	2	3	4	5	6	7	8	9	10
1.	H	H	H	2.313	4.418	7 528	8.824	8.798	8.673
2.	H	H	H	2.313	4 417	7.428	8.481	8.870	8.743
3	NH_2	H	H	2.308	6.450	7.984	8 744	8 469	8.357
4.	$NHSO_2CH_3$	H	H	2.339	4.685	10.786	6.301	6 444	6.412
5.	H	F	F	2.363	4.518	7 978	8 869	8.473	8.798
6.	H	CH_3S	CH_3S	2.331	5.013	11.162	6.301	6 173	6.152
7.	H	CH_3	CH_3	2.290	4 518	8.599	7 778	8.028	7.930
8.	H	OCH_3	OCH_3	2 323	5 013	8.825	7.671	7 862	7.774
9.	H	Cl	Cl	2.339	4.518	8.734	8 301	7.927	8.273
10.	H	F	$C_3H_3N_2$	2 353	4.757	9.314	7.377	7.508	7.435

The regression analysis of the data presented in Table 1 gave following significant equation:

$$\text{Log}(1/IC_{50}) = -0.722(\pm 0\ 07)\ ^1\chi^b + 19.23\ (\pm 0.64) \qquad (1)$$

$n = 10$, $r = 0.97$, $r^2 = 0.93$, $s = 0.25$, $F = 100.9$

where n represents the number of data presents, r the correlation coefficient, F the varience ratio between the calculated and observed activities and s the standard error of estimate. Equation (1) gave significant but negative coefficient accounts for 92.7% of varience and F ratio was found to be significant at 99% level [$(F_{2,10}) = 7.8$]

In order to study the effect of specific substituents at R, R_1, R_2 position six indicator parameters were taken, Ind_{-1} for compound possessing NH_2 at pyrrole ring, Ind_{-2} for compound possessing $NHSO_2CH_3$ at position R, Ind_{-3} for compound having F at R_1 and R_2 position, Ind_{-4} for compound CH_3S,Ind_{-5} for compound OCH_3 and Ind_{-6} for compound Cl and F at position R_1 and R_2 phenyl ring. Following significant equations were obtained.

$$\text{Log}(1/IC_{50}) = -0.703(\pm 0.07)\ {}^1\chi^b + 0.324(\pm 0.294)Ind_1 + 14.03 \quad (2)$$

$n = 10$, $r = 0.968$, $r^2 = 0.937$, $s = 0\ 27$, $F = 52.39$

$$\text{Log}(1/IC_{50}) = -0.692(\pm 0.08)\ {}^1\chi^b - 0.224(\pm 0.35)Ind_2 + 13.99(\pm 0.77) \quad (3)$$

$n = 10$, $r = 0.97$, $r^2 = 0.93$, $s = 0.25$, $F = 46.8$

$$\text{Log}(1/IC_{50}) = -0.702\ (\pm 0.07)\ {}^1\chi^b + 0.348(\pm 0\ 29)Ind_3 + 14.02(\pm 0.64) \quad (4)$$

$n = 10$, $r = 0.97$, $r^2 = 0.93$, $s = 0.26$, $F = 55.93$

$$\text{Log}\ (1/IC_{50}) = -0.761\ (\pm 0.09)\ {}^1\chi^b + 0.24(\pm 0.39)Ind_4 + 14.54(\pm .84) \quad (5)$$

$n = 10$, $r = 0.964$, $r^2 = 0.930$, $s = 0.28$, $F = 46.6$

$$\text{Log}(1/IC_{50}) = 0.722(\pm 0.07)\ {}^1\chi^b - 0.211\ (\pm 0.29)Ind_5 + 14.25(\pm 0.66) \quad (6)$$

$n = 10$, $r = 0.97$, $r^2 = 0.93$, $s = 0.28$, $F = 47.57$

$$\text{Log}(1/IC_{50}) = -0.694(\pm 0.05)\ {}^1\chi^b + 0.436\ (\pm 0.17)Ind_6 + 13.89(\pm 0.51) \quad (7)$$

$n = 10$, $r = 0.90$, $r^2 = 0.97$, $s = 0.27$, $F = 55.42$

Equation(2-7) account for 93.9%, 93.0%, 93.1 % variance of F are also found to be significant for all above equations at 99% level [$(F_{2,10})$=7.56].

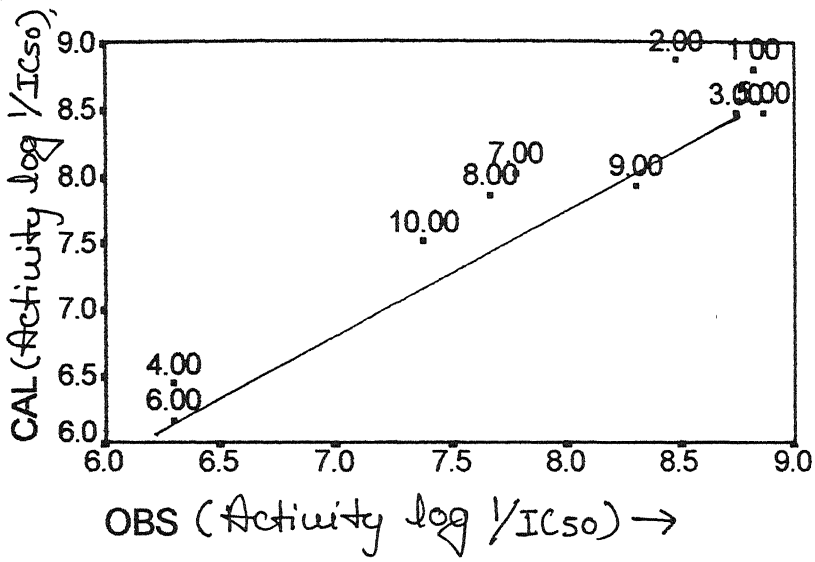

Fig 1

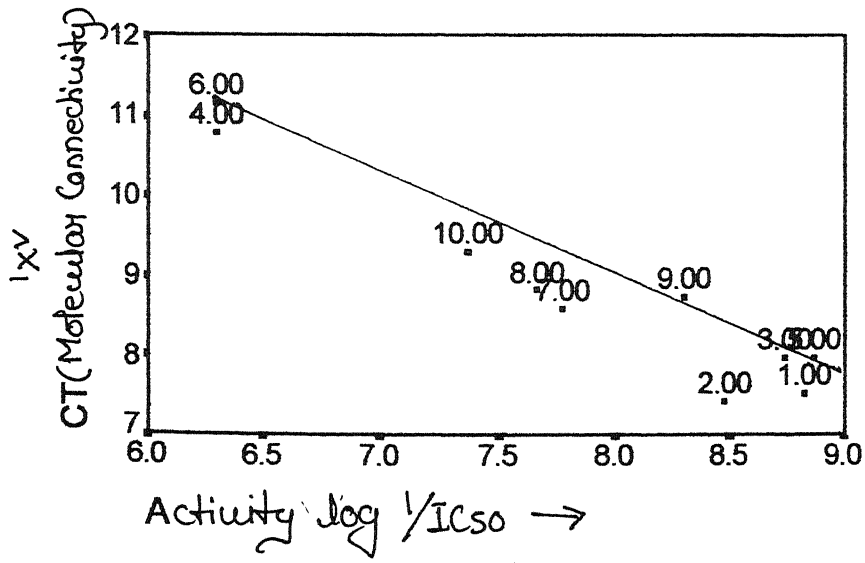

Fig 2

Conclusions

On the basis of the above study it can be inferred that steric factor $^{1}\chi^{b}$ with negative (-) coefficient plays an important role in determining the Cox-2 inhibitory potencies-the negative coefficient shows that with small increase in constituent size potency decreases sharply. The coefficient value of Ind_1, Ind_3 and Ind_6 are having positive (+) coefficient suggesting that -NH_2 at pyrrole ring (Ind_1), Halogen (Cl or F, Ind_3 and Ind_6) particularly F at para position of phenyl ring shows higher inhibitory potencies. Whereas bulky substituent like -$NHSO_2SO_3$ at pyrrole ring Ind_2 and -OCH_3 at para position (Ind_5) shows decrease in inhibitory potencies however substituent –CH_3S Ind_4 shows positive coefficient and increase inhibitory potencies suggest there may be an active pocket for CH_3S where S (Sulphur) seems to be playing active role, therefore smaller substituents group like halogen, amine at R_1 and R_2 position at phenyl ring should be preferred in future drug synthesis. In the present series these findings are in conformity with Portevin *et. al*[1]. These fact are also proved by Fig. (1 & 2) plotted between predicted and calculated inhibitory potency, steric parameter and log $1/IC_{50}$ respectively.

Acknowledgement

This research was supported by Grant (1648)/00/EMR II awarded by CSIR, New Delhi.

References

1 Portevin, Bernard & Tordjrnan, Charles, *et al* (Private communication)

2 Kujubu, D A , Fletcher, B S , Varnum, B C , Lim, R W , Herschman, H R & Tisio (1991) *J Chem, Biol* **266** 12866

3 Xie, W , Chipman, J G , Robertson, D L , Erikson R L & Simmons, D L (1992) *Proc Natl Acad Sci U S A,* **89** 3917

4 Parnham, M J (1998) *Inflamm Res* **47** 43

5 Geng, Y , Blanco, F J , Comellison, M , & Lotz, M (1995) *J Immunol* **155** 796

6 Chan, C C , DiBattista, I A , Zhao, J , Pelletier, J P , Martel-Pelletier, J , Kennedy, B P , Brideau, C & Rodger, I W (1995) *International Association of Inflammation Society,* Brighton, Sept 17

7. Amin, A R , Attur, M , Patel, R N., Thakker, G D , Marshall, P J , Rediske, J , Stuchin, S A , Patel, I R & Abramson, S B (1997) *J Clin Invest* **99** : 1231

8. Davis, R , Brodgen, R N. & Nimesulide (1994) *Drugs* **48** · 431.

9. Futaki, N , Taakahashi, S , Yokoyama, S , Arai, I , Higuchi, S & Otomo, S (1994) *Prostaglandins,* **47** 55

10 Wiesenberg-Boettcher, I , Schweizer, A & Muller, K (1989) *Agents Action* **26** 240

11 Li, C S , Black, W C , Chan, C C , Ford-Hutchinson, A W , Gauthier, J Y , Gordon, R , Guay, D , Kargman, S , Lau, C K , Manichi, J , Ouimet, N , Roy, P , Vickers, P , Wong, E , Young, R N , Zamboni, R & Prasit, P (1995) *J Med, Chem* **38** 4897

12 Penning, T D , Talley, J J , Bertenshaw, S R , Carter, J S , Collins, P W , Docter, S., Graneto, M J., Lee, L F , Malecha, J W , Miyashiro, J.M , Rogers, R S , Rogier, D.J , Yu, S S., Anderson, G D , Burton, E G , Cogburn, J N., Gregory, S.A., Koboldt, C.M , Perkins, W E , Seibert, K , Veenhuizen, A W , Zhang, Y Y & Isakson, P C (1997) *J Med Chem* **40** · 1347

13 Wallace, J., Chin, B & Celeocoxib (1999) *Curr Opin Central Peripheral Nerv Syst* **1** 132.

14 Black, C , Grimm, E , Leger, S , Prasit, P & Wang, Z.(1995) *World Patent WO* 9619469.

15 Kamali, F Rofecoxib (1999) *Curr Opin Central Peripheral* 126

16 Kupchick, E J (1985) *Quant Struct Act Relat* **4** 123

17 Kupchick, E J (1988) *Quant Struct Act Relat* **7** 57

18 Kupchick, E J (1986) *Quant Struct Act Relat* **5** · 95

PROC. NAT ACAD SCI INDIA, 74 (A), II, 2004

Wave propagation in a micropolar elastic solid with stretch

BALJEET SINGH*[1] and RAJNEESH KUMAR[2]

[1]*Department of Mathematics, Government College, Sector 11 Chandigarh - 160011, India*

[2]*Department of Mathematics, Kurukshetra University, Kurukshetra-136 119, India.*

**Correspondence address. 597/40, Krishnanagar, Hisar-125 001, India*

E-mail address. baljeet_gill@hotmail.com

Received May 16, 2002, Revised December 9, 2002, Accepted July 15, 2003

Abstract

The paper deals with the problem of the reflection and refraction of plane waves at an interface between two dissimilar micropolar elastic solid half-spaces with stretch The amplitude ratios for various reflected and refracted waves are calculated theoretically Numerical values of the amplitude ratios are computed and plotted against the angle of emergence of incident longitudinal microstretch wave

(**Keywords** reflection/refraction/micropolar elastic solid/axial stretch/amplitude ratios/ LMS wave)

Introduction

It is well known that material response to external stimuli depends heavily on the motion of its inner structures. Classical elasticity ignores this effect by ascribing only translation degrees of freedom of material point of body. Micropolar theory of Eringen and his coworkers[1,2] by including intrinsic rotations of the microstructure, provides a model that can support body and surface couples and display high frequency optical branch of the wave spectrum.

Eringen[3] extended his work to include the effect of axial stretch during the rotation of molecules and developed the theory of micropolar elastic solid with stretch. For engineering applications, composites with rigid chopped fibres, elastic solid with rigid granular inclusions, and other industrial materials such as liquid crystals may be modeled as micropolar elastic solids with axial stretch.

During last four decades, various researchers[4-14] discussed some problems on waves and vibrations in micropolar elastic solid. Recently, Tomar and Gogna[10-11] discussed some problems on reflection and refraction at an interface between two micropolar media. The present investigation is concerned with the reflection and refraction of plane waves at an interface between two dissimilar micropolar elastic solids with stretch.

Basic Equations and their Solutions

Following Eringen[2,3], the constitutive and field equations in a micropolar elastic solid with stretch without body forces and body couples can be written as

$$\sigma_{kl} = \lambda u_{r,r}\delta_{kl}+\mu(u_{k,l}+u_{l,k})+\kappa(u_{l,k}-\varepsilon_{klr}\,\phi_r), \tag{1}$$

$$m_{kl}=\beta_0\varepsilon_{rkl}\Phi^*_{,r} + \alpha\,\phi_{r,r}\delta_{kl}+\beta\phi_{k,l}+\gamma\phi_{l,k}, \tag{2}$$

$$\beta_k= \alpha_0\Phi^*_{,k}+(\beta_0/3)\varepsilon_{rkl}\phi_{r,l}, \tag{3}$$

and

$$(c_1^2+c_3^2)\nabla(\nabla.\,\mathbf{u})-(c_2^2+c_3^2))\nabla\times(\nabla\times u)+ c_3^2\nabla\times\phi=\ddot{u} \tag{4}$$

$$(c_4^2+c_5^2))\nabla(\nabla.\,\phi)-c_4^2\,\nabla\times(\nabla\times\phi) + \omega_\circ^2\nabla\times u -2\,\omega_\circ^2\phi = \ddot{\Phi}, \tag{5}$$

$$c_6^2\nabla^2\Phi^*-r_1\Phi^*=\ddot{\Phi}^*, \tag{6}$$

where

$$c_1^2=(\lambda+2\mu)/\rho, \qquad c_2^2=\mu/\rho, \qquad c_3^2=\kappa/\rho,$$

$$c_4^2=\gamma/\rho j, \qquad c^2=(\alpha+\beta)/\rho j, \qquad \omega_3^2 = c_3^2/j=\kappa/\rho j,$$

$$c_6^2=2\alpha_0/\rho j \qquad r_1=2\eta_0/\rho j, \tag{7}$$

where symbols λ, μ, κ, α, β, γ, α_0, β_0, η_0, ρ have their-usual meanings. $\mathbf{u}$, ϕ and Φ^* are displacement vector, microrotation vector and scalar micro stretch respectively. δ_{kl} is the kronecker delta. The superposed dots on right hand side of equations (4) to (6) denote the second order partial derivatives with respect time.

Parfitt and Eringen[5] have shown that there exists four basic waves propagating in an infinite micropolar solid, namely, a longitudinal displacement wave (LD wave) travelling with speed V_1, a longitudinal microrotational wave (LM wave) travelling with speed V_2 and two sets of two coupled transverse displacement and microrotational waves (CD I and CD II waves) with velocities V_3 and V_4.

In order to solve equation (6), we assume that wave propagates in a positive direction of unit vector $\boldsymbol{n}$ as

$$\Phi^* = D \exp[ik(\boldsymbol{n}.\boldsymbol{r}-Vt)], \tag{8}$$

where D is the amplitude of the wave, V is the phase velocity, $\boldsymbol{r}$ is the position vector, k is the wave number and $\omega = kV$.

Substituting equation (8) in equation (6), we get

$$\{(k^2V^2/c_6^2) - k^2 - r_2\}D \exp[ik(\boldsymbol{n}.\boldsymbol{r} - Vt)] = 0, \tag{9}$$

where $r_2 = \eta_0/\alpha_0$.

From equation (9), we have

$$V^2 = c_6^2/\{1-(r_2\ c_6^2/\omega^2)\}, \tag{10}$$

Equation (10) gives the speed of the wave given by equation (6) and we call the wave as longitudinal micro stretch (LMS) wave.

V will be real and finite only if

$$1-(r_2\ c_6^2/\omega^2) > 0,$$

i.e. $$\omega > (2\ \eta_0/\rho j)^{1/2}, \tag{11}$$

This is the condition for the existence of the longitudinal micro stretch wave.

Thus, in an unbounded micropolar elastic solid with stretch there exists five basic waves travelling with distinct speeds.

Since we are discussing a two dimensional problem in x-z plane, we have

$$\boldsymbol{u} = (u_1 0, u_3), \qquad \phi = (0, \phi_2, 0), \tag{12}$$

where

$$u_1 = \frac{\partial \phi}{\partial x} + \frac{\partial \psi}{\partial z}, \qquad u_3 = \frac{\partial \phi}{\partial z} - \frac{\partial \psi}{\partial x}, \tag{13}$$

where ϕ, ψ; are potentials satisfying certain wave equations in micropolar media with stretch.

Boundary Conditions

For two-dimensional motion in xz-plane, the appropriate boundary conditions at the interface $z = 0$ are the continuity of normal stress, tangential stress, couple stress, normal vector first moment, tangential vector first moment, normal displacement, tangential displacement and microrotation, i.e.,

$$t_{zz} = t_{zz}', \quad t_{zx} = t_{zx}', \quad m_{zy} = m'_{zy}, \quad \beta_z = \beta'_z,$$

$$\beta_x = \beta_x' \quad u_3 = u_3', \quad u_1 = u_1', \quad \phi_2 = \phi_2', \text{ at } z = 0, \tag{14}$$

The quantities with primes correspond to the medium ($z < 0$) and those without primes to the medium ($z > 0$) throughout this manuscript.

Reflection and Refraction

We consider two micropolar elastic solid half-spaces with stretch which are in welded contact along a plane interface $z = 0$. We introduce rectangular Cartesian co-ordinates (x, y, z) and place the origin at the interface separating the two half-spaces,

We now consider a plane harmonic seismic body wave [LD, CD I or LMS] with time dependence proportional to $\exp(i\omega t)$, propagating through the medium ($z > 0$) and striking obliquely at the interface $z = 0$ and making an angle θ_0 with the interface, Corresponding to this incident wave, we get waves in medium ($z > 0$) as reflected LD, CD I, CD II and LMS waves and refracted LD, CD I, CD II and LMS waves in medium ($z < 0$).

The non-vanishing potentials suitable for the problem are given by

$$\phi = A_0 \exp[ik_1(x \cos\theta_0 - z \sin\theta_0) + i\omega_1 t] + A_1 \exp[ik_1(x \cos\theta_1 + z \sin\theta_1) + i\omega_1 t], \tag{15}$$

$$\psi = A_0 \exp[i\delta_1(x \cos\theta_0 - z \sin\theta_0) + i\omega_2 t] + A_2 \exp[i\delta_1(x \cos\theta_2 + z \sin\theta_2) + i\omega_2 t], + A_3 \exp[i\delta_2(x \cos\theta_3 + z \sin\theta_3) + i\omega_3 t], \tag{16}$$

$$\phi_2 = EA_0 \exp[i\delta_1(x \cos\theta_0 - z \sin\theta_0) + i\omega_2 t] + EA_2 \exp[i\delta_1(x \cos\theta_2 + z \sin\theta_2) + i\omega_2 t] + FA_3 \exp[i\delta_2(x \cos\theta_3 + z \sin\theta_3) + i\omega_3 t] \tag{17}$$

$$\Phi^* = GA_0 \exp[ik_4(x \cos\theta_0 - z \sin\theta_0) + i\omega_4 t] + GA_4 \exp[ik_4(x \cos\theta_4 + z \sin\theta_4) + i\omega_4 t], \tag{18}$$

$$\phi' = A_1' \exp[ik_1'(x \cos\theta_1' - z \sin\theta_1') + i\omega_1' t] \tag{19}$$

$$\psi' = A_2' \exp[i\delta_1'(x \cos\theta_2' - z \sin\theta_2') + i\omega_2' t] + A_3' \exp[i\delta_2'(x \cos\theta_3' - z \sin\theta_3') + i\omega_3' t], \tag{20}$$

$$\phi_2' = E'A_2' \exp[i\delta_1'(x \cos\theta_2' - z \sin\theta_2') + i\omega_2' t]$$

$$+F'A_3' \exp[i\delta_2'(x \cos\theta_3' - z \sin\theta_3') + i\omega_3' t], \tag{21}$$

$$\Phi^* = G'A_4' \exp[ik_4'(x \cos\theta_4' - z \sin\theta_4') + i\omega_4' t] \tag{22}$$

where

$$E = \delta_1^2\left(\delta_1^2 - \frac{\omega^2}{c_2^2 + c_3^2} - pq\right) / p\left(2q - \frac{\omega^2}{c_4^2}\right)$$

$$F = \delta_2^2\left(\delta_2^2 - \frac{\omega^2}{c_2^2 + c_3^2} - pq\right) / p\left(2q - \frac{\omega^2}{c_4^2}\right) \tag{23}$$

where

$$p = \mu/(\mu + k),\ q = \kappa/\gamma,\ \delta_1^2 = \lambda_1^2\omega^2,\ \delta_2^2 = \lambda_2^2\omega^2,\ \lambda_{1,2}^2 = [B \pm (B^2 - 4AC)^{1/2}]/2,$$

$$B = \frac{q(p-2)}{\omega^2} + \frac{1}{(c_2^2 + c_3^2)} + \frac{1}{c_4^2}, \qquad C = \frac{1}{(c_2^2 + c_3^2)}\left(\frac{1}{c_4^2} - \frac{2q}{\omega^2}\right). \tag{24}$$

and G is the constant of dimension L^{-2}. Similar expressions with primes correspond to medium ($z<0$). A_0, A_1, A_2, A_3, A_4, A_1', A_2', A_3' and A_4' are the amplitudes of incident, reflected and refracted waves. For incident LD wave, $A_0=0$ in equations (16) to (18); for incident CD I wave, $A_o = 0$ in equations (15) and (18) whereas for incident LMS wave, $A_o = 0$ in equations (15) to (17).

The extension of Snell's law will be

$$V^{*-1} \cos\theta = V_1^{-1} \cos\theta_1 = \lambda_1 \cos\theta_2 = \lambda_2 \cos\theta_3 = V^{-1} \cos\theta_4$$

$$= V_1'^{-1} \cos\theta_1 = \lambda_1' \cos\theta_2 = \lambda_2' \cos\theta_3 = V^{-1} \cos\theta_4 \tag{25}$$

and

$$\omega_1=\omega_2=\omega_3=\omega_4=\omega_1'=\omega_2'=\omega_3'=\omega_4'=\omega(\text{say}) \tag{26}$$

where $V^* = V_1$, V_3 or V, for incident LD, CD 1 or LMS wave respectively.

Making use of the potentials given by equations (15) to (22) in the boundary conditions (14), after using the equations (1) to (3), (12) and (13), we obtain a system of eight nonhomogeneous equations as

$$\sum_{j=1}^{8} a_{ij} Z_j = b_i, \qquad (i=1,2,\ldots\ldots,8) \tag{27}$$

where Z_j are the amplitude ratios for reflected and refracted LD, CD I, CD II and LMS waves, a_{ij} are the coefficients of amplitude ratios and the relation between b_i and a_{ij} are given as follows

(a) for an incident LD wave

$$b_1 = -a_{11},\ b_2 = a_{21},\ b_3 = -a_{31},\ b_4 = a_{41},\ b_5 = -a_{51},$$

$$b_6 = a_{61},\ b_7 = -a_{71},\ b_8 = a_{81}.$$

(b) for an incident CD I wave

$$b_1 = a_{12},\ b_2 = -a_{22},\ b_3 = a_{32},\ b_4 = -a_{42},\ b_5 = a_{52},$$

$$b_6 = -a_{62},\ b_7 = a_{72},\ b_8 = -a_{82}$$

(c) for an incident LMS wave

$$b_1 = -a_{14},\ b_2 = a_{24},\ b_3 = -a_{34},\ b_4 = a_{44},\ b_5 = -a_{54},$$

$$b_6 = a_{64},\ b_7 = -a_{74},\ b_8 = a_{84}$$

If we neglect the stretch effect, we can obtain corresponding results for micropolar/micropolar interface as shown by Tomar and Gogna[10,11]

Numerical Analysis

Here, we shall confine our study for the case of incident LMS wave only. Following Gauthier[15], we take the following values of relevant parameters for micropolar elastic solid with stretch (medium $z>0$) as

$\rho = 2.19$ g/cm^3, $\lambda = 7.59 \times 10^{11}$ dyne/cm^2,

$\mu = 1.89 \times 10^{11}$ dyne/cm^2,

$\gamma = 0.0268 \times 10^{11}$ dyne, $j = 0.0196$ cm^2, $\kappa = 0.0149 \times 10^{11}$ dyne/cm^2,

$\alpha_o = 0.0915$ dyne, $\beta_o = 0.0726$ dyne,

$\eta_o = 0.0532$ dyne, $G = 0.05$ cm^{-2}.

and, for medium ($z < 0$), we consider

$\rho' = 2.06$ g/cm^3, $\lambda' = 6.8 \times 10^{11}$ dyne/cm^2,

$\mu' = 1.62 \times 10^{11}$ dyne/cm^2,

$\gamma' = 0.0254 \times 10^{11}$ dyne, $j' = 0.0187$ cm^2,

$\kappa' = 0.0134 \times 10^{11}$ dyne/cm^2,

$\alpha_o' = 0.0911$ dyne, $\beta_o' = 0.0717$ dyne,

$\eta_o' = 0.0528$ dyne, $G' = 0.045$ cm^{-2}.

For the above values of relevant physical constants, the system of equations (27) is solved for amplitude ratios by using Gauss-elimination method for different angle of emergence varying from 0° to 90° when $\omega^2/\omega_o^2 = 10$. The variations of these amplitude ratios with the angle of emergence of incident LMS wave are shown in Fig. (1 and 2).

In Fig. 1, the variation of the amplitude ratios for reflected LD-wave, coupled waves (CD I and CD II) and LMS wave are shown by lines S,D(1), D(2) and D(3) respectively, whereas the lines S, D(1), D(2) and D(3) in Fig. 2. show the variation of the amplitude ratios for refracted LD-wave, coupled waves (CD I, CD II) and LMS wave respectively.

The variation of the amplitude ratios for reflected and refracted LD waves are observed oscillatory in nature. The variation of the amplitude ratios for reflected coupled waves and refracted coupled waves are observed similar. They first increase to their respective maxima and then decrease. The amplitude ratio for reflected LMS wave, first decreases to its minima near $\theta_o = 89°$ and then increases sharply to its maximum value. The amplitude ratio for refracted LMS wave, first increases to its maxima near $\theta_o = 89°$ and then decreases sharply to its minimum value zero. The amplitude ratio for reflected and refracted LMS waves are shown in Fig. (1 and 2) by D(3) after multiplying their original values by 10^{-4}.

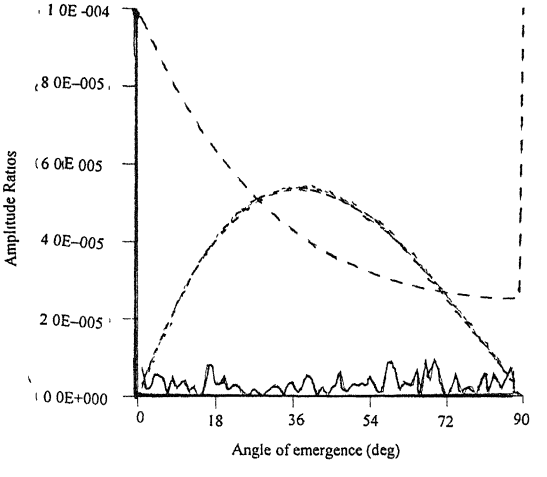

Fig. 1–Variation of amplitude ratios for reflected waves with the angle of emergence of incident LMS wave.

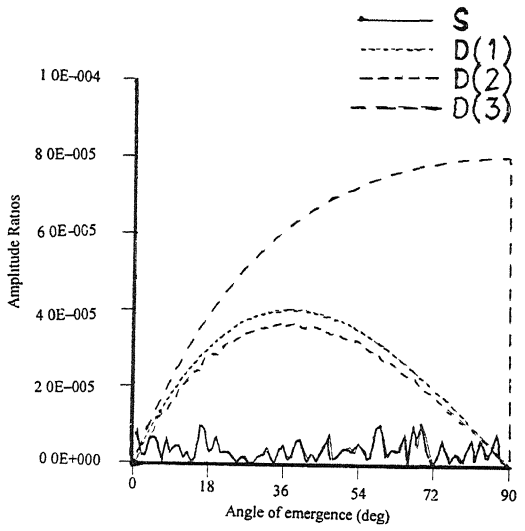

Fig. 2–Variation of amplitude ratios for refracted waves with the angle of emergence of incident LMS wave

Conclusions

The basic equations of motion for a micropolar elastic solid with stretch are solved. It is found that there exists a new wave, which we call longitudinal microstretch wave (LMS wave) in addition to waves shown by Parfitt and Eringen[5]. Theoretical calculations are presented for the cases of LD, CD I and LMS waves, incident at the interface between two dissimilar micropolar elastic solids with stretch. Numerical results are presented graphically for incident LMS wave only. If we neglect the stretch effect, the new wave (i.e LMS wave) will not exist. The problem though theoretical but is of physical interest in the fields of seismology, geophysics, earthquake engineering, etc.

References

1. Eringen, A. C. & Suhubi, E. S. (1964) *Int J Engng Sci* **2** : 189,389
2. Eringen, A. C. (1966) *J. Math. Mech.*, **15** : 909.
3. Eringen, A. C. (1971) *Ari. Kitabevi Matabaasi*, **24** : 1.
4. Ariman, T. (1972).*J. Math. Mech* , **13** : 11.
5. Parfitt, V. R. & Eringen, A. C. (1969) *J. Acoust Soc. Am.* **45** . 1258.
6. Kumar, R. & Gogna, M. L. (1988) *Proc. Ind Acad Sci (Math. Sci)* **88** : 89.

7. Kumar, R & Gogna, M. L (1992) *Int J Engng Sci*, **30** : 811.
8. Kumar, R. & Singh, B. (1996) *Proc Indian Acad Sci (Math. Sci)* **106** : 183
9. Kumar, R & Singh, B. (1998) *Ind J Pure Appl Math.*, **29** . 657.
10. Tomar, S. K. & Gogna, M L. (1992) *Int J Engng Sci* **30** · 1637.
11. Tomar, S K. & Gogna, M L. (1995) *Int J Engng Sc* **33** . 485.
12. Singh, B. & Kumar, R (1998) *Int. J. Engng Sc* **36** : 865.
13. Singh, B. & Kumar, R. (1998) *Int. J. Engng Sc.* **36** : 891.
14. Singh, B. (2002) *Proc Earth and Planet Sci, J. A. Sc* **111** : 29.
15. Gauthier, R D. (1982) *Experimental Investigations on Micropolar Media, Mechanics of micropolar media,* ed: O. Brulin , and R K. T. Hsieh, World Scientific Singapore, 395.

PROC. NAT. ACAD. SCI. INDIA, 74 (A), II, 2004

MHD free convection and mass transfer flow of a viscous fluid past a vertical plate

ATUL KUMAR SINGH* and N. P. SINGH

**Department of Mathematics, V. S. S. D. College, Kanpur -208 002, India.*

Department of Mathematics, C. L Jain (P.G.) College, Firozabad - 283203, India.

Received August 16, 2001, Revised February 20, 2002, Accepted July 15, 2003

Abstract

The present paper deals with the study of hydromagnetic free convection and mass transfer flow of an incompressible, electrically conducting, viscous fluid past an infinite vertical porous plate embedded in porous medium of time dependent permeability under oscillatory suction velocity normal to the plate. It is considered that the uniform magnetic field is applied normal to the flow and the permeability of the medium fluctuates with time. The velocity distribution, temperature distribution, concentration distribution, fluctuating parts of the velocity, amplitude and phase lead of skin-friction, rate of heat and mass transfer have also been obtained The behaviour of important parameters on the results obtained are discussed with the help of graphs and tables.

(**Keywords** . free convection/mass transfer/porous medium/variable permeability).

Introduction

The phenomenon of free convection arises in the flow of fluid when temperature changes due to density variations leading to buoyancy forces acting on the fluid elements. Such flows have been the object of extensive research due to their enhanced concern in science and technology about buoyancy induced motions in the atmosphere, in bodies of water and quasi-solid bodies such as earth. Unsteady oscillatory free convective flows play an important role in chemical engineering, turbomachinery and aerospace technology. In addition, many transport process exists where the transfer of heat and mass takes place simultaneously as a result of combined buoyancy effects of thermal diffusion and diffusion of chemical species.

Several authors[1-6] have studied free convection and mass transfer flow of a viscous fluid through porous medium assuming the permeability of the porous medium to be constant. However, the porosity of the medium may not necessarily be constant because the porous material containing the fluid is a non-homogeneous

medium. In the light of this fact, several authors[7-11] have investigated the effects of permeability variation.

To the knowledge of authors, the effects of time dependent permeability variation along with time dependent suction velocity in unsteady flow have not been discussed, though these effects show their significant role in chemical engineering, turbomachinery and aerospace technology. Therefore, the aim of the present investigation is to study the effects of permeability variation and oscillatory suction velocity on free convection and mass transfer flow of a viscous fluid past an infinite vertical porous plate. The permeability of the porous medium is considered as $K(t') = K_0(1+\varepsilon e^{int'})$ and the suction velocity is assumed as $v(t') = -v_0(1+\varepsilon e^{int'})$ where $v_0 > 0$ and $\varepsilon << 1$ is a positive constant.

Mathematical Analysis

We consider unsteady free convection and mass transfer flow of an incompressible, electrically conducting, viscous fluid past an infinite vertical porous plate in a porous medium. In cartesian coordinate system, x'-axis is taken along the plate in the direction of the flow and y'-axis normal to it. A uniform magnetic field is introduced normal to the direction of flow. In the analysis, we assume that the magnetic Reynold's number is much less then unity so that the induced magnetic field is neglected in comparison to the applied magnetic field. Further, all the fluid properties are assumed constant except that of the influence of density variation with temperature. Therefore the basic flow in the medium is entirely due to buoyancy force caused by temperature difference between the wall and the medium. Initially at $t' \le 0$, the plate as well as fluid are assumed to be at same temperature and the concentration of species is very low. When $t' > 0$, the temperature of the plate is instantaneously raised to T_w' and the concentration of species is raised to C_w'. By use of the Boussineseq's approximation, the governing equations in dimensionless form are as follows.

Momentum equation :

$$\frac{1}{4}\frac{\partial u}{\partial t} - \left(1+\varepsilon e^{imt}\right)\frac{\partial u}{\partial y} = G_r T + G_m C + \frac{\partial^2 u}{\partial y^2} - \frac{u}{k_0\left(1+\varepsilon e^{imt}\right)} - M^2 u \qquad (1)$$

Energy equation :

$$\frac{1}{4}\frac{\partial T}{\partial t}-\left(1+\varepsilon e^{int}\right)\frac{\partial T}{\partial y}=\frac{1}{P_r}\frac{\partial^2 T}{\partial y^2} \tag{2}$$

Concentration equation :

$$\frac{1}{4}\frac{\partial C}{\partial t}-\left(1+\varepsilon e^{int}\right)\frac{\partial C}{\partial y}=\frac{1}{S_c}\frac{\partial^2 C}{\partial y^2} \tag{3}$$

where the symbols have their usual meaning as defined a Acharya *et al.*[11]

The non-dimensional quantities introduced in the above equations are defined as :

$$y=\frac{v_0 y'}{\partial},\quad t=\frac{v_0^2 t'}{4\partial},\quad n=\frac{4\partial n'}{v_0^2},\quad u=\frac{u'}{v_0},\quad T=\frac{T'-T_\infty}{T_w-T_\infty},\text{ and }\quad C=\frac{C'-C_\infty}{C_w-C_\infty},$$

$$G_r=\frac{\partial g\beta^{+}(T_w-T_\infty)}{v_0^3},\text{(Grashof number)}\quad S_c=\frac{\partial}{D},\text{(Schmidt number),}$$

$$P_r=\frac{\mu C_p}{K_T},\text{(parandtl number),}\quad M=\frac{B_0}{v_0}\sqrt{\frac{\sigma\partial}{\rho}}\text{(Magnetic parameter)}$$

and $$G_m=\frac{\partial g\beta(C_w-C_\infty)}{v_0^3},\text{(Modified Grashof number)}$$

The relevant boundary conditions in dimensionless form are :

$$u=0,\quad T=1+\varepsilon e^{int},\quad C=1+\varepsilon e^{int},\qquad \text{at } y=0$$

$$u\to 0,\quad T\to 0,\quad C\to 0,\qquad \text{at } y=\infty$$

In order to solve the system of equations (1), (2) and (3) under the boundary conditions (4) we assume

$$u(y,t)=u_0(y)+\varepsilon u_1(y)e^{int}$$

$$T(y,t)=T_0(y)+\varepsilon T_1(y)e^{int}$$

and $$C(y,t)=C_0(y)+\varepsilon C_1(y)e^{int} \tag{5}$$

Substitution (5) into the equations (1) to (3) and equating the harmonic and non-harmonic terms, we get :

$$u_0^{\#}+u_0'-a_1u_0=-G_rT_0-G_mC_0 \tag{6}$$

$$u_1^{\#}+u_1'-a_2u_1=-G_rT_1-G_mC_1-u_0'-\frac{1}{K_0}u_0 \tag{7}$$

$$T_0^{\#}+P_rT_0'=0 \tag{8}$$

$$T_1^{\#}+P_rT_1'-\frac{in}{4}P_rT_1=-P_rT_0' \tag{9}$$

$$C_0^{\#}+S_cC_0'=0 \tag{10}$$

$$C_1^{\#}+C_cC_1'-\frac{in}{4}S_cC_1=-S_cC_0' \tag{11}$$

where the primes denote differentiation with respect to y.

The boundary conditions (4) reduce to :

$$u_0=u_1=0,\quad T_0=T_1=1,\quad C_0=C_1=1,\qquad \text{at } y=0$$

$$u_0=u_1\to 0,\quad T_0=T_1\to 0,\quad C_0=C_1\to 0,\qquad \text{as } y=\infty \tag{12}$$

Substituting the solutions of equations (6)-(11) under the boundary conditions (12), we obtain :

$$T(y,t) = e^{-P_r y} + \in \left[\left(1 - i\frac{4p_r}{n} \right) e^{-m_1 y} + i\frac{4p_r}{n} e^{-p_r y} \right] e^{int} \tag{13}$$

$$C(y,t) = e^{-S_c y} + \in \left[\left(1 - i\frac{4S_c}{n} \right) e^{-m_2 y} + i\frac{4S_c}{n} e^{-S_c y} \right] e^{int} \tag{14}$$

$$u(y,t) = (a_3 + a_4) e^{-m_3 y} - a_3 e^{-P_r y} - a_4 e^{-S_c y}$$

$$+ \in \left[a_{15} e^{-m_4 y} - a_{10} e^{-m_1 y} - a_{11} e^{-m_2 y} + a_{12} e^{-m_3 y} + a_{13} e^{-P_r y} + a_{14} e^{-S_c y} \right] e^{int} \tag{15}$$

With convention that the real parts of complex quantities have physical significance in the problem, the velocity, temperature and concentration field can be expressed in fluctuating parts as :

$$u(y,t) = u_0(y) + \in (M_r \cos nt - M_i \sin nt) \tag{16}$$

$$T(y,t) = T_0(y) + \in (K_r \cos nt - K_i \sin nt) \tag{17}$$

$$C(y,t) = C_0(y) + \in (L_r \cos nt - L_i \sin nt) \tag{18}$$

where

$$M_r = (N_{11} \cos B_3 y + N_{12} \sin B_3 y) e^{-A_3 y} - (N_1 \cos B_1 y + N_2 \sin B_1 y) e^{-A_1 y}$$

$$+ (N_3 \cos B_2 y + N_4 \sin B_3 y) e^{-A_3 y} + N_5 e^{-m_3 y} + N_7 e^{-P_r y} + N_9 e^{-S_c y}$$

$$M_i = (N_{12} \cos B_3 y + N_{11} \sin B_3 y) e^{-A_3 y} - (N_2 \cos B_1 y + N_1 \sin B_1 y) e^{-A_1 v}$$

$$+ (N_4 \cos B_2 y + N_3 \sin B_2 y) e^{-A_2 y} + N_6 e^{-m_3 y} + N_8 e^{-P_r y} + N_{10} e^{-S_c y}$$

$$K_r = \left(\cos B_1 y - \frac{4P_r}{n} \sin B_1 y \right) e^{-A_1 y}$$

$$K_r = \left(\sin B_1 y - \frac{4P_r}{n}\cos B_1 y\right)e^{-A_1 y} + \frac{4P_r}{n}e^{-P_r y}$$

$$L_r = \left(\cos B_2 y - \frac{4S_c}{n}\sin B_2 y\right)e^{-A_2 y}$$

$$L_i = \left(\sin B_2 y - \frac{4S_c}{n}\cos B_2 y\right)e^{-A_2 y} + \frac{4S_c}{n}e^{-S_c y}$$

Hence expression for transient velocity, temperature and concentration field for $nt = \frac{\pi}{2}$ are :

$$u\left(y, \frac{\pi}{2n}\right) = u_0(y) - \epsilon M_i \tag{19}$$

$$T\left(y, \frac{\pi}{2n}\right) = T_0(y) - \epsilon K_i \tag{20}$$

$$C\left(y, \frac{\pi}{2n}\right) = C_0(y) - \epsilon L_i \tag{21}$$

Skin-Friction, Rate of Heat and Mass Transfer

Skin-friction coefficient (ι) at the plate, in terms of amplitude and phase, is

$$\tau = \left(\frac{\partial u}{\partial y}\right)_{y=0} = \iota_0 + \epsilon |N| \cos(nt + \alpha) \tag{22}$$

Heat transfer coefficient (N_u) at the plate terms of amplitude and phase

$$N_u = -\left(\frac{\partial T}{\partial y}\right)_{y=0} = P_r + \epsilon |R| \cos(nt + \beta) \tag{23}$$

Mass transfer coefficient (S_h) at the plate in terms of amplitude and phase

$$S_h = -\left(\frac{\partial C}{\partial y}\right)_{y=0} = S_c + \epsilon |Q| \cos(nt + \gamma) \tag{24}$$

Discussion and Conclusions

In order to get physical insight into the problem, velocity field, temperature and concentration field, skin-friction coefficient, rate of heat transfer and rate of mass transfer have been discussed by assigning numerical values to various parameters encountered into the equations. To be realistic, the values of Prandtl number (P_r) are chosen to be $P_r = 11.4$ which represents water at 4°C, $P_r = 0.71$ and $P_r = 7.0$ which represent air and water at 20°C respectively. The values of Schmidt number S_c are taken for hydrogen ($S_c = 0.22$), oxygen ($S_c = 0.66$) and ammonia ($S_c = 0.78$). In these numerical calculations Grashof number for heat transfer $G_r = 5.0, 10.0, 20.0$, modified Grashof number for mass transfer $G_m = 5.0, 10.0, 15.0$, magnetic parameter $M = 0.5, 1.0$, permeability parameter $K_0 = 10.0, 20.0$ and frequency parameter $n = 5.0, 10.0, 15.0$ are chosen arbitrarily.

It is of immense important to mention here that the series solutions obtained for velocity u, temperature T and concentration C are expended in powers of ε.

Therefore to judge the convergence of these series solutions, a computer program was setup to calculate $\sqrt{M_r^2 + M_i^2}$, $\sqrt{K_r^2 + K_i^2}$, and $\sqrt{L_r^2 + L_i^2}$, under the conditions $\sqrt{M_r^2 + M_i^2} << u_0$ $\sqrt{K_r^2 + K_i^2} << T_0$ and $\sqrt{L_r^2 + L_i^2} << C_0$. In this manner it was observed that the solutions in series form are valid the above mentioned restriction.

Fig. 1 shows transient velocity field at $\varepsilon = 0.002$, $P_r = 0.71$ and $nt = \pi/2$. It represents the curves due to change in the numerical values of Grashof number for heat transfer G_r, modified Grashof number for mass transfer G_m, Schmidt number S_c, magnetic parameter M and permeability parameter K_0. Fig. 2 shows transient temperature and concentration fields at $\varepsilon = 0.002$ and $nt = \pi/2$. It represents the curves due to change in Prandtl number P_r and Schmidt number S_c respectively. The numerical values skin-friction coefficient (ι) in terms of amplitude $|N|$ and phase tan α are tabulated in Table 1 for variations in G_r, G_m, S_c, M, K_0 and n respectively. Table 2 represents the numerical values due to variations in the numerical values of P_r and frequency n on the rate of heat transfer in terms of amplitude $|R|$ and phase tan β.

Table 3 represents the numerical values due to variations in the numerical values of S_c and frequency n on the rate of mass transfer in terms of amplitude $|Q|$ and phase tan γ.

Table 1– Values of amplitude $|N|$ and phase tan α for skin-friction coefficient

G_r	G_m	S_c	M	K_o	n	$\|N\|$	tan α
5.00	5.00	0 22	0 5	10.0	5.00	30.00448	-0.25451
10 0	5 00	0 22	0 5	10.0	5 00	49 46438	-0.29118
5.00	10.0	0.22	0 5	10.0	5 00	41.16401	-0.21461
5.00	5 00	0 60	0.5	10.0	5 00	24.98689	-0.22516
5 00	5 00	0 22	1 0	10.0	5.00	01 66431	1 30813
5 00	5 00	0 22	0 5	20.0	5 00	47 36441	-0 27686
5 00	5 00	0 22	0 5	10 0	10.0	25 94993	-0.40371

Table 2 – Values of amplitude $|R|$ and phase tan β for rate of heat transfer.

S. No.	P_r	n	$\|R\|$	tan β
1	0 71	5.00	01 48214	0 29255
2	7.00	5 00	13 82601	0.00671
3	11 4	5 00	22.67623	0 00179
4	0.71	10.0	01.75014	0 46111
5	0.71	15 0	02.00082	0 55456

Table 3– Values of amplitude $|Q|$ and phase tan γ for rate of mass transfer

S. No.	S_r	n	$\|Q\|$	tan γ
1	0.22	5.00	0.64138	0 58794
2	0.66	5.00	1.42431	0.37536
3	0.78	5.00	2 04135	0 31725
4	0 22	10 0	0.85512	0 74467
5	0.22	15.0	1.02098	0.80761

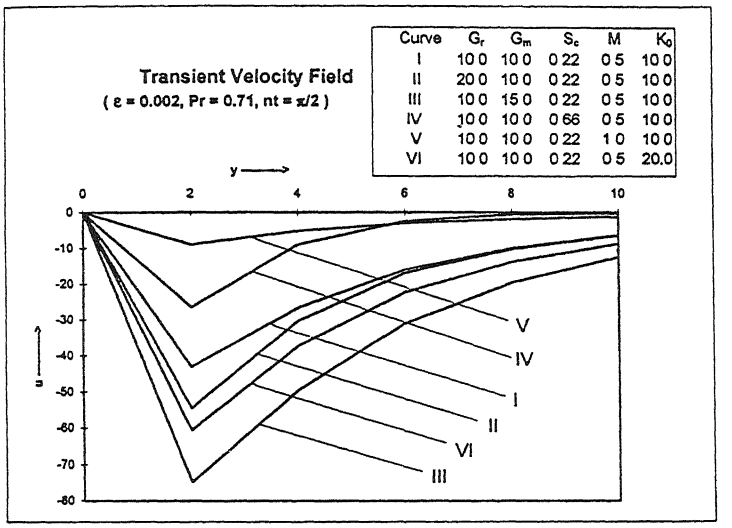

Fig. 1– Transient velocity field

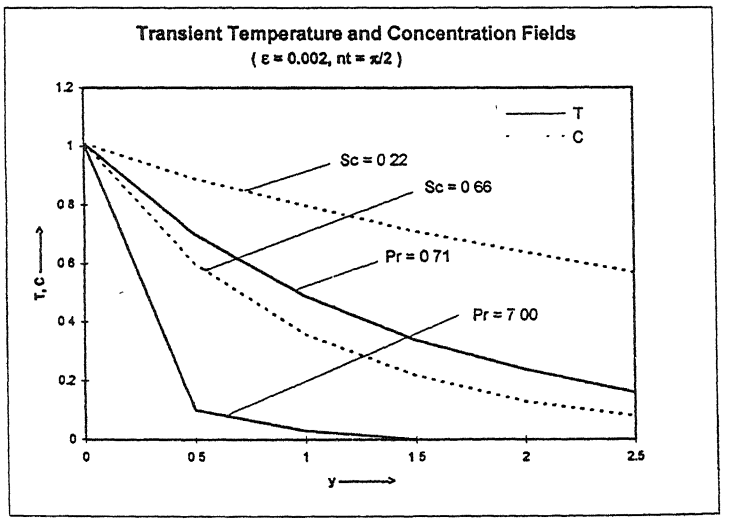

Fig. 2– Transient temperature and concentration fields.

The conclusions of the study are :

(i) An increase in G_r or G_m or K_0 decreases the transient velocity field.

(ii) An increase in S_c or M increases the transient velocity field.

(iii) Comparison of transient velocity distribution curves show that the curves rise gradually after attaining minimum value near the plate.

(iv) An increase in P_r decreases the transient temperature field indicating that transient temperature field falls more rapidly for water in comparison to air.

(v) An increase in S_c decreases the transient concentration field indicating that transient concentration field falls gradually for hydrogen in comparison to oxygen.

(vi) An increase in G_r or G_m or K_0 leads to an increase in the value of amplitude $|N|$ where as an increase in S_c or M or n leads to a decrease in the value of $|N|$.

(vii) There is always a phase lag in the case of skin-motion except for magnetic parameter M where phase lead is observed.

(viii) An increase in P_r or n leads to an increase in the value of amplitude $|R|$.

(ix) There is always a phase lead in the rate of heat transfer.

(x) An increase in S_c or n leads to an increase in the value of amplitude $|Q|$.

(xi) There is always a phase lead in the rate of mass transfer.

Acknowledgements

The authors thank the learned referee for valuable suggestions to improve the paper.

References

1. Agrawal, H. L., Ram, P C & Singh, V. (1983) *Astrophys Space Sci* **91** 445.
2. Singh, N P (1994) *Proc Math. Soc B H U* **10** : 59.
3. Soundalgekar, V. M. & Lahurikar, R. M. (1996) *Proc Math Soc B H U* **12** 99
4. Singh, N. P., Singh, Ajay Kumar & Kumar, R (1996) *Ind Jour Theo Phys* **44** 255
5. Singh, N. P. (1996) *Proc. Math Soc B H U* **12** . 109
6. Agrawal, A. K., Samria, N. K. & Gupta, S. N. (1998) *J. Energy Heat Mass Transfer* **20** · 35

7. Chandrasekhara, B. C , Namboodiri, P. M. S. & Hanumanthappa, A. R. (1984) *Warmi-und-stoffubertranung* **18** 17

8. Vedhanayagam, M., Jain, P. & Fairweather, G (1987) *Int Comm. Heat Mass Trans* **14** . 495

9. Singh, P., Mishra, I. K & Narayana, K. A. (1989) *Int J Numerical and Analytical Methods in Geomechanics* **13** 443.

10. Shreekanth, S., Venkataramana, S. & Ramakrishna, S (1996) *Acta Ciencia Indica* **XXII M** · 267.

11 Acharya, M., Dash, G C. & Singh, L. P (2000) *Ind J. Pure Appl Math* **31** : 1.

Appendix

$$m_1 = \frac{1}{2}\left[P_r + \sqrt{P_r^2 + \imath n P_r}\right] = A_1 + \imath B_1,$$

$$m_2 = \frac{1}{2}\left[S_c + \sqrt{S_c^2 + \imath n S_c}\right] = A_2 + \imath B_2 \ , \qquad 2m_3 = 1 + \sqrt{1 + 4a_1}\ ,$$

$$m_4 = \frac{1}{2}\left[1 + \sqrt{1 + 4a_2}\right] = A_3 + \imath B_3, \quad a_1 = M^2 + \frac{1}{K_0}, \quad a_2 = a_1 + \frac{\imath n}{4},$$

$$a_3 = \frac{G_r}{P_r^2 - P_r + a_1}, \quad a_4 = \frac{G_m}{S_c^2 - S_c + a_1}, \quad a_5 = G_r + \imath C_1,$$

$$a_6 = G_m + \imath C_2,\ a_7 = (a_3 + a_4)\left(m_3 - \frac{1}{K_0}\right), a_8 = a_3\left(\frac{1}{K_0} - P_r\right) + \imath C_1,$$

$$a_9 = a_4\left(\frac{1}{K_0} - S_c\right) + \imath C_2, \qquad a_{10} = N_1 + \imath N_2 = \frac{a_5}{m_1^2 - m_1 - a_2},$$

$$a_{11} = N_3 + \imath N_4 = \frac{a_6}{m_2^2 - m_2 - a_2}, \quad a_{12} = N_5 + \imath N_6 = \frac{a_7}{m_3^2 - m_3 - a_2},$$

$$a_{13} = N_7 + \imath N_8 = \frac{a_8}{P_r^2 - P_r - a_2}, \quad a_{14} = N_9 + \imath N_{10} = \frac{a_9}{S_c^2 - S_c - a_2},$$

$$a_{15} = N_{11} + \imath N_{12} = a_{10} + a_{11} - a_{12} - a_{13} - a_{14}, \qquad C_1 = -\frac{4P_r G_r}{n},$$

$$C_2 = -\frac{4S_c G_m}{n}, \quad C_3 = a_3\left(\frac{1}{K_0} - P_r\right), \quad C_4 = a_4\left(\frac{1}{K_0} - S_c\right),$$

$$N_1 = \frac{C_1 K_2 + G_r K_1}{K_1^2 + K_2^2}, \quad N_2 = \frac{C_1 K_1 - G_r K_2}{K_1^2 + K_2^2}, \quad N_3 = \frac{C_2 K_4 + G_m K_3}{K_3^2 + K_4^2},$$

$$N_4 = \frac{C_2 K_3 - G_m K_4}{K_3^2 + K_4^2}, \quad N_5 = \frac{16 a_7 K_5}{16K_5^2 + n^2}, \quad N_6 = \frac{4n a_7}{16K_5^2 + n^2},$$

$$N_7 = \frac{16C_3 K_6 - 4nC_1}{16K_6^2 + n^2}, \qquad N_8 = \frac{16C_1 K_6 + 4nC_3}{16K_6^2 + n^2},$$

$$N_9 = \frac{16C_4 K_7 - 4nC_2}{16K_7^2 + n^2}, \qquad N_{10} = \frac{16C_2 K_7 + 4nC_4}{16K_7^2 + n^2},$$

$$N_{11} = N_1 + N_3 - N_5 - N_7 - N_9, \quad N_{12} = N_2 + N_4 - N_6 - N_8 - N_{10},$$

$$K_1 = A_1^2 - B_1^2 - A_1 - a_1, \qquad K_2 = 2A_1B_1 - B_1 - \frac{n}{4},$$

$$K_3 = A_2^2 - B_2^2 - A_2 - a_1, \qquad K_4 = 2A_2B_2 - B_2 - \frac{n}{4},$$

$$K_5 = m_3^2 - m_3 - a_1, \quad K_6 = P_r^2 - P_r - a_1, \quad K_7 = S_c^2 - S_c - a_1,$$

$$A_1 = \frac{P_r}{2} + \frac{1}{2}\sqrt{\frac{P_r}{2}}\left[\sqrt{P_r^2 + n^2} + P_r\right]^{1/2},$$

$$A_2 = \frac{S_c}{2} + \frac{1}{2}\sqrt{\frac{S_c}{2}}\left[\sqrt{S_c^2 + n^2} + S_c\right]^{1/2},$$

$$A_3 = \frac{1}{2} + \frac{1}{2\sqrt{2}}\left[\sqrt{(1+4a_1)^2 + n^2} + (1+4a_1)\right]^{1/2},$$

$$B_1 = \frac{1}{2}\sqrt{\frac{P_r}{2}}\left[\sqrt{P_r^2 + n^2} - P_r\right]^{1/2}, \quad B_2 = \frac{1}{2}\sqrt{\frac{S_c}{2}}\left[\sqrt{S_c^2 + n^2} - S_c\right]^{1/2},$$

$$B_3 = \frac{1}{2\sqrt{2}}\left[\sqrt{(1+4a_1)^2 + n^2} - (1+4a_1)\right]^{1/2},$$

$$\tau_0 = a_3P_r + a_4S_c - m_3(a_3 + a_4),$$

$$N = N_r + iN_i = \left(\frac{du_1}{dy}\right)_{y=0}, \qquad \tan\alpha = \frac{N_i}{N_r},$$

$$R = R_r + iR_i = -\left(\frac{dT_1}{dy}\right)_{y=0}, \qquad \tan\beta = \frac{R_i}{R_r},$$

$$Q = Q_r + iQ_i = -\left(\frac{dC_1}{dy}\right)_{y=0}, \qquad \tan\gamma = \frac{Q_i}{Q_r},$$

$$N_r = A_1N_1 - B_1N_2 + A_2N_3 - B_2N_4 - (A_3N_{11} - B_3N_{12}) - m_3N_5 - P_rN_7 - S_cN_9$$

$$N_i = A_1N_2 + B_1N_1 + A_2N_4 + B_2N_3 - (A_3N_{12} + B_3N_{11}) - m_3N_6 - P_rN_8 - S_cN_{10}$$

$$R_r = A_1 + \frac{4P_rB_1}{n}, \qquad R_i = B_1 - \frac{4P_rA_1}{n} + \frac{4P_r^2}{n},$$

$$Q_r = A_2 + \frac{4S_cB_2}{n}, \qquad \text{and} \qquad Q_i = B_2 - \frac{4S_cA_2}{n} + \frac{4S_c^2}{n}.$$

PROC. NAT. ACAD. SCI. INDIA, 74 (A), II, 2004

Effects of time dependent suction on heat and mass transfer flow of a viscous fluid in rotating system

ATUL KUMAR SINGH* and N. P. SINGH

**Department of Mathematics, V. S. S. D. College, Kanpur-208002, India.*

Department of Mathematics, C. L. Jain (P.G) College, Firozabad-283203, India

Received March 14, 2002, Revised July 6, 2002, Re-Revised December 9, 2002, Accepted July 15, 2003

Abstract

In the present paper free convection and mass transfer flow of an incompressible, viscous liquid through a porous medium in a rotating system past an infinite vertical porous plate is studied In the analysis, the heat flux is considered constant and the suction velocity is assumed to be time dependent.Two different cases namely externally cooled plate ($G_r > 0$) and externally heated plate ($G_r < 0$) have been analysed The solutions for steady primary velocity, steady secondary velocity, time dependent primary velocity, time dependent secondary velocity, temperature distribution and concentration field have been obtained using perturbation technique The results obtained have been discussed

(**Keywords** · time dependent suction/mass transfer/rotating system/porous medium/heat flux)

Introduction

In recent years, free convection and mass transfer flow of viscous fluids through porous medium have attracted the attention of a number of authors in view of its application to geophysics, astrophysics, meteorology, physiology, aerodynamics, boundary layer control and so on. In addition, convective flow through porous medium have applications in the field of chemical engineering for filtration and purification processes; in the field of agriculture engineering to study the underground water resources; in petroleum industry to study the movement of natural gases oil and water through the oil channels / reservoirs; in metal industry to study the flow pattern of the melted solids at different temperatures. The development of aeronautical, chemical, mechanical and computer engineering during last few decades, on the one hand and finding oil wells in oceans on the other hand, have added stimuli to the study of viscous fluid flows.

Ahmadi and Manvi[1] derived the equations of motion for viscous flow through a rigid porous medium. Gersten and Gross[2] applied these equations to study the effects

of transverse sinusoidal suction velocity on flow and heat transfer along an infinite porous wall and Ram and Mishra[3] used them to study the unsteady flow of a viscous fluid through porous medium. Raptis[4] investigated the unsteady flow through a porous medium bounded by an infinite porous plate subject to a variable plate temperature and constant suction velocity. Raptis and Perdikis[5] further studied oscillatory flow of a viscous fluid through porous medium by the presence of free convective flow. Several authors[6-12] have studied free convection / mass transfer flow in rotating system under various boundary conditions. Recently, Singh *et al.*[13] have analysed MHD free convection and mass transfer in dusty flow of a rotating viscous liquid. More recently, Singh *et al.*[14] have studied free convection effect in the unsteady MHD flow of an incompressible viscous fluid in a rotating system past an isothermal vertical plate under constant suction velocity.

The present paper deals with free convection and mass transfer flow through a porous medium in a rotating system past an infinite vertical porous plate with time dependent suction and constant heat flux. The effects of various parameters for two different cases namely externally cooled plate ($G_r > 0$) and externally heated plate ($G_r < 0$) have been discussed with the help of graphs and tables.

Formulation of the Problem

We consider the unsteady flow of an incompressible, viscous liquid by the presence of free convection and mass transfer through a porous medium past an infinite vertical porous plate. A cartesian coordinate system (x, y, z) rotating uniformly with the liquid in a rigid state of rotation is considered and a constant angular velocity (0,0, Ω) is taken into account about z-axis. The vertical porous plate is considered in the plane and z-axis is chosen normal to the plate pointing towards the flow medium. Besides, in the analysis a time dependent section velocity $w = -w_0[1+\varepsilon e^{-nt}]$ has been taken into account normal to the plate (w_0 and n are positive constants).

Therefore, for the present configuration, the momentum equations, diffusion equation and energy equation governing the flow, in non-dimensional from (ignoring the stars introduced ahead), are :

$$\frac{\partial u}{\partial t} - 2Ev + \left(1 + \varepsilon e^{-nt}\right)\frac{\partial u}{\partial z} = G_r T + G_m C + \frac{\partial^2 u}{\partial z^2} - \frac{1}{k}u \qquad (1)$$

$$\frac{\partial v}{\partial t}+2Ev+\left(1+\varepsilon e^{-nt}\right)\frac{\partial v}{\partial z}=\frac{\partial^2 v}{\partial z^2}-\frac{1}{k}v \tag{2}$$

$$\frac{\partial C}{\partial t}-\left(1+\varepsilon e^{-nt}\right)\frac{\partial C}{\partial z}=\frac{1}{S_c}\frac{\partial^2 C}{\partial z^2} \tag{3}$$

and

$$-P_r\frac{\partial T}{\partial t}+\frac{\partial^2 T}{\partial z^2}+P_r\left(1+\varepsilon e^{-nt}\right)\frac{\partial T}{\partial z}=0 \tag{4}$$

The non-dimensional boundary conditions relevant to the present problem are :

$$t>0:\ W=0,\quad \frac{dT}{dz}=-L_1,\quad C=1+\varepsilon L_2 e^{-nt}\ \text{ at }\quad z=0$$

$$W=0,\quad T\to 0,\quad C\to 0,\quad \text{as}\quad z\to\infty, \tag{5}$$

where u and v are the velocities in x and y directions, T is the temperature of the fluid T_∞ is the temperature of the fluid far away from the plate, C is the concentration of species, C_∞ is the concentration of species far away from the plate, β^* is the volumetric coefficient of thermal expansion, β is the volumetric coefficient of thermal expansion with concentration, K' is the thermal conductivity, C_p is the specific heat at constant pressure, D is the chemical molecular diffusivity, k is the permeability of the medium, q is constant heat flux and the other symbols have their usual meaning.

The non dimensional quantities introduced in the above equations are defined as :

$$u^*=\frac{u}{w_0},\quad v^*=\frac{v}{w_0},\quad z^*=\frac{zw_0^2}{\upsilon},\quad \frac{\mu}{\rho}=\upsilon,\quad K^*=\frac{w_0^2K'}{\upsilon},$$

$$n^*=\frac{n\upsilon}{w_0^2},\quad k^*=\frac{\upsilon^2 k}{w_0^2},\quad t^*=\frac{tw_0^2}{\upsilon},\quad C^*=\frac{C-C_\infty}{C_w-C_\infty},$$

$$T^*=\frac{(T-T_\infty)K'}{q\upsilon},$$

where $G_r = \frac{\upsilon^2 q g \beta^*}{K' v_0^4}$, (Grashof Number), $S_c = \frac{\upsilon}{D}$, (Schmidt Number),

$E = \frac{\Omega \upsilon}{v_0^2}$, (Rotation Parameter), $P_r = \frac{\mu C_p}{K}$, (Prandtl Number)

$G_m = \frac{\upsilon g \beta (C_w - C_\infty)}{v_0^3}$, (Modified Grashof Number), $L_1 = \frac{T_w}{T_w - T_\infty}$,

and $L_2 = \frac{C_w}{C_w - C_\infty}$,

Assuming $W = u + iv$, the equations (1) and (2) transform to :

$$\frac{\partial W}{\partial t} + 2iEv - \left(1 + \varepsilon e^{-nt}\right)\frac{\partial W}{\partial z} = G_r T + G_m C + \frac{\partial^2 W}{\partial z^2} - \frac{1}{k} W \tag{6}$$

Solution of the Problem

To obtain the solution of (6), (3) and (4), we assume

$$W = W_1(z) + \varepsilon W_2(z) e^{-nt} + \ldots \ldots \ldots \ldots$$

$$T = T_1(z) + \varepsilon T_2(z) e^{-nt} + \ldots \ldots \ldots \ldots \tag{7}$$

$$C = C_1(z) + \varepsilon C_2(z) e^{-nt} + \ldots \ldots \ldots \ldots \ldots$$

Using (7) is equations (3), (4) and (6) and comparing the coefficients of harmonic and non-harmonic terms, we obtain six equations. The solution of these equations under the transformed boundary conditions yield :

$$C_1(z) = e^{-S_c z} \tag{8}$$

$$C_2(z) = \left(L_2 \frac{S_c}{n} \right) e^{-K_1 z} + \frac{S_c}{n} e^{-S_c z} \tag{9}$$

$$T_1(z) = \frac{L_1}{P_r} e^{-P_r z} \tag{10}$$

$$T_2(z) = \frac{L_1 P_r}{K_2} e^{-K_2 z} - L_1 e^{P_r z} \tag{11}$$

$$W_1(z) = K_5 \left(e^{-P_r z} - e^{-K_3 z} \right) + K_6 \left(e^{-K_3 z} - e^{-S_c z} \right) \tag{12}$$

$$W_2(z) = K_{12} e^{-K_1 z} + K_{13} e^{-K_2 z} + K_{14} e^{-K_3 z} + K_{15} e^{-P_r z} + K_{16} e^{-S_c z} + K_{17} e^{-K_4 z} \tag{13}$$

where $L_3 = \frac{1}{k} + 2iE$, $K_1 = \frac{S_c + \sqrt{S_c(S_c - 4n)}}{2}$, $K_2 = \frac{P_r + \sqrt{P_r(P_r - 4)}}{2}$,

$K_3 = A_1 + iB_1 = \frac{1 + \sqrt{1 - 4L_3}}{2}$, $K_4 = A_2 + iB_2 = \frac{1 + \sqrt{1 - 4(L_3 - n)}}{2}$,

$K_5 = A_3 + iB_3 = \frac{L_1 G_r}{P_r(P_r^2 - P_r - L_3)}$, $K_6 = A_4 + iB_4 = \frac{-G_m}{S_c^2 - S_c - L_3}$,

$K_7 = -G_m \left(L_2 - \frac{S_c}{n} \right)$, $K_8 = -\frac{L_1 G_r P_r}{K_2}$,

$K_9 = A_5 + iB_5 = -K_3(K_5 + K_6)$, $K_{10} = A_6 + iB_6 = L_1 G_r + K_5 P_r$,

$K_{11} = A_7 + iB_7 = S_c \left(\frac{G_m}{n} - K_6 \right)$, $K_{12} = A_8 + iB_8 = \frac{K_7}{K_1^2 - K_1 - (L_3 - n)}$

$$K_{13}= A_9+iB_9= \frac{K_8}{K_2^2 - K_2 - (L_3 - n)}$$

$$K_{14}= A_{10}+iB_{10}= \frac{K_9}{K_3^2 - K_3 - (L_3 - n)}$$

$$K_{15}= A_{11}+iB_{11}= \frac{K_{10}}{P_r^2 - P_r - (L_3 - n)}$$

$$K_{16}= A_{12}+iB_{12}= \frac{K_{11}}{S_c^2 - S_c - (L_3 - n)}$$

$$K_{17}= A_{13}+iB_{13}=-(K_{12}+ K_{13}+ K_{14}+ K_{15}+ K_{16})$$

$$A_1=\frac{1}{2}+\frac{1}{2\sqrt{2}}\left[\sqrt{(1+4\alpha_0)^2+64E^2}+(1+4\alpha_0)\right]^{\frac{1}{2}}$$

$$B_1=\frac{1}{2\sqrt{2}}\left[\sqrt{(1+4\alpha_0)^2+64E^2}-(1+4\alpha_0)\right]^{\frac{1}{2}}, \qquad \alpha_0=-\frac{1}{k},$$

$$A_2=\frac{1}{2}+\frac{1}{2\sqrt{2}}\left[\sqrt{(1-4n+4\alpha_0)^2+64E^2}+(1-4n+4\alpha_0)\right]^{\frac{1}{2}},$$

$$B_2=\frac{1}{2\sqrt{2}}\left[\sqrt{(1-4n+4\alpha_0)^2+64E^2}-(1-4n+4\alpha_0)\right]^{\frac{1}{2}},$$

$$A_3=\frac{L_1G_rM_1}{M_1^2+4E^2P_r^2}, \qquad B_3=\frac{2EL_1G_rP_r}{M_1^2+4E^2P_r^2}, \qquad A_4=\frac{-M_2G_m}{M_2^2+4E^2},$$

$$B_4=\frac{-2EG_m}{M_2^2+4E^2}, \qquad A_5=B_1(B_3+B_4)-A_1(A_3+A_4),$$

$B_5=-[A_1(B_3+B_4)-B_1(A_3+A_4)]$, $A_6=L_1G_r+A_3P_r$,

$B_6=B_3P_r$, $A_7=S_c\left(\frac{G_m}{n}-A_4\right)$, $B_7=-S_cB_4$,

$A_8=\frac{K_7M_3}{M_3^2+4E^2}$, $B_8=\frac{2EK_7}{M_3^2+4E^2}$, $A_9=\frac{K_8M_4}{M_4^2+4E^2}$,

$B_9=\frac{2EK_8}{M_4^2+4E^2}$, $A_{10}=\frac{A_5M_5+B_5M_6}{M_5^2+M_6^2}$, $B_{10}=\frac{B_5M_5-A_5M_6}{M_5^2+M_6^2}$,

$A_{11}=\frac{A_6M_7-2EB_6}{M_7^2+4E^2}$, $B_{11}=\frac{B_6M_7+2EA_6}{M_7^2+4E^2}$, $A_{12}=\frac{A_7M_8-2EB_7}{M_8^2+4E^2}$,

$B_{12}=\frac{B_7M_8+2EA_7}{M_8^2+4E^2}$, $A_{13}=-(A_8+A_9+A_{10}+A_{11}+A_{12})$,

$B_{13}=-(B_8+B_9+B_{10}+B_{11}+B_{12})$, $M_1=P_r(P_r^2-P_r+\alpha_0)$,

$M_2=S_c^2-S_c+\alpha_0$, $M_3=K_1^2-K_1+n+\alpha_0$, $M_4=K_2^2-K_2+n+\alpha_0$,

$M_5=A_1^2-B_1^2-A_1+n+\alpha_0$, $M_6=2A_1B_1-B_1-2E$,

$M_7=P_1^2-P_r+n+\alpha_0$, $M_8=S_c^2-S_c+n+\alpha_0$,

Substituting the values of $C_1(z)$, $C_2(z)$, $T_1(z)$, $T_2(z)$, $W_1(z)$, and $W_2(z)$, in (7), we obtain

$$C=e^{-S_cz}+\varepsilon\left[\left(L_2-\frac{S_c}{n}\right)e^{-k_1z}+\frac{S_c}{n}e^{-S_cz}\right]e^{-nt} \tag{14}$$

$$T=\frac{L_1}{P_r}e^{-P_rz}+\varepsilon\left[\frac{L_1P_r}{K_2}e^{-K_2z}-L_1e^{-P_rz}\right]e^{-nt} \tag{15}$$

and $$W = K_5\left(e^{-p_r z} - e^{-k_3 z}\right) + K_6\left(e^{-K_3 z} - e^{-S_c z}\right)$$

$$+\varepsilon\left[K_{12}e^{-K_1 z} + K_{13}e^{-K_2 z} + K_{14}e^{-K_3 z} + K_{15}e^{-P_r z} + K_{16}e^{-S_c z} + K_{17}e^{-K_4 z}\right] \quad (16)$$

Hence, primary velocity (u) is :

$$u(z,t) = u_1 + \varepsilon u_2 e^{-nt} = A_3\left(e^{-P_r z} - e^{-A_1 z}\cos B_1 z\right) + B_3 e^{-A_1 z}\sin B_1 z$$

$$+ A_4\left(e^{-A_r z}\cos B_1 z - e^{-S_c z}\right) - B_4 e^{-A_1 z}\sin B_1 z$$

$$+ \varepsilon e^{-nt}\left[A_8 e^{-K_1 z} + A_9 e^{-K_2 z} + A_{10}e^{-A_1 z}\cos B_1 z\right.$$

$$\left. A_{11}e^{-P_r z} + A_{12}e^{-S_c z} + A_{13}e^{-A_2 z}\cos B_2 z\right] \quad (17)$$

The secondary velocity (v) is :

$$v(y,t) = v_1 + \varepsilon v_2 e^{-nt} = B_3\left(e^{-P_r z} - e^{-A_1 z}\cos B_1 z\right) + A_3 e^{-A_1 z}\sin B_1 z$$

$$+ B_4\left(e^{-A_1 z}\cos B_1 z - e^{-S_c z}\right) - A_4 e^{-A_1 z}\sin B_1 z$$

$$+ \varepsilon e^{-nt}\left[B_8 e^{-K_1 z} + B_9 e^{-K_2 z} + B_{10}e^{-A_1 z}\sin B_1 z\right.$$

$$\left. B_{11}e^{-P_r z} + B_{12}e^{-S_c z} + A_{13}e^{-A_2 z}\cos B_2 z\right] \quad (18)$$

Skin-Friction, Heat and Mass Transfer

The skin-friction coefficient of the fluid (τ_f) at the plate

$$\tau_f = \left(\frac{\partial W}{\partial z}\right)_{z=0}$$

$$= K_5(K_3 - P_r) + K_6(S_c - K_3) - \varepsilon(K_1K_{12} + K_2K_{13} + K_3K_{14}$$

$$+ P_rK_{15} + S_cK_{16} + K_4K_{17})e^{-nt} \qquad (19)$$

Hence, skin-friction (τ_p) due to primary velocity is :

$$\tau_p = A_3(A_1 - P_r) - B_3B_1 + A_4(S_c - A_1) + B_4B_1$$

$$-\varepsilon e^{-nt}[K_1A_8 + K_2A_9 + A_1A_{10} - B_1B_{10}$$

$$+ P_rA_{11} + S_cA_{12} + A_2A_{13} - B_2B_{13}] \qquad (20)$$

Hence, skin-friction (τ_s) due to primary velocity is :

$$\tau_s = B_3(A_1 - P_r) - A_3B_1 + B_4(S_c - A_1) - A_4B_1$$

$$-\varepsilon e^{-nt}[K_1B_8 + K_2B_9 + A_1B_{10} - B_1A_{10}$$

$$+ P_rB_{11} + S_cB_{12} + B_2A_{13} + A_2B_{13}] \qquad (21)$$

The rate of heat transfer *i.e.* the heat transfer coefficient in terms of Nusselt number (N_u) at the plate is

$$N_u = \left(\frac{\partial T}{\partial z}\right)_{z=0} = -L_1 \qquad (22)$$

which satisfies the boundary condition.

The rate of mass transfer i.e. the mass transfer coefficient in terms of Sherwood number S_h is :

$$S_h = \left(\frac{\partial C}{\partial z}\right)_{z=0} \tag{23}$$

$$= -S_c - \varepsilon\left[K_1\left(L_2 - \frac{S_c}{n}\right) + \frac{S_c^2}{n}\right] \tag{24}$$

Table 1– Rate of mass transfer; (ε = 0 002, L_2 = 1.0 and n = 0.05)

t	S_c = 0.22	S_c = 0.30	S_c = 0.60	S_c = 0 66	S_c = 0 78
1 0	- 0.22092	-0 30117	- 0 60229	- 0 66252	- 0 78298
2 0	- 0.22087	- 0.30112	- 0 60218	- 0 66240	- 0.78283
3.0	- 0.22083	- 0.30106	- 0 60208	- 0 66228	- 0 78269
4.0	- 0.22079	- 0 30101	- 0 60197	-0 66217	- 0.78256
5.0	- 0 22075	- 0.30096	- 0.60188	- 0.66206	- 0 78244

Table 2- Skin friction due to primary velocity; (Cooling case at ε = 0 002)

k	E	n	P_r	S_c	G_r	G_m	t	τ_p
10.0	1.0	0 10	0.71	0.66	10.0	8.00	1 0	- 33 2582
20.0	1.0	0.10	0.71	0.66	10.0	8.00	1.0	- 32 1045
10.0	2.0	0 10	0.71	0.66	10.0	8.00	1 0	- 32.4167
10.0	1 0	0.05	0.71	0.66	10 0	8 00	1.0	- 33 3728
10.0	1.0	0 10	7.00	0.66	10.0	8.00	1 0	- 12 2919
10 0	1.0	0.10	0.71	0.78	10.0	8.00	1 0	- 33 0048
10.0	1.0	0.10	0.71	0.66	15.0	8.00	1 0	- 43 8016
10.0	1 0	0.10	0 71	0.66	10.0	12 0	1.0	- 39.3439
10.0	1.0	0.10	0.71	0 66	10.0	8 00	2.0	- 33 2494

Table 3– Skin friction due to secondary velocity, (Cooling case at ε = 0 002)

k	E	n	P_r	S_c	G_r	G_m	t	τ_s
10 0	1 0	0.10	0.71	0 66	10 0	8 00	1 0	5 7471
20.0	1.0	0.10	0.71	0.66	10 0	8 00	1 0	6 8939
10 0	2.0	0.10	0 71	0.66	10 0	8 00	1 0	8 4749
10 0	1 0	0 05	0.71	0.66	10 0	8 00	1 0	6 3176
10 0	1 0	0 10	7.00	0 66	10 0	8.00	1 0	9 7743
10 0	1.0	0.10	0 71	0 78	10 0	8 00	1 0	6 4867
10 0	1 0	0 10	0 71	0 66	15.0	8 00	1 0	3 7729
10.0	1.0	0.10	0.71	0 66	10 0	12 0	1 0	10.5947
10.0	1.0	0.10	0 71	0.66	10 0	8 00	2 0	5 7387

Table 4– Skin friction due to primary velocity; (Heating case at ε = 0 002)

k	E	n	P_r	S_c	G_r	G_m	t	τ_p
10.0	1.0	0.10	0.71	0 66	-10.0	-8 00	1 0	33 2582
20.0	1.0	0 10	0 71	0 66	-10 0	-8 00	1 0	32 1045
10.0	2.0	0 10	0 71	0 66	-10 0	-8 00	1 0	32 4167
10.0	1.0	0 05	0 71	0.66	-10.0	-8 00	1 0	33 3728
10.0	1.0	0.10	7.00	0.66	-10 0	-8 00	1 0	12.2919
10.0	1.0	0 10	0 71	0 78	-10 0	-8.00	1 0	33.0048
10.0	1.0	0.10	0.71	0 66	-15.0	-8.00	1.0	43.8016
10.0	1.0	0 10	0 71	0.66	-10 0	-12.0	1.0	39.3439
10.0	1.0	0.10	0.71	0 66	-10.0	-8.00	2.0	33.2494

Table 5– Skin friction due to secondary velocity, (Heating case at ε = 0 002)

k	E	n	P_r	S_c	G_r	G_m	t	τ_s
10 0	1 0	0 10	0 71	0 66	-10 0	-8 00	1 0	- 5 7471
20 0	1 0	0 10	0 71	0 66	-10 0	-8 00	1 0	- 6 8939
10 0	2 0	0 10	0 71	0 66	-10 0	-8 00	1 0	- 8 4749
10 0	1 0	0 05	0 71	0 66	-10 0	-8.00	1.0	-6 3176
10 0	1 0	0.10	7 00	0 66	-10 0	-8 00	1 0	- 9 7743
10 0	1 0	0 10	0 71	0.78	-10 0	-8 00	1.0	- 6 4867
10 0	1 0	0 10	0 71	0 66	-15.0	-8.00	1 0	- 3 7729
10 0	1 0	0 10	0 71	0 66	-10 0	-12 0	1 0	- 10.5947
10 0	1 0	0 10	0 71	0 66	-10 0	-8 00	2 0	- 5 7387

Discussion and Conclusions

In order to get physical insight into the problem, the effects of permeability parameter (k), rotation parameter (E), Schmidt number (S_c), Grashof number (G_r) and modified Grashof number (G_m) on primary velocity field and secondary velocity field in case of externally cooled plate (G_r>0) and externally heated plate (G_r<0) are studied taking numerical values of various parameters. To study the effect of Schmidt number (S_c) on primary and secondary velocities, the values of Schmidt number (S_c) are chosen for Oxygen (S_c = 0.66) and Ammonia (S_c = 0.78). The value of Prandtl number (P_r) is chosen as P_r = 0.71 which corresponds to air at 20°C and one atmospheric pressure. For concentration of species and mass transfer the values of Schmidt number (Sc) are chosen for Hydrogen (S_c = 0.22). Helium (S_c=0.30), Water-vapour (S_c := 0.60), Oxygen (Sc = 0.66) and Ammonia (S_c := 0.78). The numerical values of the remaining parameters are chosen arbitrarily.

Fig. 1 shows primary velocity profiles (u) for heating case (G_r < 0) and cooling case (G_r > 0) at P_r = 0.71 to observe the effects of permeability parameter (k), rotation parameter (E), Schmidt number (S_c), Grashof number (G_r) and modified Grashof number (G_m). It is observed that in case of externally heated plate the primary velocity (u) increases rapidly near the plate and after attaining a maximum value, it decreases

while in case of externally cooled plate the primary velocity (u) decreases near the plate and after attaining a minimum value it increases. It is also observed that an increase in G_r or G_m results in an increase in the primary velocity field while an increase in k, E or S_c leads to a decrease in the primary velocity field in case of externally heated plate. The effects of these parameters in the case of externally cooled plate are just reverse. It is interesting to note that numerically, the effects of the parameters on primary velocity are equal in value but opposite in sign.

It is worth while to mention here that the effects of permeability parameter (k), rotation parameter (E), Schmidt number (S_c) Grashof number (G_r) and modified Grashof number (G_m) on secondary velocity profiles (v) for cooling case ($G_r > 0$) and heating case ($G_r < 0$) at $P_r = 0\ 71$ were observed on the screen of the computer and it was noted that in case of externally cooled plate the secondary velocity (v) increases rapidly in the vicinity of the plate and after attaining a maximum value, it decreases but in case of externally heated plate the secondary velocity (v) decreases in the vicinity of the plate and after attaining a minimum value it increases. It was also observed that an increase in k, G_r or G_m results in an increase in the secondary velocity field while an increase in E or S_c leads to a decrease in the secondary velocity field in case of externally heated plate. The effects of these parameters in the case of externally cooled plate were noted just reverse.

The equation (14) shows concentration of species. It is obvious that for various values of Schmidt number (S_c) the concentration field decreases as z increases for given values of ε, t, n and L_2. It is also obvious that an increase in S_c results in a decrease in the concentration of species for all z. Thus concentration field is maximum in case of Hydrogen (S_c = 0.22) and minimum for Ammonia (S_c = 0.78). The concentration for the gases Helium (S_c = 0.30), Water-vapour (S_c = 0.60), Oxygen (S_c = 0.66) lies in the said range.

Table 1 indicates the rate of mass transfer in terms of Sherwood number (S_h) with respect to time (t) for Hydrogen (S_c = 022), Helium (S_c = 0.30), Water-vapour (S_c = 0.60), Oxygen (S_c = 0.66) and Ammonia (S_c = 0.78). It is observed that an increase in Schmidt number (S_c) decreases the rate of mass transfer (S_h) while an increase in time (t) increases the rate of mass transfer (S_h). Thus the rate of mass transfer for Ammonia is highest in comparison to other said gases.

Table 2 represents the skin-friction (τ_p) due to primary velocity for cooling case at ε = 0.002 to observe the effects of k, E, n, P_r, S_c, G_r, G_m and t. It is observed that an increase in k, E, n, P_r, S_c or t leads to an increase the skin. friction (τ_p) while an increase in G_r or G_m decreases the skin-friction (τ_p).

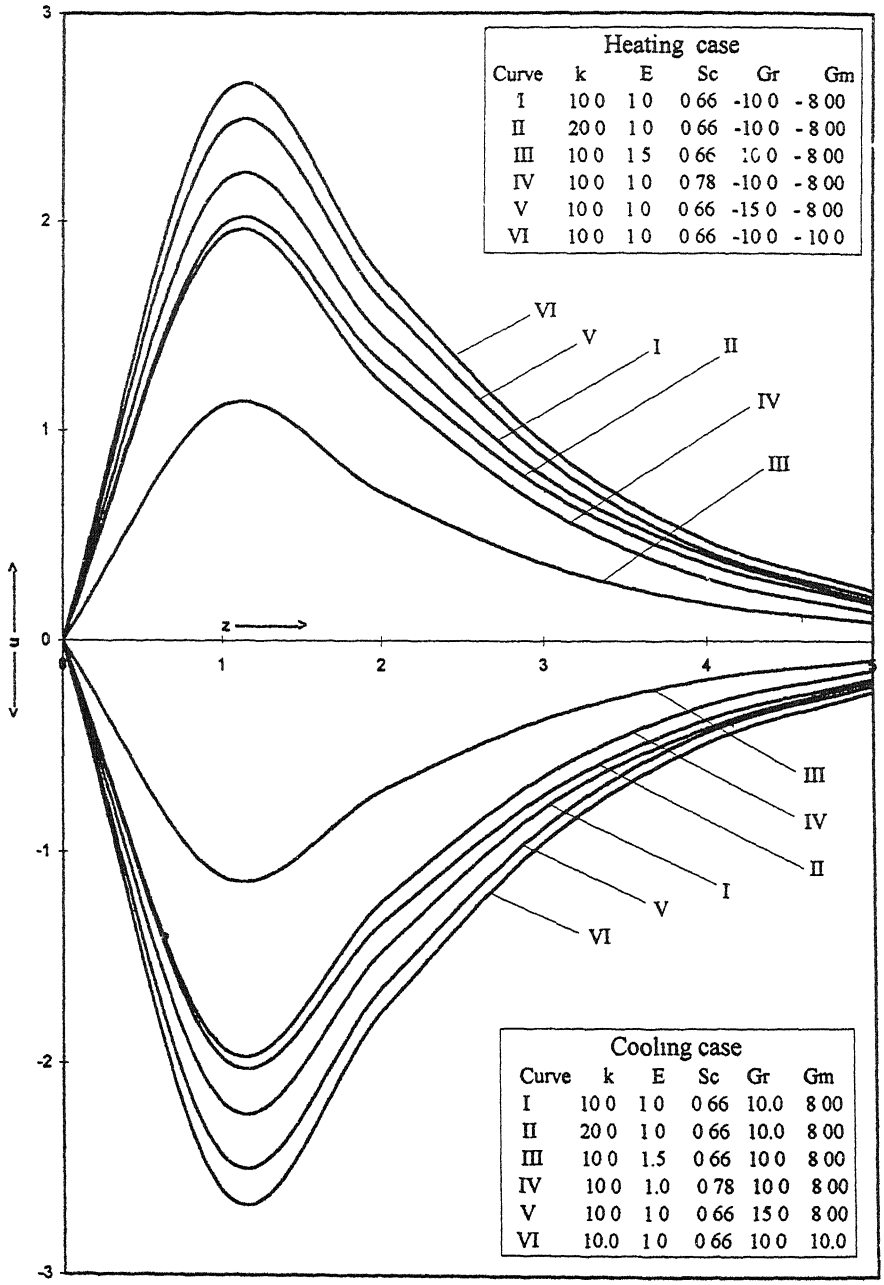

Fig. 1– Primary velocity profiles

Table 3 represents the skin-friction (τ_s) due to secondary velocity for cooling case to observe the effects of k, E, n, P_r, S_c, G_r, G_m and t. It is observed that an increase in n, G_r or t leads to a decrease in the skin. friction (τ_s) while an increase in k, E, P_r, S_c or G_m increases the skin-friction(τ_s).

Table 4 represents the skin-friction (τ_p) due to primary velocity for heating case to observe the effects of k, E, n, P_r, S_c, G_r, G_m and t. It is observed that an increase in k, E, n, P_r, S_c or t leads to a decrease in the skin-friction (τ_p) while an increase in G_r or G_m increases the skin-friction (τ_p).

Table 5 represents the skin-friction (τ_s) due to secondary velocity for heating case to observe the effects of k, E, n, P_r, S_c, G_r, G_m and t. It is observed that an increase in n, G_r or t leads to an increase in the skin-friction (τ_s)while an increase in k, E, P_r, S_c or G_m decreases the skin-friction(τ_s).

References

1. Ahmadı, G. & Manvı, R (1971) *Ind J. Techno* **9** 441
2. Gersten, K & Gross, I. F (1974) *ZAMP* **25** 399
3 Ram, G & Mishra, R. S (1977) *Ind J Pure Appl Math* **8** 637
4 Raptıs, A. A (1983) *Int J. Engng Scı* **21** · 345
5. Raptis, A & Perdıkıs, C. P (1985) *Int J Engng Scı* **23** . 51
6 Sıngh, H. P. & Trıpathı, D D. (1988) *Ind J Pure Appl Math* **19** . 677
7. Prasadarao, D R. V, Krishna, D V. & Debnath, L. (1981) *Acta Mech* **39** 225.
8. Senger, R. S., Singh, B D. & Gupta, I (1987) *Proc. Nat Acad Scı Indıa* **57A** . 230
9. Hatzikonstantinou, P. (1990) *ZAMM* **70** : 457.
10 Srivastava, A. C. & Sharma, B. R. (1992) *J Math Phy. Scı* **26** : 539
11. Sattar, M. A. & Alam, M. M. (1995) *Ind J. Theo Phy* **43** . 169.
12. Sıngh, N. P., Gupta, S. K., Singh, Ajay Kumar & Sıngh, Atul Kumar (1999) *JMACT* **32** . 33.
13. Sıngh, N. P., Gupta, S K & Singh, Atul Kumar (2000) *Ind J Theo Pıty* **48** 161
14. Singh, N. P., Gupta, S. K. & Singh, *Atul Kumar* (2001) *Proc Nat Acad Scı. Indıa* **71 :** 149.

PROC NAT. ACAD. SCI. INDIA, 74 (A), II, 2004

Heat and water transport in thermally damaged skin

V.P. SAXENA, A. JUNEJA and A.S. YADAV

School of Mathematics and Allied Sciences, Jiwaji University, Gwalior - 474 011, India.

Received April 25, 2001, Revised August 23, 2001, Accepted June 01, 2002

Abstract

Extreme variations in atmospheric temperature results in the damage of exposed human skin and subcutaneous region The present paper deals with the study of mathematical and numerical computation of disturbed thermo-regulation with damage causing excessive fluid or water migration. In particular, the coetaneous region is assumed to be exposed to excessive heating for a long period of time which leads to bum injury in dermal skin The physical parameters like rate of blood mass flow, the rate of metabolic heat generation and thermal conductivity are taken to be variable while rate of sweat generation is a function of tissue temperature The mathematical model which consists of heat and mass diffusion equations has been solved using variational finite element method.

(**Keywords** : human skin/thermo regulation/damage function)

Introduction

The exposure of skin region of human body to heat source either in direct contact or kept at a distance for a long period of time results in bum injury. The degree of injury depends both on the temperature of the source and time of exposure along with the thermal nature of the tissue. Mortiz and Henriques[1] demonstrated graphically the time and temperature required to produce a specific level of bum injury. Guyton[2] pointed out that the average critical temperature at which the pain starts is 45°C. Stole[3] has mentioned that the range of thermal sensation extends above and below the temperature levels of comfort into heat and pain on one side and cold and pain on the other side. Each limit is reached when the tissue is destroyed. For practical purposes these limits may be stated as instantaneous tissue temperature of 27°C as upper limit where the process of systematic progression of thermal-coagulation can be demonstrated[4,5] while the lower limit is mentioned as 0 to 4°C.

In the present paper, we have estimated the damage by investigating the process of heat and water migration in dermal region by mathematical modelling in the form

of partial differential equations. For computation of the temperature distribution the use of finite element method has been made. The severity of burn has also been studied using the damage function defined in the following section.

The Mathematical Model

Energy equation including the effects of convection due to blood circulation, conduction and metabolic heat generation[15]

$$\text{div } [k \text{ grad } T] + mc_b (T_A - T) + S = 0 \tag{1}$$

in which k, m, c_b and S are the thermal conductivity, blood mass flow rate, specific heat and metabolic heat generation rate respectively. T_A is the temperature at the deepest subcutaneous tissue. There is evaporation of sweat from the skin surface so that the equation (1) subject to the following boundary condition :

$$K\frac{\partial T}{\partial x} = h(T - T_a) + LE \tag{2}$$

where, h is heat transfer coefficient, T_a is environmental temperature, and L and E are the latent heat of water (also sweat) and rate of sweat evaporation respectively. The burn injury causes (a) metabolic change (b) circulatoery change and (c) body fluid alteration. Due to burn injury large amount of fluid is lost from the body by evaporation through the burn wound.

Due to water transport through tissue, eqn. (1) along with boundary condition (2) is then coupled with the following mass diffusion equation governing water magration.

$$\text{div } [\ \overline{D} \text{ grad } \overline{C}\ ] + \overline{R} = 0 \tag{3}$$

in which $\overline{D}$ is the mass diffusivity of water in the tissue, $\overline{C}$ is the water concentration in tissue and $\overline{R}$ is the rate of sweat generation. The appropriate boundary condition at the skin surface is given by

$$\overline{D}\frac{\partial \overline{C}}{\partial x} = h_D((\overline{C} - C_a) \tag{4}$$

where h_D is defined as the mass transfer coefficient and C_a is the water concentration environment.

To complete the thermal (burn) injury model, a damage function devised by Henriques and Moritz[6] has to be included. This damage function has subsequently been used quite widely by several workers[3,5,7-10]. With this injury function the cumulative damage incurred during a burn can be predicted.

The total injury, Ω, at any point in the tissue is obtained by knowing the local transient temperature history, i.e.,

$$\Omega(x) = A \int_0^t \exp\left[\frac{-\Delta E}{RT(x,t)}\right] dt \qquad (5)$$

The function $\Omega(x)$ was quantified by Henrique to identify various injury thresholds. At $\Omega = 0.53$ is the starting value of irreversible epidermal injury, whereas at $\Omega = 10^4$ complete transepidermal necrosis occurrs. In between there exist several stages of the thermal damage. The mathematical study of thermal thermo-regulation in *in vitro* tissue was taken up by several authors[11-14, 16,17]. Saxena and his co-workers[18-20]. obtained interesting results for normal atmospheric conditions and abnormal growth in skin layers. Diller and Hayes[21] modeled simple burn process using finite element technique in blood perfused skin.

In the present work we have studied the thermal effect of hot atmospheric conditions on the SST region upto the extent of burn in one dimensional steady state case. The region under study has been assumed to be divided into three layers with total thickness c. The first layer, epidermis, is of thickness c measured from the skin surface; dermis, the second layer has thickness b and the third layer, the sub dermal tissue, is of thickness measured from the outer skin surface. The assumptions regarding external and internal conditions are given in Table 1. The boundary conditions are :

At the skin surface (outer boundary) (x=0), we have the condition given by eqn. (2) and eqn. (4) with

$$T = T_o$$

$$\text{and } \overline{C} = \overline{C} \qquad (6)$$

At the inner boundary ($x = c$)

$$T = T_3 = T_b \text{ (body core temperature)}$$

$$\text{and } T_A = T_b \tag{7}$$

Method of Solution

Solving eqn. (3) along with boundary condition (4) in view of the values assigned to $\overline{C}, \overline{D}$ and $\overline{R}$ in tissue layers and at interfaces conditions (Table 1), we obtain :

$$\overline{C}_1 = [1/2\mu(b\text{-}a)/\overline{D}_1 + (T_1 + T_2)x + 1/2\ \mu(b\text{-}a)/h_D(T_1+T_2) + C_a$$

$$\overline{C}_2 = -\mu[1/2(bT_1+aT_2)/b\text{-}a)x^2 + 1/3)T_2\text{-}T_1)/(b\text{-}a)x^3]/\overline{D}_2$$

$$+[1/2\mu/\overline{D}_2(b\text{-}a)\{b^2T_1+b(b\text{-}2a)T_2\}]x$$

$$+1/2\mu(b\text{-}a)(a/\overline{D}_1+1/h_D)\ (T_1 + T_2)$$

$$+1/6\ \mu a/\overline{D}_2(b\text{-}a)\{(3ab\text{-}a^2\text{-}3b^2)T_1+(6ab\text{-}3b^2\text{-}2a^2)T_2)\}$$

Accordingly the rate of sweat evaporation E is estimated as

$$E = \frac{1}{2}\mu(b\text{-}a)(T_1+T_2) \tag{8}$$

where T_1 and T_2 are unknown temperatures to be determined.

Now coupling eqn. (1) with eqn. (2) and comparing with Euler's Largrange's equation, we get the following equivalent integral form :

$$I = \frac{1}{2}\int_0^c [k(\frac{\partial T}{\partial x})^2 + mc_b(T_A - T)^2 - 2ST]dx + 1/2h(T-T_a)^2 + LET \tag{9}$$

Table 1–

Interior of the region			At interfaces	
Epidermis	Dermis	Subcutaneous	First interface	Second interface
$(0 < x < a)$	$(a < x < b)$	$(B < x < c)$	$(x = a)$	$(x = b)$
$k = K_1$	$k = K_2 = (bK_1 - aK_3) / (b-a) + (K_3 - K_1)\, x/(b-a)$	$k = K_3$	$k_1 = K_2$	$K_2 = K_3$
$m = m_1 = 0$	$m = m_2 - (x-a)\, m_3 / (b-a)$	$m = m_3$	$m_1 = m_2$	$m_2 = m_3$
$S = S_1 = 0$	$S = S_2 = (x\text{-}a)\, S_3 / (b\text{-}a)$	$S = S_3$	$S_1 = S_2$	$S_2 = S_3$
$T^{(1)} = T_0 + (T_1 - T_0)x/a$	$T^{(2)} = (bT_1 - aT_2)/(b-a) + (T_2 - T_1)\, x/(b-a)$	$T^{(3)} = (cT_1 - bT_3) / (c-b) + (T_3 - T_2)\, x/(c-a)$	$T = T_1$	$T = T_2$
	$T_A^{(2)} = (x - a)\, T_b /(c-a)$	$T_A^{(3)} = (x-a)\, Tb /(c-a)$		
			$\overline{C}_1 = \overline{C}_2$	
$\overline{D} = \overline{D}_1$ (Cons)	$\overline{D} = \overline{D}_2$ (const)		$\overline{D}_1 \frac{\partial \overline{C}_1}{\partial x} = \overline{D}_2 \frac{\partial \overline{C}_2}{\partial x}$	$\overline{D}_2 \frac{\partial \overline{C}_2}{\partial x} = 0$
$\overline{R} = \overline{R}_r = 0$	$\overline{R}_2 = \mu T^{(2)}$; $\mu = \frac{\overline{R}}{T_b}$			

The variational integral (9) for the whole region can be given as the sum of all I's defined for each layer. Thus,

$$I = \sum_{i=1}^{3} I_1 \tag{10}$$

Evaluating the integral (9) for each layer by substituting layerwise expressions and interface conditions given in Table 1 and boundary conditions (7) and (8) respectively, we obtain:

$$I_1 = K_1/\ 2a(T_1 - T_0)^2 + 1/2h(T_0 - T_a)^2 + 1/2L\mu(b-a)T_0(T_1+T_2)$$

$$I_2 = F_1(T_2-T_1)^2 + F_2(bT_1 - aT_2)^2 + F_3(T_2-T_1) + F_4(bT_1 - aT_2)$$

$$+ F_5(T_2-T_1)(bT_1 - aT_2) + F_6$$

$$I_3 = E_1(T_3-T_2)^2 + E_2(cT_2 - bT_3)^2 + E_3(T_3-T_2) + E_4(cT_2 - bT_3)$$

$$+ E_5(T_3-T_3)(cT_2 - bT_3) + F_6$$

The values of $F_i's$, $E_i's$ for $i = 1$ to 6 are given in Appendix I.

Minimizing I for T_0, T_1 and T_2, as $T_3 = T_b$, a constant, we get the following system of equations :

$$XT = Y \tag{11}$$

Here

$$\mathrm{X} = \begin{vmatrix} L_1 & L_2 & L3 \\ M_1 & M_2 & M_3 \\ N_1 & N_2 & N_3 \end{vmatrix} \quad ; \quad T = \begin{vmatrix} T_0 \\ T_1 \\ T_2 \end{vmatrix} \quad ; \quad Y = \begin{vmatrix} W_1 \\ W_2 \\ W_3 \end{vmatrix}$$

where $L_i's$, $M_i's$ and $W_i's$ W/s (i= 1,2,3) are defined in Appendix II.

Results and Discussion

For numerical computation, following values of the quantities[6,15,23-25] have been used

$K_1 = 0.5 \times 10^{-3}$ cal/cm sec°C; $K_3 = 1.0 \times 10^{-3}$ cal/cm sec°C

$m_3 c_b = 0.525 \times 10^{-3}$ cal/cm^3 – sec°C; $S_3 = 0.3 \times 10^{-3}$ cal/cm^3 sec°C,

$h = 3 \times 10^{-3}$ cal/cm^2 - sec°C; $L = 579$ cal/g,

$T_b = 37$°C; $\overline{R} = 0.33 \times 10^{-4}$ gm/cm^3/sec.,

$\overline{D_1} = 0.97 \times 10^{-5}$cm^2/sec; $\overline{D_2} = 0.34 \times 10^{-4}$ cm^2/sec,

$h_d = 59.5 \times 10^{-2}$ cm/sec, ; $\overline{C_a} = 4.51498 \times 10^{-4}$ g/cm^3

$a = 0.10$ cm; $b = 0.35$ cm; $c = 0.50$ cm,

$A = 3.x\ 10^{98}$/sec.; $\Delta E = 6.3 \times 10^8$/Kmol; $R = 8.31 \times 10^3$ J/Kmol°C

Using these numerical values in set of eqn. (11), we get the values of nodal temperature and sweat evaporation at different values of heat source temperature (Table 2).

Table 2–

T_a(°C)	T_0(°C)	T_1(°C)	T_2(°C)	E_2 (g/cm^2–min)
60	50.97	46.70	41 06	5.929 X 10-4
65	54.30	49 07	41.91	6 147 X 10-4
70	57.63	51 43	42.77	6 365 x 10-4
75	60.95	53.80	43.63	6.582 X 10-4
80	64.28	56.16	44.49	6.8 X 10-4

Nodal temperatures (T_{i}, i = 0.1.2.) and rate of sweat evaporation (E) at different values of source temperature (T_a)

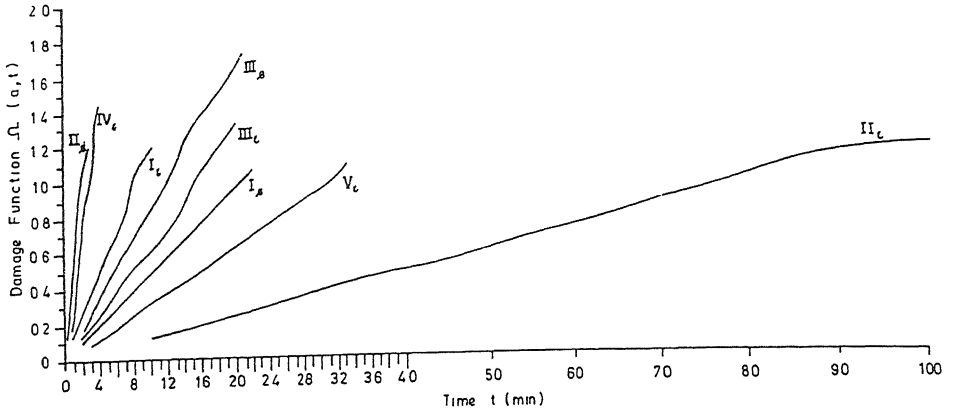

Fig 1– The curves numbered I, II, III, IV and V are drawn for T_a = 60°C, 65°C, 75°C and 80°C respectively Subscript 's' stands for skin surface and 'i' for interface of epidermis and dermis

By substituting the nodal values of tissues temperature (Table 2) in $T^{(i)}$ (i=1,2,3) we get temperature profiles in dermal region at different values of source temperature. After the completion of steady state, we obtained damage function at skin surface and at interface of epidermis and dermis where nodal temperatures are above critical temperature. Using eqn. (6), Table 2 and corresponding numerical values of constants, we get damage ions(Fig. 1).

From the Table 2 we observe that the tissue temperature T increases as the value of T_a increases and the rate of sweat evaporation also increases as value of T_a increases. We also find that the extent of burn increases as source temperature (T_a) increases. With increment in the extent of burns, the rate of sweat evaporation also increases.

From Fig. 1, we observe that

(i) At T_a = 60°C and at skin surface, irreversible burn is obtained after the time 11 min. 24 sec and injury into entire epidermis may be available after the time 21 min. 24 sec. approximately.

(ii) At T_a = 60°C and at first interface (interface of epidermis and dermis), irreversible injury is available after the time 04 hrs 21 min. approximately. Injury into whole dermis may be available after the time 08 hrs 06 min. approximately.

(iii) At T_a = 65°C and at skin surface, irreversible burn is obtained after the time 1.04 min. and entire epidermis may be affected after the time 1.99 min. approximately.

(iv) At T_a = 65°C and at first interface, irreversible injury is available after the time 45 min. and injury into whole dermis may be available after the time 85.50 min. approximately.

(v) At T_a = 70°C and at skin surface, irreversible injury is available after the time 6.20 sec. and entire epidermis may be affected after the time 11.6 sec. approximately.

(vi) At T_a = 70°C and at the first interface, irreversible injury is obtained after the time 8.2 min. and entire dermis may be affected after the time 15.4 min. approximately.

(vii) At T_a = 75°C entire epidermis may be affected within 1.5 sec. and at the first interface irreversible burn is available after the time 1.5 min. and injury into entire dermis may be available after the time 2.85 min. approximately.

(viii) At T_a = 80°C entire epidermis may be affected within 0.15 sec. and at the first interface irreversible burn is obtained after the time 17.2 sec. and injury into entire dermis may be available after the time 32.2 sec. approximately.

From the Fig. 1, we also notice that initially the damages are linear, however, afterwards they show little fluctuations with time.

References

1. Moritz, A.R & Henriques, H C (1947) *The Ameri Jour of Pathology* **23** 695
2. Guyton, A C. (1976) *Text book of Medical Physiology*, W E Saunders Co
3. Stoll, A M. & Green, L. C (1959) *Jour of Appld Physiol* **14** . 373
4 Henriques, F C. (1947) *Jr Arch Pathol.* **43** : 489.
5 Stoll, A.M. (1960) *Trans of Medi Electronics* **7** . 355.
6. Henriques, F & Moritz, A.R (1947) *Amer J Path.* **23** . 531
7. Buettner, K. (1951) *J Appld Physio.* **3** . 691
8 Weaver, J A & Stoll, A M (1961) *Aerospace Medicine* **40** 24.

9. Mainster, M A., White, T.J , Tips, J H & Wilson, P W , (1970) *Bull. of Math Biophys,* **32** 303.
10. Takata, A N., Zaneveld, & Richter, W (1977) SAM-TR-77-38, *USAF School of Aerospace Medicine* **1** 159.
11. Pennes, H.H (1948) *J Appl Physiol* **1**(2) . 93
12. Perl, W. (1962) *J Theo Biol* **2** : 201.
13. Wissler, E.H. (1961) *J Appl Physiol.* **16** . 734
14. Cooper, T.E & Trezek, G J. (1968) *Thermal Problems in Bio-Technology,* ASME, NY, **1** 15.
15. Chao, KN., Eisley, J.G & Yang, W.J. (1973) *Bio-Mech Symp* , ASME, **69** 72
16. Patterson, AM. (1976) *S Afr J Sc* **72** · 78
17. Chao, K.N & Yang, W J. (1975) *Bio-Mech Symp* ASME **69** 71
18. Saxena, V P & Arya, D (1981) *J Theo Biol.* **89** : 423
19. Saxena, V.P. (1979) *Numerical Methods on Thermal Problems* ed Levis and Morgan, Pineridge Press, UK, p 1067.
20. Saxena, V P. & Pardasani, K.R (1991) *Bull Math Bio* **53**(4) : 525.
21. Diller, K R. & Hayes, L.J. (1983) *Bio Mech Engg,* **105** · 300
22. Ponder, E. (1962) *J. Gen Physiol* **45** : 545.
23. Poppendiek, H F *et al* (1966) *Cryobiol* **3** : 318
24. Hodgson, T (1974) *Ph D Thesis,* South African C.S.I.R

Appendix I

$L_1 = [K_1/a + h]$; $L_2 = [1/2\ p\mu L(b-a)-K]la)$,. $L_3 = [1/2\ \mu L(b-a)]$

$W_1 = [hT_a]$; $W_2\ [F_3-bF_4]$

$W_3 = [(2E_1+2bcE_2-(b+c)E_5\}\ T_b-F_3+aF_4+E_3- cE_4)]$

$M_1 = [1/2\ \mu L\ (b-a)- K_1/a]$,. $M_2 = [K_1/a+ 2F_1 + 2b^2F_2 - 2bF_5]$,.

$M_3 = [-2F_1 - 2abF_2 + (a+c)\ F_5]$

$N_1 = [1/2\ \mu L\ (b-a)]$

$N_2 = [\ -2F_1 - 2abF_2\ (a+b)\ F_5]$

$N_3 = [2F_1 + 2a^2F_2 - 2aF_5 + 2E_1 + 2c^2E_2 - 2cE_5]$,

Appendix II

$F_1 = [1/4(K_1 + K_3/(b-a) + 1/24(b-a)\ m_3c_b(a^2+2ab+ 3b^2)]$;

$F_2 = [1/4(b-a)m_3c_b]$;

$F_3 = [-1/12(c-a)\ m_3c_bT_b\ (b-a)\ (a+3b)\ -1/6\ S_3\ (a+2b)]$;

$F_4 = [\ -1/3(c-a)\ m_3c_bT_b\ (b-a)\ -1/2\ S_3]$, $F_5 = [1/6\ (b-a)\ m_3C_b\ (a+2b)]$

$F_6\ [\ 1/8\ (c-a)^2\ m_3c_b\ T',2\ (b-a)_3]$;

$E_1 = [1/2(c-b)K_3 + 1/6(c-b)m_3c_b\ (b^2+C^2\ +bc)$;. $E_2 = [\ 1/2(b-c)\ m_3c_b]$,.

$E_3 = [-1/6(c-a)\ m_3c_bT_b\ (2b^2\ +2C^2 + 2bc - 3ab - 3ac)\ -1/2\ S_3\ (b-c)]$;

$E_4 = [-1/2(c-a)\ m_3c_bT_b\ (b+c-2a) - S_3]$; $E_5 = [1/2(c-b)m_3c_b(b+c)]$;.

$E_6 = [1/6(c-a)\ m_3c_bT_b(b-a)(a^2+b^2 + 3c^2+ab\ -3bc\ -3ac)]$

PROC. NAT. ACAD. SCI INDIA, 74 (A), II, 2004

A note on Mond-Shisha inequality and its extension to certain classes of operators

K. C. DAS, M. DAS GUPTA and K. PAUL[1]

[1]*Department of Mathematics, New Alipore College, Kolkata-700032, India.*

Department of Mathematics, Jadavpur University, Kolkata-700032, India.

E-mail jumath@cal.vsnl.net.in,kalloplaul@hotmail.com

Received October 1, 1999, Revised February 14, 2000, Accepted April 6, 2000

Abstract

A simple analytic proof of Mond-Shisha inequality for operators with a complete orthonormal set of eigenvectors is given. We then generalize the inequality for normal operators It is then generalized to a pair of selfadjoint commutative operators under certain conditions. The structure of the vectors for which one of the inequalities becomes an equality is also studied.

(Keywords : strictly accretive operators/mean of order *r*/stationary vectors)

Introduction

Let $q_1, q_2,....q_n$ be positive numbers with $\Sigma_{k=1}^{n} q_k = 1$. For every sequence (x_1, $x_2,...x_n$), with all $x_k > 0$ and for every $r \neq 0$, consider the mean of order r, M_r (x_1, $x_2,...x_n$) defined as $\left\{\sum_{k=1}^{n} q_k x_k^r\right\}^{\frac{1}{r}}$. Let r, s be given reals $r < s$, $rs \neq 0$, then by a classical inequality (see Hardy *et al.*[1] or Beckenbach and Bellman[2]) we have

$$1 \leq M_s\,(x_1, x_2,...x_n)/M_r\,(x_1, x_2,...x_n). \tag{1}$$

Cargo and Shisha[3] gave an upper bound for the ratio in (1). They assumed that $0 < \alpha < \beta$ and $\alpha \leq x_k \leq \beta$, $k = 1, 2....n$. Then setting $\gamma = \beta/\alpha$, they found

$$M_s\,(x_1, x_2,...x_n)/M_r\,(x_1, x_2,...x_n) \leq \Delta \tag{2}$$

$$\text{where } \Delta = \left\{\frac{r\left(\gamma^s-\gamma^r\right)}{(s-r)\left(\gamma^r-1\right)}\right\}^{1/s}\left\{\frac{s\left(\gamma^r-\gamma^s\right)}{(r-s)\left(\gamma^s-1\right)}\right\}^{-1/r}.$$

Mond and Shisha[4] showed that these inequalities between means give rise to inequalities involving a bounded, selfadjoint operator A on a Hilbert Space H. In fact, they proved the following.

Theorem (Mond-Shisha) Let A be a bounded linear selfadjoint operator on a Hilbert space H with $mI \le A \le MI$ and $0 < m < M$, I being the identity operator on H. Then

$$1 \le (A^s f, f)^{1/s}/(A^r f, f)^{1/r} \le \Delta, \tag{3}$$

where $f \in H$, $\|f\| = 1$ and Δ is given by (2) which $\gamma = M/m$.

For other related results the reader may refer to Mond and Pecaric[5-11].

In this paper we study the structure of the vectors that make $(A^s f, f)^{1/s}/(A^r f, f)^{1/r} = \phi_A(f)$ (say), for $\|f\| = 1$, stationary, which we call stationary vectors. The concept of stationary value and stationary vector was introduced by the first author Das[12] in studying the Rayleigh quotient of an operator and it was later used by us Das *et al.*[13] in studying the anteigenvectors of a strictly accretive operator. We here give the definition of stationary value and stationary vector as follows. A function $\phi_A(f)$ of a unit vector f is said to have a stationary value at f if the function $w_g(t)$ of a real variable t, defined by

$$w_g(t) = \phi_A\left(\frac{f+tg}{\|f+tg\|}\right) = \frac{\left(A^s(f+tg), f+tg\right)^{1/s}\left(f+tg, f+tg\right)^{1/r-1/s}}{\left(A^r(f+tg), f+tg\right)^{1/r}}$$

has a stationary value at $t = 0$ for any arbitrary but fixed vector $g \in H$. In other words $w_g'(0)=0$ for all g. Then f is called a stationary vector.

We show that a suitable linear combination of two eigenvectors is a stationary vector.

If A is a bounded linear selfadjoint operator with a complete orthonormal set of eigenvectors then we find the stationary values of A in terms of the eigenvalues of A. In case the maximum of $\phi_A(f)$ is attained, the stationary vector is a linear combination of eigenvectors corresponding to the minimum and maximum eigenvalues. If the maximum is not attained, by our method we obtain an upper bound of $\phi_A(f)$, which serves as an alternative proof of Mond-Shisha inequality for operators with a complete orthonormal set of eigenvectors.

Next we generalize this inequality first to a strictly accretive ($Re\ A > 0$) normal operator and then to a pair of bounded, selfadoint and commutative operators.

Throughout this paper H denotes a complex Hilbert space, with inner product (,) and norm $\| \|$, I is the identity operator on H and A is a bounded linear operator on H, and λ_i and e_i denotes the eigenvalues and eigenvectors of A respectively.

Stationary vectors of $(A^s f,f)^{1/s}/(A^r f,f)^{1/r}$

Here we find the necessary and sufficient condition for a unit vector f to be a stationary vector of $\phi_A(f)$ when A is selfadjoint and show that for any two eigenvectors e_1, e_2 there exists a suitable linear combination $f = \alpha_1 e_1 + \alpha_2 e_2$ of e_1 and e_2 such that f is a stationary vector of $\phi_A(f)$. Then we find the stationary values of $\phi_A(f)$ in terms of eigenvalues of A assuming that A has a complete orthonormal set of eigenvectors.

Theorem 1 : Let A be a bounded, linear, selfadjoint operator on H and e_1, e_2 be two eigenvectors of A with corresponding eigenvalues λ_1, λ_2. Then there exists a linear combination f of e_1 and e_2 such that f is a stationary vector of $\phi_A(f)$.

Proof : If $\phi_A(f)$ has a stationary value at a unit vector f then we have $w_g'(0) = 0$, where $w_g(t)$ is defined as

$$w_g(t) = \phi A\left(\frac{f+tg}{\|f+tg\|}\right) = \frac{\left(A^s(f+tg), f+tg\right)^{1/s}\left(f+tg, f+tg\right)^{\frac{1}{r}-\frac{1}{s}}}{\left(A^r(f+tg), f+tg\right)^{1/r}}$$

For $\|f\| = 1$ set $(A^s f,f) = a^s$ and $(A^r f,f) = b^r$, then $w_g'(0) = 0$ implies

$$\frac{a^{1-s}b}{s}\mathrm{Re}\left(A^s f,g\right) - \frac{ab^{1-r}}{r}\mathrm{Re}\left(A^r f,g\right) + \frac{s-r}{sr}ab\,\mathrm{Re}(f,g) = 0.$$

Since g is arbitrary we have

$$rb^r A^s f - sa^s A^r f + (s-r)\, a^s b^r f = 0. \tag{4}$$

This equation characterises the vector for which $\phi_A(f)$ is stationary.

Suppose $f = \alpha_1 e_1 + \alpha_2 e_2$, $|\alpha_1|^2 + |\alpha_2|^2 = 1$

Then

$$A^s f = \alpha_1 \lambda_1^s e_1 + \alpha_2 \lambda_2^s e_2$$

$$A^r f = \alpha_1 \lambda_1^r e_1 + \alpha_2 \lambda_2^r e_2$$

$$(A^s f, f) = |\alpha_1|^2 \lambda_1^s + |\alpha_2|^2 \lambda_2^s$$

$$(A^r f, f) = |\alpha_1|^2 \lambda_1^r + |\alpha_2|^2 \lambda_2^r .$$

Choose

$$|\alpha_1|^2 = \frac{s\lambda_2^s\left(\lambda_1^r - \lambda_2^r\right) - r\lambda_2^r\left(\lambda_1^s - \lambda_2^s\right)}{(r-s)\left(\lambda_1^r - \lambda_2^r\right)\left(\lambda_1^s - \lambda_2^s\right)}$$

so that

$$|\alpha_2|^2 = \frac{r\lambda_1^r\left(\lambda_1^s - \lambda_2^s\right) - s\lambda_1^s\left(\lambda_1^r - \lambda_2^r\right)}{(r-s)\left(\lambda_1^r - \lambda_2^r\right)\left(\lambda_1^s - \lambda_2^s\right)}.$$

Now L.H.S. of (4)

$$= rb^r A^s f - sa^s A^r f + (s-r)\, a^s b^r f$$

$$= \{r(|\alpha_1|^2 \lambda_1^r + |\alpha_2|^2 \lambda_2^r)\, \alpha_1 \lambda_1^s - s(|\alpha_1|^2 \lambda_1^s + |\alpha_2|^2 \lambda_2^s)\, \alpha_1 \lambda_1^r$$

$$+ (s-r)\,(|\alpha_1|^2\lambda_1^s+|\alpha_2|^2\lambda_2^s)\,(|\alpha_1|^2\lambda_1^r+|\alpha_2|^2\lambda_2^r)\,\alpha_1\}\,e_1 +$$

$$\{r(|\alpha_1|^2\lambda_1^r+|\alpha_2|^2\lambda_2^r)\,\alpha_2\lambda_2^s - s(|\alpha_1|^2\lambda_1^s+|\alpha_2|^2\lambda_2^s)\,\alpha_2\lambda_2^r$$

$$+ (s-r)\,(|\alpha_1|^2\lambda_1^s+|\alpha_2|^2\lambda_2^s)\,(|\alpha_1|^2\lambda_1^r+|\alpha_2|^2\lambda_2^r)\,\alpha_2\}\,e_2$$

$$= 0.$$

so that f is a stationary vector of $\phi_A(f)$. This completes the proof.

Also in this case

$$(A^s f, f) = |\alpha_1|^2\lambda_1^s + |\alpha_2|^2\lambda_2^s$$

$$= \frac{r\left(\lambda_2^r\lambda_1^s - \lambda_1^r\lambda_2^s\right)}{(s-r)\left(\lambda_1^r - \lambda_2^r\right)},$$

$$(A^r f, f) = |\alpha_1|^2\lambda_1^r + |\alpha_2|^2\lambda_2^r$$

$$= \frac{r\left(\lambda_2^r\lambda_1^s - \lambda_1^r\lambda_2^s\right)}{(s-r)\left(\lambda_1^s - \lambda_2^s\right)}$$

so that

$$\phi_A(f) = \left\{\frac{r\left(u^s - u^r\right)}{(s-r)\left(u^r - 1\right)}\right\}^{1/s}\left\{\frac{s\left(u^s - u^r\right)}{(s-r)\left(u^s - 1\right)}\right\}^{-1/r}, u = \frac{\lambda_1}{\lambda_2}.$$

Next suppose A has a complete orthonormal set of eigenvectors e_i with eigenvalues λ_i. We now prove the following theorem.

Theorem 2 : Let A be a bounded, linear, selfadjoint operator on H with a complete orthonormal set of eigenvectors e_i and corresponding eigenvalues λ_i. Let r, s, m, M be

given reals where $0 < m < M$, $r < s$ and $rs \neq 0$. Let A be such that $mI \leq A \leq MI$. Then $(A^s f, f)^{1/s}/(A^r f, f)^{1/r} \leq \Delta$ for $f \in H$, $\|f\| = 1$, where Δ is given by eqn. (2) ($\gamma = M/m$).

Proof: Suppose $f \in H$, $\|f\| = 1$ be a stationary vector of $\phi_A(f)$ and let $f = \Sigma(f,e_i)e_i$, $Af = \Sigma\lambda_i(f,e_i)e_i$. Substituting the values of f, Af in (4) and equating to zero the coefficients of e_i we obtain

$$(rb^r \lambda_i^s - sa^s \lambda_i^r + (s-r)a^s b^r)(f,e_i) = 0 \quad \forall i$$

If $(f,e_i) \neq 0$ then

$$rb^r \lambda_i^s - sa^s \lambda_i^r + (s-r)\, a^s b^r = 0 \tag{5}$$

If f is an eigenvector then the characteristic eqn. (4) is satisfied for which $a = b = \lambda$, where λ is the corresponding eigenvalue. Then $\phi_A(f) = 1$, which gives the minimum value.

If f is not an eigenvector then the following cases arise.

Case 1 : Eqn. (5) is satisfied by only two λ_i's, in which case f is a linear combination of the corresponding two eigenvectors.

Case 2 : Eqn. (5) is satisfied by more than two λ_i's, in which case f is a linear combination more than two eigenvectors corresponding to two distinct eigenvalues.

We shall however show that there always exists a suitable linear combination g, of two eigenvectors corresponding to two eigenvalues λ_i and λ_j, $\lambda \neq \lambda_j$ such that $\phi_A(f) = \phi_A(g)$ and ϕ_A is stationary at g.

It suffices now to find α and α_j such that

$$g = \alpha_i e_i + \alpha_j e_j, \qquad |\alpha_i|^2 + |\alpha_j|^2 = 1,$$

$$a^s = (A^s f, f) = (A^s g, g), \qquad b^r = (A^r f, f) = (A^r g, g)$$

and (4) is satisfied for g. Now

$$a^s = |\alpha_i|^2 \lambda_i^s + |\alpha_j|^2 \lambda_j^s \qquad \text{and} \qquad b^r = |\alpha_i|^2 \lambda_i^r + |\alpha_j|^2 \lambda_j^r .$$

Since $|\alpha_i|^2 + |\alpha_j|^2 = 1$, we get

$$|\alpha_i|^2 = \frac{a^s - \lambda_j^s}{\lambda_i^s - \lambda_j^s} \text{ and also } |\alpha_i|^2 = \frac{b^r - \lambda_j^r}{\lambda_i^r - \lambda_j^r}.$$

But since λ_i and λ_j satisfy (5) we have

$$rb^r\lambda_i^s - sa^s\lambda_i^r + (s-r)a^s b^r = 0,\ rb^r\lambda_j^s - sa^s\lambda_i^r + (s-r)a^s b^r = 0.$$

From these equations, it follows that

$$a^s = \frac{r\left(\lambda_j^r\lambda_i^s - \lambda_i^r\lambda_i^s\right)}{(s-r)\left(\lambda_i^r - \lambda_j^r\right)} \text{ and } b^r = \frac{r\left(\lambda_j^r\lambda_i^s - \lambda_i^r\lambda_j^s\right)}{(s-r)\left(\lambda_i^s - \lambda_j^s\right)}$$

With these values it is seen that the two values of $|\alpha_i|^2$ are the same. Hence a suitable g is obtained.

Thus we get $\phi_A(f)$ in terms of the eigenvalues of A. Next let

$$F(u) = \left\{\frac{r\left(u^s - u^r\right)}{(s-r)\left(u^r - 1\right)}\right\}^{1/s}\left\{\frac{s\left(u^s - u^r\right)}{(s-r)\left(u^s - 1\right)}\right\}^{-1/r},$$

where $u = \frac{\lambda_i}{\lambda_j}$, $\lambda_i > \lambda_j$.

A little calculation shows that $F(u)$ is an increasing function of u.

So Δ (eqn. (2), where $\gamma = M/m$) is an upper bound of $\phi_A(f)$. In case the maximum of $\phi_A(f)$ is attained, it is given by Δ and $f = \alpha_i e_i + \alpha_j e_j$, where e_i and e_j are eigenvectors corresponding to the eigenvalues m and M resp.

This completes the proof.

Extension of Mond-Shisha Inequality to Strictly Accretive Normal Operators

Here we study the structure of the stationary vectors of

$$\Phi_A(f) = \frac{\left(\left(\sqrt{A^*A}\right)^s f, f\right)^{\frac{1}{s}}}{\left(\left(\frac{A+A^r}{2}\right)^r f, f\right)^{\frac{1}{r}}},$$

where A is a strictly accretive (Re $A > 0$) normal operator with a complete orthonormal set of eigenvectors. We obtain its stationary values in terms of eignevalues of A and taking the supremum of these values we get an upper bound of $\Phi_A(f)$.

Theorem 3 : Let A be a strictly accretive (Re $A > 0$) normal operator on H such that for any unit vector $f \in H$, $Af = \Sigma\lambda_i(f,e_i)\, e_i$. Let r and s be given reals where $r < s$, $rs \neq 0$. If f is a stationary vector of $\Phi_A(f)$ then it is an eigenvector of A or a linear combination of two eigenvectors corresponding to two conjugate eigenvalues or there exists a linear combination of two eigenvectors corresponding to two eigenvalues with unequal real parts and moduli, say g, such that $\Phi_A(g) = \Phi_A(f)$ and Φ_A is stationary at g. Further, a stationary value of $\Phi_A(f)$ is given by

$$\left\{\frac{r\left(\lambda^s\mu^r\cos^r\phi - \mu^s\lambda^r\cos^r\theta\right)}{(s-r)\left(\lambda^r\cos^r\theta - \mu^r\cos^r\phi\right)}\right\}^{1/s} \left\{\frac{r\left(\lambda^s\mu^r\cos^r\phi - \mu^s\lambda^r\cos^r\theta\right)}{(s-r)\left(\lambda^s - \mu^s\right)}\right\}^{-1/r}$$

where $\lambda e^{i\theta}$ and $\mu e^{i\phi}$ are the distinct eigenvalues referred to above and are such that $\lambda \neq \mu$, $\lambda\cos\theta \neq \mu\cos\phi$.

Proof: As in Theorem 1, $\Phi_A(f)$ has a stationary value at a unit vector f if

$$w_g(t) = \frac{\left(\left(\sqrt{A^*A}\right)^s (f+tg),(f+tg)\right)^{1/s} (f+tg,f+tg)^{(s-r)/sr}}{\left(\left(\frac{A+A^*}{2}\right)^r (f+tg),(f+tg)\right)^{1/r}}$$

has a stationary value at $t = 0$. For $\|f\| = 1$, set $a^s = \left(\left(\sqrt{A^*A}\right)^s f, f\right)$ and $b^r = \left(\left(\frac{A+A^*}{2}\right)^r f, f\right)$.

Then we get

$$rb^r \left(\sqrt{A^*A}\right)^s f - sa^s \left(\frac{A+A^*}{2}\right)^r f + (s-r)\, a^s b^r f = 0. \tag{6}$$

This equation characterises the vector for which $\Phi_A(f)$ is stationary. Substituting $Af = \Sigma\lambda_i(f,e_i)e_i$ and $A^*f = \Sigma\,\overline{\lambda}_i(f,e_i)e_i$ in (6) we obtain as before

$$\{rb^r|\lambda_i|^s - sa^s \operatorname{Re}\lambda_i^r + (s-r)\, a^s b^r\}\,(f,e_i) = 0 \;\forall i.$$

If $(f,e_i) \neq 0$ then

$$\{rb^r|\lambda_i|^s - sa^s \operatorname{Re}\lambda_i^r + (s-r)\, a^s b^r\} = 0. \tag{7}$$

If f is an eigenvector then the characteristic eqn. (6) is satisfied for which $a = |\lambda|$, $b = \operatorname{Re}\lambda$, where λ is the corresponding eigenvalue.

If f is not an eigenvector then the following cases arise.

Case 1 : Eqn. (7) may be satisfied by only one pair $(|\lambda_i|, \operatorname{Re}\lambda_i)$, in which case $(f,e_i) \neq 0$ for two e_i's corresponding to two distinct λ_i's. So the only way this can happen is that $Af = \lambda\,(f,e_i)\,e_i + \overline{\lambda}_j(f,e_j)e_j$. Here $a = |\lambda|$, $b = \operatorname{Re}\lambda$.

Case 2 : Eqn. (7) is satisfied by more than one pair $(|\lambda_i|, \text{Re } \lambda_i)$, then f is a linear combination of more than two eigenvectors corresponding to distinct eigenvalues.

Proceeding as in Theorem 1 we shall however show that there always exists a suitable linear combination g, of two eigenvectors e_i and e_j corresponding to two eigenvalues with unequal real parts and moduli such that $\Phi_A(f) = \Phi_A(g)$ and Φ_A is stationary at g.

Let $\lambda_i = \lambda e^{i\theta}$ and $\lambda_j = \mu e^{i\phi}$, $\lambda \neq \mu$, $\lambda \cos\theta \neq \mu \cos\phi$. It suffices now to find α_i and α_j such that $g = \alpha_i e_i + \alpha_j e_j$, $|\alpha_i|^2 + |\alpha_j|^2 = 1$, $a^s = \left(\left(\sqrt{A^*A}\right)^s f, f\right) = \left(\left(\sqrt{A^*A}\right)^s g, g\right)$, $b^r = \left(\left(\frac{A+A^*}{2}\right)^r f, f\right) = \left(\left(\frac{A+A^*}{2}\right)^r g, g\right)$ and (6) is satisfied for g. Now

$$a^s = |\alpha_i|^2\lambda^s + |\alpha_j|^2\mu^s,\ b^r = |\alpha_i|^2\lambda^r \cos^r\theta + |\alpha_i|^2\mu^r \cos^r\phi.$$

Since $|\alpha_i|^2 + |\alpha_j|^2 = 1$, we get

$$|\alpha_i|^2 = \frac{a^s - \mu^s}{\lambda^s - \mu^s} \text{ and also } |\alpha_i|^2 = \frac{b^r - \mu^r \cos^r\phi}{\lambda^r \cos^r\theta - \mu^r \cos^r\phi}.$$

But since λ_i and λ_j satisfy (7) we have

$$rb^r\lambda^s - sa^s\lambda^r\cos^r\theta + (s-r)\,a^sb^r = 0,$$

$$rb^r\mu^s - sa^s\mu^r\cos^r\phi + (s-r)\,a^sb^r = 0.$$

From these equations it follows that

$$a^s = \frac{r\left(\lambda^s\mu^r\cos^r\phi - \mu^s\lambda^r\cos^r\theta\right)}{(s-r)\left(\lambda^r\cos^r\theta - \mu^r\cos^r\phi\right)}, \qquad b^r = \frac{s\left(\lambda^s\mu^r\cos^r\phi - \mu^s\lambda^r\cos^r\theta\right)}{(s-r)\left(\lambda^s - \mu^s\right)}.$$

With these values it is seen that the two values of $|\alpha_i|^2$ are the same. Hence $a\,g$ is obtained. Further a/b gives a stationary value of $\Phi_A(f)$.

If the operator is positive then $\sqrt{A^*A} = A$ and $\frac{A+A^*}{2} = A$ also the eigenvalues are then real so that $\phi = 0$, $\theta = 0$ and Mond-Shisha inequality follows clearly as a corollary.

Extension of Mond-Shisha Inequality to two Selfadjoint Commutative Operators

Here we obtain the stationary values and the structure of the stationary vectors of $(A^sf, f)^{1/s}/(B^rf, f)^{1/r}$, where A and B are selfadjoint, commutative operators. The supremum of these stationary values gives an upper bound of the same. By taking $P(A)$ and $Q(A)$ in place of A and B respectively, where $P(A)$ and $Q(A)$ are polynomials in A, we have generalized it in yet another direction.

Theorem 4 : Let A and B be two bounded, linear, selfadjoint, commutative operators on H with $0 < m_1I \le A \le M_1I$ and $0 < m_2I \le B \le M_2I$. Let λ_i and μ_i be the eigenvalues of A and B respectively with corresponding eigenvectors e_i. For any unit vector $f \in H$, let $Af = \Sigma\lambda_i(f,e_i)e_i$, $Bf = \Sigma\mu_i(f,e_i)e_i$ and $(A^sf, f)^{1/s}/(B^rf, f)^{1/r} = \psi(f)$ (say), where r and s are reals with $r < s$, $rs \neq 0$.

If f is a stationary vector of $\psi(f)$ then either it is an eigenvector of A and B both or a linear combination of two eigenvectors corresponding to two distinct pairs of eigenvalues of A and B, else there exists a linear combination of two eigenvectors, corresponding to two distinct pairs of eigenvalues, say g, such that $\psi(g) = \psi(f)$ and ψ is stationary at g. Also a stationary value of $\psi(f)$ is

$$\left\{\frac{r\left(\lambda_i^s\mu_j^r - \lambda_j^s\mu_i^r\right)}{(s-r)\left(\mu_i^r - \mu_j^r\right)}\right\}^{1/s} \left\{\frac{s\left(\lambda_i^s\mu_j^r - \lambda_j^s\mu_i^r\right)}{(s-r)\left(\lambda_i^s - \lambda_j^s\right)}\right\}^{-1/r}$$

where (λ_i, μ_i) and (λ_j, μ_j) are the two distinct pairs of eigenvalues of A and B referred to above.

Proof : It can be shown that if f is a stationary vector of $\psi(f)$ it satisfies the following equation

$$rb^r A^s f - sa^s B^r f + (s-r)\, a^s b^r f = 0. \tag{8}$$

where $a^s = (A^s f, f)$, $b^r = (B^r f, f)$ $\|f\| = 1$. Substituting $A^s f = \Sigma \lambda_i^s (f, e_i)\, e_i$, and $B^r f = \Sigma \mu_i^r (f, e_i)\, e_i$ in (8) we get

$$rb^r \lambda_i^s - sa^s \mu_i^r + (s-r)\, a^s b^r = 0. \tag{9}$$

if $(f, e_i) \neq 0$. If f is an eigenvector then eqn. (8) is satisfied, for which $a = \lambda_i$ and $b = \mu_i$, where (λ_i, μ_i) is the corresponding pair of eigenvalues.

If f is not an eigenvector then the following cases arise.

Case 1 : Eqn. (9) is satisfied by only two pairs of (λ_i, μ_i), in which case f is a linear combination of the corresponding eigenvectors.

Case 2 : Eqn. (9) is satisfied by more than two pairs of (λ_i, μ_i), then f is a linear combination of more than two eigenvectors corresponding to distinct pairs of eigenvalues. Proceeding as in the previous theorem we can show, that there always exists a suitable linear combination g, of eigenvectors corresponding to the distinct pairs (λ_i, μ_i) and (λ_j, μ_j) such that $\psi(g) = \psi(f)$ and ψ is stationary at g. Also the stationary value of $\psi(f)$ can be calculated similarly.

Corollary 1 : If $B = A$, $r = -1$, $s = 1$, the Kantorovich inequality follows (see Greub and Rheinboldt[14], and Kantorovich[15]).

Corollary 2 : If $B = A$, Mond-Shisha inequality follows.

Corollary 3 : By taking $P(A)$ and $Q(A)$ in place of A and B respectively in $\psi(f)$, where $P(A)$ and $Q(A)$ are polynomials in A of the same degree, with positive coefficients so that $P(A) > 0$, $Q(A) > 0$, we get the stationary values of $(P(A)^s f, f)^{1/s} / (Q(A)^r f, f)^{1/r}$ which is given by

$$\left[\frac{r\left\{P(\lambda_i)^s Q(\lambda_j)^r - P(\lambda_j)^s Q(\lambda_i)^r\right\}}{(s-r)\left\{Q(\lambda_i)^r - Q(\lambda_j)^r\right\}}\right]^{1/s} \left[\frac{s\left\{P(\lambda_i)^s Q(\lambda_j)^r - P(\lambda_j)^s Q(\lambda_i)^r\right\}}{(s-r)\left\{P(\lambda_i)^s - P(\lambda_j)^s\right\}}\right]^{-1/r}$$

Thus we have extended the Mond-Shisha inequality in two directions. In Theorem 3 we considered a strictly accretive normal operator A in place of a selfadjoint

operator A whereas in Theorem 4 we considered two selfadjoint operators A and B in place of a selfadjoint operator A. Since positive operator comes as a particular case of strictly accretive normal operator so Mond-Shisha inequality follows from Theorem 3 and the same inequality follows from Theorem 4 by taking $A = B$ in Theorem 4.

Acknowledgments

Authors thank Professor T.K. Mukherjee for his valuable suggestions while preparing this paper.

References

1. Hardy, G H , Littlehood, J E. & Polya, G (1952) *Inequalities*, 2nd ed. Cambridge Univ Press
2. Beckenbach, E F. & Bellman, R (1961) *Inequalities*, Springer-Verlag.
3 Cargo, G T & Shisha, O. (1962) *J Res Nat Bur Standards* **66** . 169
4 Mond, B & Shisha, O (1970) *Inequalities II*, Oved Shisha e , Academic Press NY and London, p 241
5. Mond, B. & Pecaric, J. (1993) *Houston J Math* **19** : 405
6 Mond, B. & Pecaric, J. (1993) *Indian J Math* **35** : 121
7. Mond, B. & Pecaric, J. (1994) *Rev Anal Numer Theor Approx (Cluj-Napoc)* **23** 179.
8. Mond, B & Pecaric, J. (199[illegible] *Anal Univ Timsoara* **31** . 223
9 Mond, B. & Pecaric, J (1994) *Houston J Math* **20** : 645
10. Mond, B. & Pecaric, J. (1995) *Houston J Math* **21** . 103.
11 Mond, B. & Pecaric, J. (1995) *Houston J Math* **21** : 739
12 Das Kiran Chandra (1974) *J Math Anal Appl.* **48** : 527.
13. Das, K.C., Das, Gupta, M. & Paul, K. (1998) *Internat J Math, and Sci.* **21** 761.
14 Greub, W & Rheinboldt, W. (1959) *Proc Amer Math Soc* **10** . 407
15. Kantorovich, L.V. (1948) *Uspehi Mat Nauk.* **3** . 89. Translated from the Russian by Curtis D. Benster, National Bureau of Standards. Report No. 1509, March 7, 1952 In particular p 106.

PROC. NAT. ACAD. SCI. INDIA, 74 (A), II, 2004

Earthquake predictions using geoelectrical precursors*

P. N. NAYAK

Formerly in Geological Survey of India, Kolkata, India.

Address: 464, Nayapalli (Nuasahi), Bhubaneswar-751 012, India, Tel· 0674-2408871

Received December 12, 2002; Accepted May, 12 2003

Abstract

Earth current variations related to earthquakes have been reported since the late 19th century One of the earliest reports pertain to 1872 Bhavnagar earthquake which was preceded by strong currents flowing through telegraph lines. The other case involves the 1897 Great Assam Earthquake when the telegraph operators at Shillong experienced strong electric shocks prior to the incidence of aftershocks in the Meghalaya plateau. In that plateau, hundreds of millivolts of electromechanical potentials observed on hills showed significant changes prior to earthquakes in nineteen eighties The Russian scientists predicted many earthquakes in Kamchatka area analysing variations of earth currents and they also detected pressure induced polarization while rupturing large granite samples in the laboratory A programme based on the seismo-electrical signals predicted 18 out of 23 earthquakes in Greece. In China, the variations of geopotentials were used to predict the M 7.3 1975 Haicheng and many other earthquakes However, the natural ground potentials are vitiated by rains, extraterrestrial and man made cultural noises unlike the georesistivity methods where the noises can be filtered out

The georesistivity investigations conducted by the geoscientists on the San Andreas fault, California and Garm region, Tadzhik republic since the nineteen seventies near the focal points using powerful deep resistivity units probing to depths of kilometers have shown that the rock resistivities decrease to a large extent before earthquakes. This has been corroborated by the results of rock fracturing experiments in America They lead to enunciation of dilatancy-diffusion models.

The Chinese scientists have been monitoring the variation of earth resistivities covering the seismically active northern parts of their country by a network of more than 100 geoelectric stations. They have also conducted *in situ* experiments to relate minor changes in strains to the pattern of changes in resistivities of rocks. Based on the observed georesistivity precursors to more than 30 strong events over 25 years, they have developed travel time curves for the front of resistivity anomalies to locate the would be epicenters of the impending earthquakes They have deduced the magnitudes of the earthquakes in advance from three different parameters

*This paper is dedicated to the memory of people who died in 26th January, 2001 Bhuj Earthquake

such as the duration of the precursor, length of total anomalous area and maximum amplitude of the anomaly at the epicenter It has been possible to determine the medium term, short term and imminent stages of earthquakes from the trends of georesistivity anomalies. The imminent time of the earthquake has been determined from the appearance of the resistivity pulses induced by crustal tides of weakened crust on the verge of breaking supplemented by sharp changes in the self potentials

At sensitive sites selected on geological and geophysical considerations in Shillong and Nagpur, the monitored earth resistivities have been observed to change and return to pre-anomaly level immediately before earthquakes occurring at 40 to 400 km from the sites The maximum change in magnitude of resistivities has been shown to be proportional to the hypocentral distance

It is possible to integrate the methods developed by the Chinese and Japanese scientists with the indigenous methods and predict earthquakes in India using simple instruments.

(**Keywords** . earthquakes/geoelectrical precursors)

Introduction

Earthquakes are generally caused by sudden movement within the lithosphere to release the strain that accumulates gradually over a period. The high pressure conditions and strains developing in the focal regions before and during earthquakes manifest themselves in changes of physical parameters of rocks and can be measured in the epicentral regions as well as at sites on ground surface several kilometers away from the epicenter. These parameters include seismic velocities, magnetism, self-potentials, electrical resistivities, radon concentrations, land deformation, tilt and strain and geohydrological conditions[1]. The changes in these parameters have been monitored to predict earthquakes by many geoscientists. In this paper, the discussions will be restricted to geoelectrical (earth resistivities and self potentials) indications as they have been found to be more effective in forecasting earthquakes in China[2], Japan[3], Greece[4], erstwhile USSR [5,6], USA[7] and also in India[8]. These studies are important for our country as six disastrous earthquakes have occurred during the thirteen years between 1988 and 2001. The earthquake striking Bihar Nepal border on 20th August, 1988 killed 1000 people. This was followed by the Uttarakashi earthquake on 20th October, 1991 with a death toll of more than 1000 people. The 30th September 1993 Latur earthquake damaged nearly 4000 houses killing 9000 and injuring 20,000 people. The death tolls were 43 and 110 in 22nd May, 1997 Jabalpur and 23rd April 1999 Chamoli earthquakes respectively. The 26th January, 2001 Bhuj earthquake demolished lacs of houses killing 195000 and injuring 17,000 people. It is true that loss of life and property can be minimized by insisting on construction of

earthquake resistant buildings, but it is not possible to replace or strengthen all the weak buildings in crowded cities located in earthquake prone belts of this poor country in near future. Hence, there is an urgent need to predict earthquakes.

The seismic zoning map of India proposed on the basis of past earthquakes, seismicity and geological features is a process of forecasting the risk factors and indirectly earthquakes. The same process can be improved and supplemented by information regarding the ground conditions based on direct measurement of parameters to identify the vulnerable areas where earthquakes are likely to occur so that proper arrangements can be made in advance to mitigate the sufferings of the people. The objective of this paper is to describe some significant observations and relevant experiments carried out in the laboratory and in the field and highlight the fact that earthquakes can be predicted through scientific methods.

In the self potential method, the potential difference is measured between two fixed electrodes using sensitive voltmeters or potentiometers to detect the electrical signals related to earthquakes. Unfortunately, these signals are vitiated by artificial or cultural noises such as leakage from power lines, and natural noises such as rainfall, solar flares and ionospheric currents. In contrast, resistivity methods employs an array of four or more electrodes. While current is passed into ground through a pair of buried electodes, the potential difference induced by electric field is simultaneously measured by other pair of electrodes. By varying the magnitude of current and frequency, the extraneous noise can be effectively eliminated. Hence, the earth resistivity methods are considered superior to the SP method. It is always desirable to work at sites away from the towns and combine these two methods as far as possible.

Earthquake related Geoelectric Potentials

Old classic cases : Yamazaki[3] has summarized many classical and modern reports pertaining to relation between natural ground potentials and earthquakes. According to him, the Indian (Bhavnagar) earthquake of 14th December, 1872 was the first which was reported to induce strong currents through telegraph line connecting Valentia with London just before the event. Intensive studies on earth potentials were carried out in Japan by Noto in the nineteen thirties and subsequently by Yoshimatsu in the nineteen forties and fifties. They observed significant changes in earth potentials associated with earthquakes. The studies were followed up by the Earthquake Research Institute, Japan in the nineteen sixties. Rikitake and others buried spiral lead tubes in the ground at depths of about 1m keeping the distances between the N-S and E-W pairs of electrodes 64m and 72m respectively. They observed a sudden change in earth

potentials for an earthquake of magnitude 5 centered at Matushiro on 23rd November, 1965, While the N-S pair of electrodes recorded 22 millivolts, the E-W pair recorded 30 millivolts of earth potentials.

SP studies in Kamchatka area

In Kamchatka area, Fedotov *et. al.*[9] observed earth-potentials as large as 50mV/km several hours prior to earthquake as well during the events between September 1967 and February, 1968. According to them, anomalous geoelectric potentials might be related to stress variations that caused piezo-electric effects in rocks at the focal regions. In the same area, Sobolev[6] took continuous observations of electrotelluric field as a part of prediction studies. Potential differences were monitored at six stations along N-S and E-W directions maintaining a separation of 200m between the pairs of electrodes. They observed changes varying from 8 to 13 millivolts in geoelectric potential about one week before a deep earthquake of magnitude 6 at a distance of about 250 km on 27.05.1972. Sobolev could predict 8 out of 12 earthquakes combining earth current observations with seismic wave velocities and statistical analysis. Later, Sobolev *et. al.*[10] carried out experiments in laboratories rupturing large granite samples and observed that the samples emit transient electric current before rupture. Varotsos and Alexopoulos[4] explain that the transient electric current comes from the orientation of the dipoles due to pressure induced polarization under changing stress on rocks at the focal regions.

SP monitoring in Haicheng and Tangshan (China)

An abnormal earth potential change was observed at a site about 20 km from Haicheng (China) before the M 7.3 earthquake on 4th February, 1975. The equipment comprised two pairs of electrodes one of copper and other of graphite buried at a depth of about 1m with a separation of 50m for E-W and 60 m for N-S electrodes. A group of geophysicists experienced in electrical prospecting monitored the potential differences using a self balancing potentiometer. As shown in Fig. 1a, the potential differences gradually increased to 170 mV for the N-S pair of electrodes. It is remarkable that the differences decreased to –90 mV the day before the earthquake (Fig. 1b), and then suddenly increased to zero before the shock. The sharp changes observed on 2nd and 3rd February, 1975 were accompanied by foreshocks and the earthquake was successfully predicted.

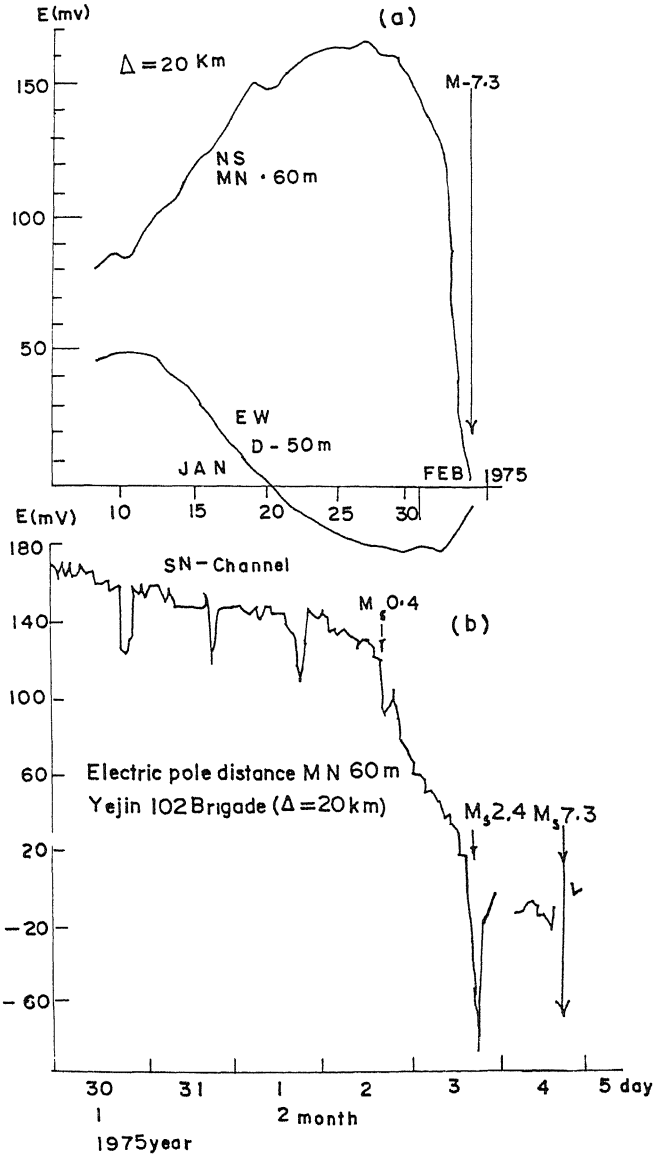

Fig. 1(a) Geoelectrical potentials observed at dist. 20 km from Haicheng (China) from 5th January to 5th February 1975 before M 7.3 4th February 1975 Haicheng earthquake; (b) The kinks on detailed graph on 2nd and 3rd February 1975 related to foreshocks. The sharp decrease of potentials started on 2nd February. This decrease and foreshocks helped in predicting earthquake (after Zhao *et. al*, 1996).

Besides the work done by experienced geophysicists many amateurs participated in the programme. At every site, the amateurs buried two pairs of electrodes of dissimilar materials in N-S and E-W arrays as reported by the U.S Haicheng Earthquake Study Delegation. They monitored telluric currents using microammeters and helped the scientists. Fig 2 shows the self potentials observed at the station Xiji in the N-S and E-W channels The sharp changes and slow recoveries are attributed to the disposition of faults in the vicinity of the station in relation to the movement of fluid due to the M 7.8 July 1976 Tangshan earthquake[24].

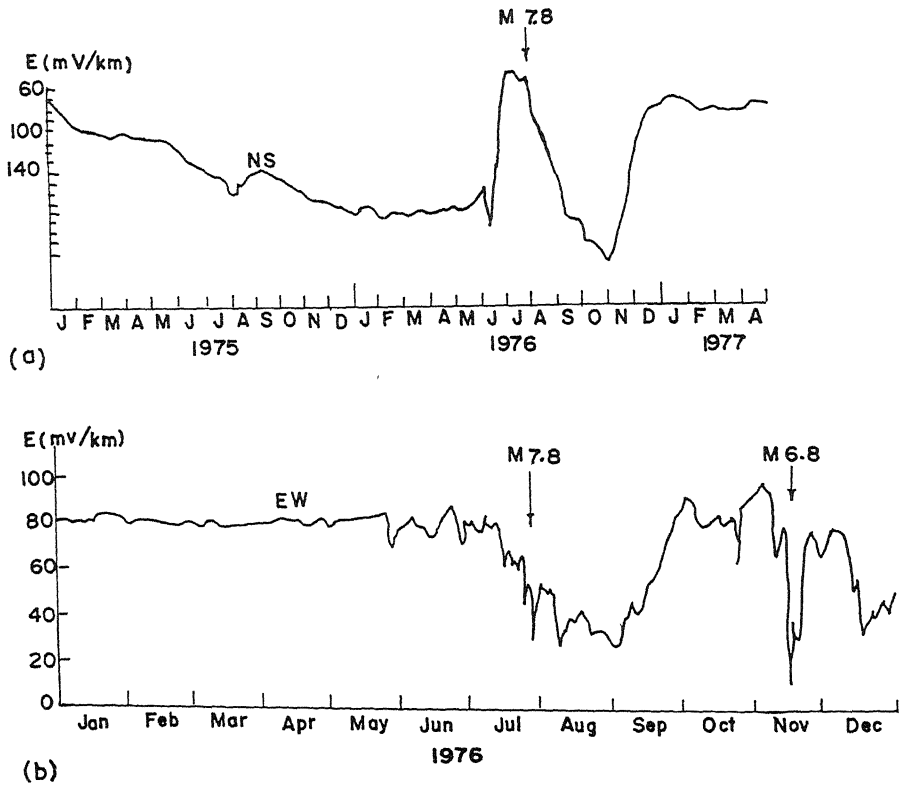

Fig 2 (a) The self-potentials in N-S channel were observed at the station Xiji from January 1975 to April 1977. Mark the anomalous sharp change in S.P. before M 7.8 Tangshan (China) earthquake; (b) S.P. in the E-W channel at the same station showed decrease. (after Zhao *et. al.*, 1997).

Seismic electrical signals in Greece

The changes in seismic electrical signal of the earth preceding earthquakes were studied in a network of 18 stations in Greece between 1981 and 1984 for earthquakes with magnitudes from 3.2 to 6.8[4]. The electric field beyond the usual disturbances due to atmospheric and magnetic storms was observed measuring the potential differences between two pairs of electrodes in E-W and N-S directions at each station. A pair of brass (or lead or non-polarized) electrodes were buried at depths of about 2m at separations varying from 30 to 200m. The stations were installed as far as possible from electric power sources to keep the cultural noise less than 0.2 mV. The potential differences observed at stations telemetrically connected to a center located at Glyfada about 15 km from Athens were measured after amplifying and filtering out frequencies higher than 0.3 Hz and depicted in multipen recorders or strip chart recorders with speeds varying 1-20 cm/h for each pair separately.

The precursor seismic signals occurred 6-115 h before the earthquakes and had duration varying from 1-90 min. The signals appeared as transient changes of the potential differences between the electrode pairs measuring upto a few millivolts which are related to magnitude of earthquakes, epicentral distances and local inhomogeneities. Fig. 3 shows the seismic electric signal recorded at PIR-station at 20-50 GMT on 17th February 1983. After about 56 h, an earthquake M4.8 occurred at a distance of about 10$\pm$5 km from the station.

The current density in a particular direction was determined dividing the change of potential differences with a suitable effective resistivity. Measurements and calculations in two directions (E-W, N-S) gave the relative signal densities at that station. Considering that the signals are inversely proportional to the epicentral distances, the epicenter was located using the relative signal densities with an accuracy of 100 km. The magnitude of earthquake was deduced empirically with an accuracy of 0.6 units considering the relative signal densities and distances. Varotsos and Alexopoulos (1984)[4] predicted 21 out of 23 events with magnitudes more than 5.

Electromechanical potentials of Shillong Plateau

Geoelectrical potentials were monitored over a hillock located in the reserve forest near Shillong from February to August, 1980. The site was selected on the basis of results of a systematic geophysical investigation carried out to detect occurrence of sulphide bearing rocks. High negative potentials were observed over quartzites

exposed on hill and the S.P profiles appeared like reflected images of the hills. The magnitude of potential in the vicinity of a peak point of a hill at a height of 1520m was – 1940 mV[23]. The quartzites strike NE-SW and dip steeply towards south near the site. Since these rocks characterised by very high resistivities are devoid of graphite and sulphides as proved by drilling, the self potentials appeared to be caused by electromechanical properties of rocks[11].

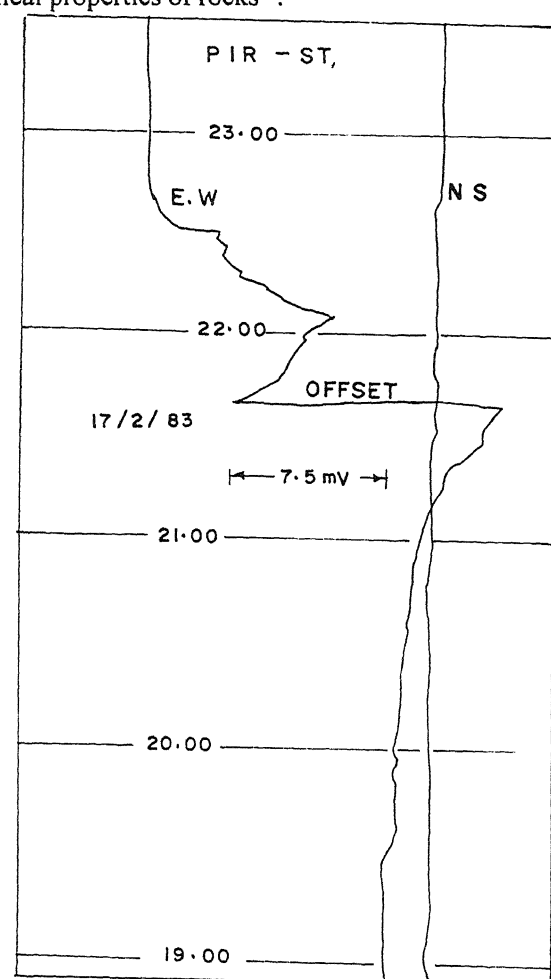

Fig. 3 (a)–A strong seismoelectrical signal recorded on E-W channel (L-50m) at PIR Greece on 17th February 1983. It is a precursor to M 4.8 earthquake that occurred at 05 45 hrs on 20th February 1983 with its epicenter close to the station (after Varotsos andf Alexopoulos, 1984).

The high electromechanical potentials were monitored keeping one potential electrode at the center of negative potential and the other electrode in a valley at a slope distance of 350m. As shown in Fig. 4, the potential difference decreased from 1500 mV on 2-3-1980 to 1340 mV on 9-3-1980. An earthquake of 4.5 occurred on 9-3-80 at a distance of 55 km from the station, and after that the self-potentials increased. It is rather difficult to correlate the trend of anomaly with the instant of the

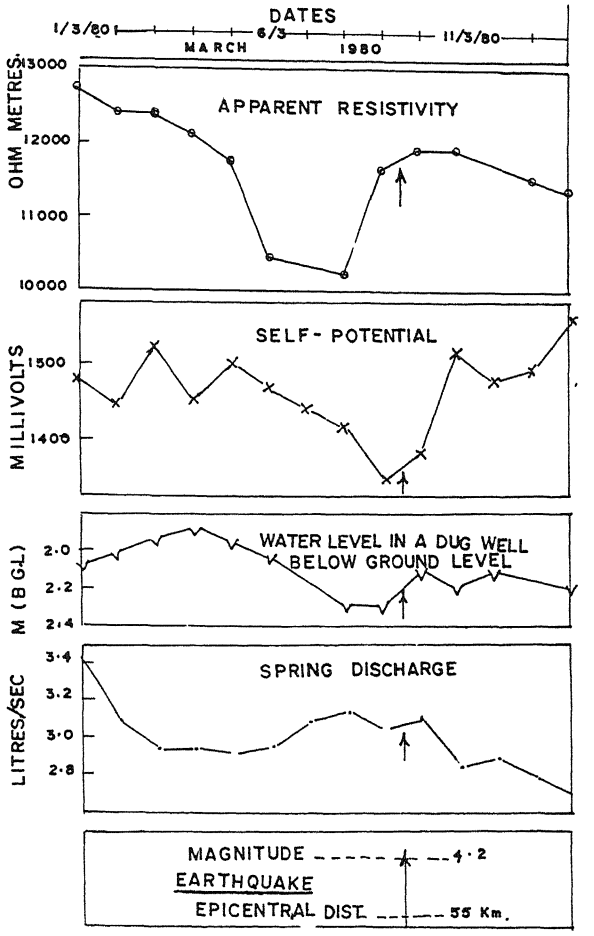

Fig 4– Variation of apparent resistivity, self-potential, water level in a dugwell and rate of spring discharge before M 4 2 earthquake near Shillong (Nayak *et al* 1983) The earthquake occurred when resistivities approached pre-anomaly level and S.P. was low

earthquake, as measurement was taken only once daily. The potentials returned to the pre-anomaly level 4 days after that event. Another earthquake related potential change was observed for the earthquake that was felt in the area on 26-4-1980. No clear correlation was observed during the rainy season when the potential difference decreased to 900 mV.

The electromechanical potentials are generally due to formation of a double layer of ions at the interface of the mineral particles and liquid. The potential difference is caused by displacement of the liquid phase of the double layer or movement of water through arenaceous rocks[11,12]. It was envisaged that the height and steep slopes on the hill flanks provide hydraulic gradients for movement of water through permeable formations causing large potential difference. Although this phenomenon has been observed at other places, the magnitudes are much less than that at Shillong. This high earth potential may also be caused by electrification of rocks either due to piezo-electric effects[9] associated with an earthquake or electro-elastic effects associated with an earthquake source[1]. It cannot be ruled out in this seismically active area where as many as 25-30 micro-earthquakes are recorded per day with about 2 medium events per month. In this context, it is worthwhile to quote from the classic work by Oldham[13] in his memoir on the Great Assam Earthquake of 12th June, 1897. "Telegraph workers experienced many electric shocks, some of them of considerable severity. Nearly all these shocks were preceded, but more often followed by an earth tremor, which rendered it impossible to utilize the earth as a return path for the current. The intensity of these currents was too great for them to be explained as a purely mechanical results of the disturbance of soil in contact with the earth plates. Though this is known to produce slight electric currents, the cause must be looked for at greater depth and more directly connected with the origin of the disturbances".

It is necessary to investigate the change in geoelectric potential related to the earthquake, whether it is entirely due to the charged rocks at the focus or due to changes of characteristics of rocks at the measuring station by taking simultaneous observations at a number of sites. If it is due to the former, the magnitude of change in potentials will be inversely proportional to the distance from the epicenter as in Greece. If it is due to the latter phenomenon, the magnitude of S.P. will depend on the rock type and hillocks irrespective of the distance from the hypocenter.

Results of Experiments on Georesistivities under Controlled Conditions

(1) Changes in electrical resistivities as a function of compressive stress in many crystalline rocks were observed by Brace and Orange[14]. The samples were subjected

to confining pressure upto 5 kb and to pore pressure of water of 500 bars. In majority of rocks, resistivity increased slightly upto about half the fracture stress. Beyond half and within 20 percent of the fracture stress, resistivity dropped sharply becoming one tenth of the initial value corresponding closely to an increase in porosity or dilatancy which took place under compressive stress. According to them, at low compressive stress, all cracks are closed resulting in decrease of the conducting paths, and hence the resistivity of rock samples increase. At stresses, prior to the fracture stresses, new cracks form in the compressed rocks and the electrical resistivity of rock sample decreases if conducting fluids fill these cracks. In another set of laboratory experiments Brace showed that the changes in rock resistivities in the focal region are entirely due to dilatant volume and not due to liquid to vapour transition of pore fluid as envisaged by some workers.

(2) Scholz[15] showed through experimental study of fracturing process in brittle rocks that at about 92% of the fracture stress, a rapid acceleration of microfracturing occurs, and there is marked clustering of microfractures on the eventual fault plane. This suggests that there is increase of stress along the potential fault plane and relaxation at other points immediately before the onset of fracture and movement. It may help in indicating the time and place of imminent fracture.

(3) Rikitake[16] observed a certain relationship between changes in earth resistivity and earth strain caused by tidal loading in 1952. Yamazaki[3] undertook compression tests in the laboratory in 1965 which revealed that resistivity changes are larger than the mechanical strain by a factor several hundred particularly for porous and permeable rocks. He suspected that the contact section between the pores increases when the specimen is compressed giving rise to tremendous increase in the conductivity.

(4) Zhao *et. al.*[17] conducted *in situ* experiments in the field to determine the relationship between the strains of partially saturated soils to the variations of the resistivities. They applied horizontal pressure on walls of soil layers in trenches. Two hydraulic spiral jacks of 10-20 tons were used to exert pressure through steel plates on thick boards fixed to the walls of the trenches (Fig. 5a). To study resistivity changes of extended (bent) soil layers, two long parallel trenches were dug through soil layer and a bending moment was exerted on the soil body between the two trenches (Fig. 5b).To study the resistivity changes due to compression on rock layer, they selected a tunnel at depths of 100-200 m (Fig. 5c). The compressional stress was exerted vertically or horizontally by jacks on arenaceous limestones and electrodes were fixed on the side walls of the tunnels.

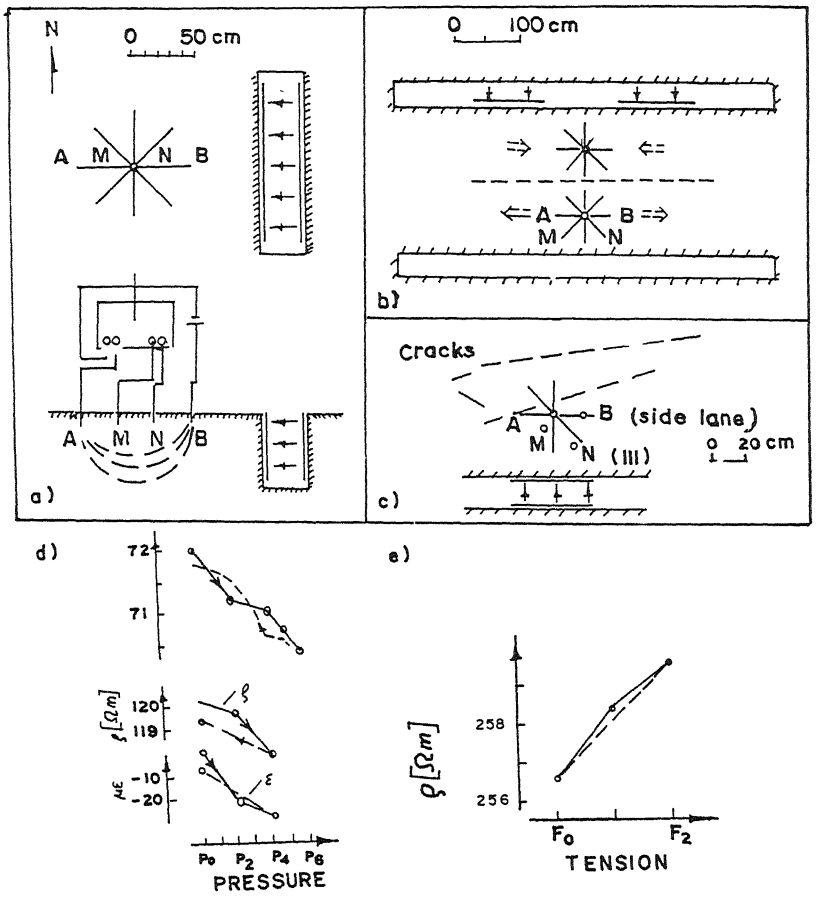

Fig. 5–Schematic diagram of the experimental set-up using jack as a loader (the arrows represent the force source in the area (ANMB-the electric system). (a) Schematic diagram illustrating the loading of soil layer, and the vertical view (top) and sectional view (bottom) of the electrode arrangement. (b) Measurement points in the bending of soil layer experiment (c) The arrangement for measurement on the rock layer in a tunnel with cracks on side walls in the compressional experiment using jack as a loader (circle denotes the location of strain gauge) Fig (d) & (e) The resistivity on soil decreases with increase of pressure and *vice-versa* (after Zhao *et al*, 1990)

To measure the strain, a rubber plug with an inner strain gauge was buried at depth of 22.5 cm at the center of the four electode system sticking the resistant strain

gauge on an intact part of the rock surface. The distance between the electrodes varied from 0.9 to 1.5m so that the deformation was uniform inside the volume of soil/rock to be tested. At each measuring point 3-4 profiles parallel, perpendicular and at 45^0 angles to the pressure direction (Fig 5a) were taken.

Zhao *et al.*[17] observed that resistivity decreases (or increases) when the soil layer is compressed (or dilated) The relative resistivity variation is sensitive to strain changes, and smaller the strain, the higher is the amplification factor The resistivity change is directly proportional to intensity of force, size of the source, but inversely proportional to the distance between the source and measuring point The resistivity change shows a delay as this distance increases. It was also observed that the isotropic soil layers develop resistivity anisotropy due to stress. The resistivity decreases on contraction and increases with extension of the volume under testing (Fig. 5d & e)

The experiments are very useful to understand the apparently anomalous phenomenon such as simultaneous increase and decrease of resistivities before earthquakes, appearance of anisotropy at the measuring point and propagation of anomalies from the epicenter. The experimental results have shown that the resistivities are very sensitive to changes in strain, and the area of the anomalous zone increases with increase of force at the focal region. It also explains the phenomenon observed in Japan by the Yamazaki variometer[3] for earthquakes at teleseismic distances. Most importantly, the experiment proves that georesistivity variations are dependable precursors to tectonic earthquakes.

Field Investigations on Geogesistivity Precursors

As a sequel to the rock fracturing experiments in laboratories, geophysicists attempted to investigate the temporal variations of the resistivities of the crustal rocks prior to earthquakes under actual field conditions. They were aware that the success of the study depends on the location, depth and dimension of the hypocenters. The length of the slipped fault plane is known to vary from about one km in case of magnitude 4 to about 500 km in case of 8.5 magnitude earthquakes. In spite of uncertainties about location of focii, early investigations were carried out at a few sites, over active fault zones in Garm regions. Tadzhik republic and San Andreas fault, California, USA. In contrast, the Chinese geoscientists monitored earth resistivities at more than 100 sites in the earthquake prone northern China to detect the anomalous focal zones and then

to plan intensive measurements to study the precursors of earthquakes. The results of these studies have been summarized in the following paragraphs.

Observations close to the hypocentral regions

In the Garm district of Tadzhik republic, the apparent resistivities of the crustal rocks were measured employing a modified dipole-dipole configuration of electrodes. While the electric pulses of about 100 amperes amplitude were passed into the ground through a pair of current electrodes[5], the potential differences due to this current were measured by a pair of electodes at about 6 km from the current dipoles. The ratio of the voltage observed by the potential electrodes to the electric current reflects the apparent resistivities. The relative or apparent resistivities assuming the value of 30-6-67 as reference decreased prior to the occurrence of earthquakes. The maximum change of resistivities varying from 7-18 percent was observed to depend on the distance between the hypocenter of the earthquake and the center of the dipole unit. It was also observed that the magnitude of an impending earthquake is directly proportional to the total precursor time.

Mazzella and Morrison[7] measured apparent resistivities on the San Andreas fault, California deploying a deep resistivity unit comprising of 85 kW generator, a switching rectifier bridge and receivers. The electrodes comprising of aluminium plates were buried in pits and the current dipoles were separated by a distance of 1.5 km. Out of the potential electrodes, one pair was kept at a distance of about 1.5 km to the north east of current dipoles The 2nd pair of potential electrode was kept at a distance of about 10 km to the South west of the current dipoles. The 3rd pair was kept at 15 km to the South west, i.e., about 5 km from the 2nd pair. The arrays of electrodes were arranged along NW-SE direction across the fault plane. A square wave current with an amplitude of 200 A and a period of 10s was passed into ground, and the potential differences were measured by the receivers. Measurements were carried out from January, 1973 to February, 1974. Precursory changes of about 20 percent in the resistivity preceded the magnitude 3.8 earthquake on 22nd June, 1973. These changes started since middle of April, 1973. Another activity occurred 8-13 October, but no significant changes were observed.

The above measurements at Park Field have been continued until the present time, but no significant variations due to earthquakes have been noticed. This leads to the conclusion that any possible changes are below the detection level[18]. Considering the

resistivity and other precursors, Scholz *et.al.*[15] proposed dilatancy diffusion model in which diffusion of water into the dilatant volume is envisaged and earthquake occurs near the maximum stress. According to another model proposed by Myachkin *et al* [19] no diffusion of water is required and in this model, earthquake occurs after the pre-anomaly level is reached during a period of falling stress.

Georesistivity precursors in China

The Chinese scientists started an elaborate programme of systematic geoelectrical investigation establishing a national network of 14 stations in 1966, which increased to more than 100 permanent stations in northern China by 1994[2]. They set up additional stations to cover the anomalous areas where impending earthquakes are suspected. They carry out repetitive measurements once daily increasing the frequency to 6 times per day or continuous if required to study the effects of crustal tides.

In China, georesistivity and geopotential methods have been accepted as most effective and powerful techniques for predicting earthquakes. They studied more than 30 geoelectric precursors to strong earthquakes. The M 7.3 Haicheng event on 4th February, 1975 (the first major earthquake to be successfully predicted), M 6.7 Xiaojin event on 22nd September, 1989 and the M 6.2 Zhang Hei event on 10th January, 1998 were successfully predicted to their credit. The M 7.8 Tangshan event of 28th July, 1976 was thoroughly investigated, the suspected epicenter was visited (Zhao, personal communication), but this disastrous earthquake was not predicted for reasons not disclosed yet. However, the wealth of data collected before during and after the event has provided insight for refining the interpretation techniques to predict other earthquakes.

In Beijing-Tangshan area within a length of 150 km 8 out of 11 stations showed persistent decrease, 2 stations showed increase and one station did not show any change in the resistivities over a period of 3 years preceding the 1976 Tangshan event. The change with greater amplitude appeared earliest around the epicentral zone. The anomalies advanced outward with progressively decreasing amplitude from the epicenter to the surrounding areas and the maximum amplitude at every station could be contoured on a map. According to Zhao *et. al.*[20], the decrease reflects the process of strain accumulation in the area. As shown in Fig. 6, the resistivity anomalies appeared late 1973 at Tangshan and Changli (distance-70 km), but after about 3 months at Baodi (distance-80 km).

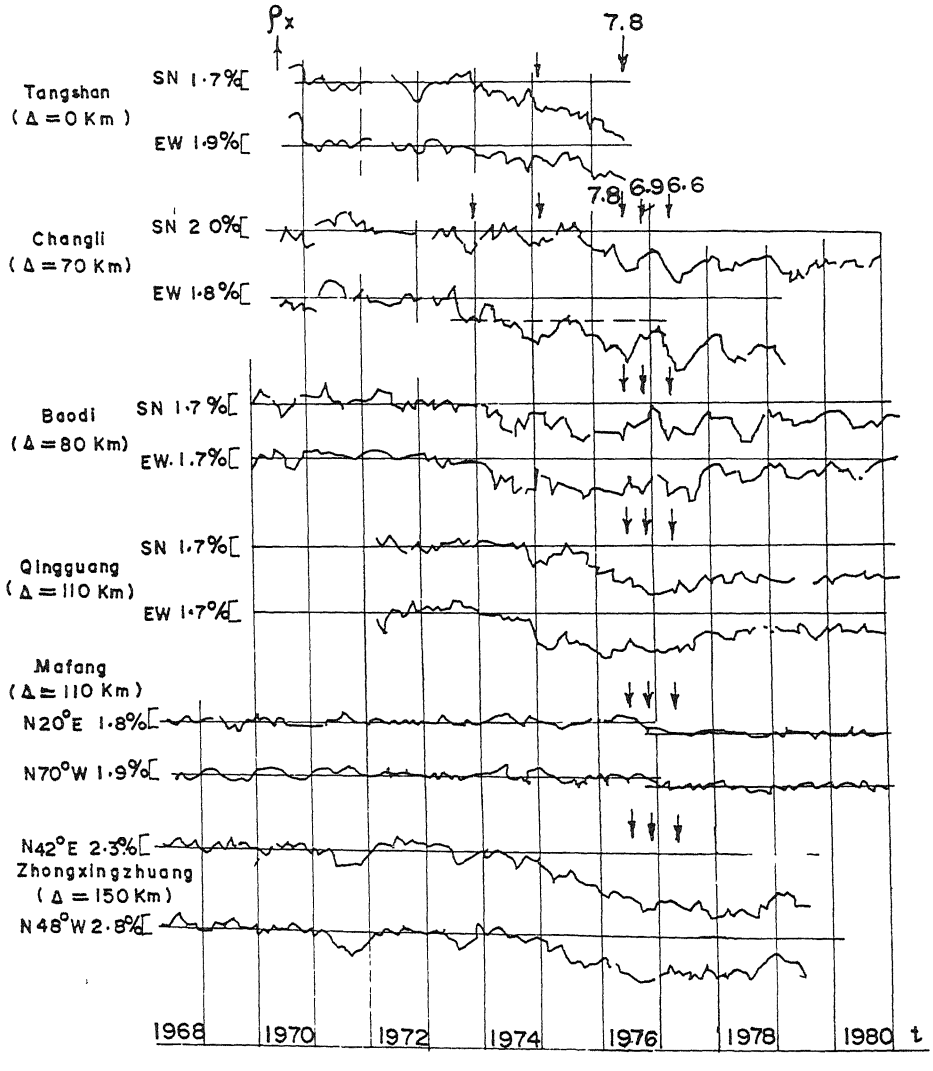

Fig. 6–Graph of monthly anomalies in resistitivities recorded continuously at six stations around the M. 7.8 Tangshan (China) earthquake epicenter. The resistivity decreases were detected after middle of 1973 near the epicentral area. The anomalies were observed by the end of 1974 at QG and ZXZ stations located 110 and 150 Kms from the epicenter (after Zhao *et. al*, 1994).

In a new area, the pattern of migration of the anomalies can indicate the location of the would-be epicenter Analysing the pattern for many strong earthquakes, Zhao *et al.*[4] have prepared a travel time curve for the front of resistivity precursors (Fig 10b) that can be used to locate the epicenter using the travel time or duration of onset of anomalies observed at three or more stations using the simple technique of intersection of circles

The scientists computed the magnitude of impending earthquake using the empirical formulae one each for three parameters namely total duration of the anomaly observed at the epicenter, ratio of maximum change in resistivity anomaly to pre-anomaly value, and the distance to the farthest station where anomaly was detected from epicenter. These formulae have been given elsewhere in this paper.

The factor for predicting time has been divided into four stages. The long term stage depends on the characteristics of the deep crustal conductor mapped by magnetotelluric method, which is outside the purview of this paper. The second stage or medium term stage starts with appearance of resistivity precursor that develops rather slowly. It has been estimated to become about 5 percent over a period of 3 years or a rate of 5×10^{-5} per day. The speed of change increases with onset of short term stage. It was observed more than 3 months before the main Tangshan event when the rate increased from 5×10^{-5} to 6.7×10^{-4} per day. The rate increased further in imminent stage during the last 15 days and it was 3×10^{-3} as shown in Fig. 7[20]. During the imminent stages, the farthest stations exhibited recovery. At the last two stages, some stations showed anisotropy, i.e., while the resistivities increased in S-N direction, it decreased in E-W direction.

The critical or imminent stage is associated with some triggering phenomena. One of them is the sharp changes or kinks impressed on accelerated S.P. anomaly (Fig. 1). These features are accompanied by foreshocks. Under normal conditions, as in the case of Bhuj earthquake[21], it is difficult to discern the foreshocks. This is rendered simpler with awareness created by the geolectrical forerunners. Besides the resistivity (Fig. 7z) pulses apparently correlatable with lunar phases show large amplitudes, and at this stage, appearance of oil gushes in otherwise old abandoned wells were seen near Tangshan. In the final stage, SP may change abruptly before the shock.

The Chinese scientists believe that monitoring resistivity and self potential are not only simple methods for detecting stress-strain within the crust, but also effective techniques in the study of earthquake prediction. They caution that negative cases have been recorded, which has created trouble with predictions.

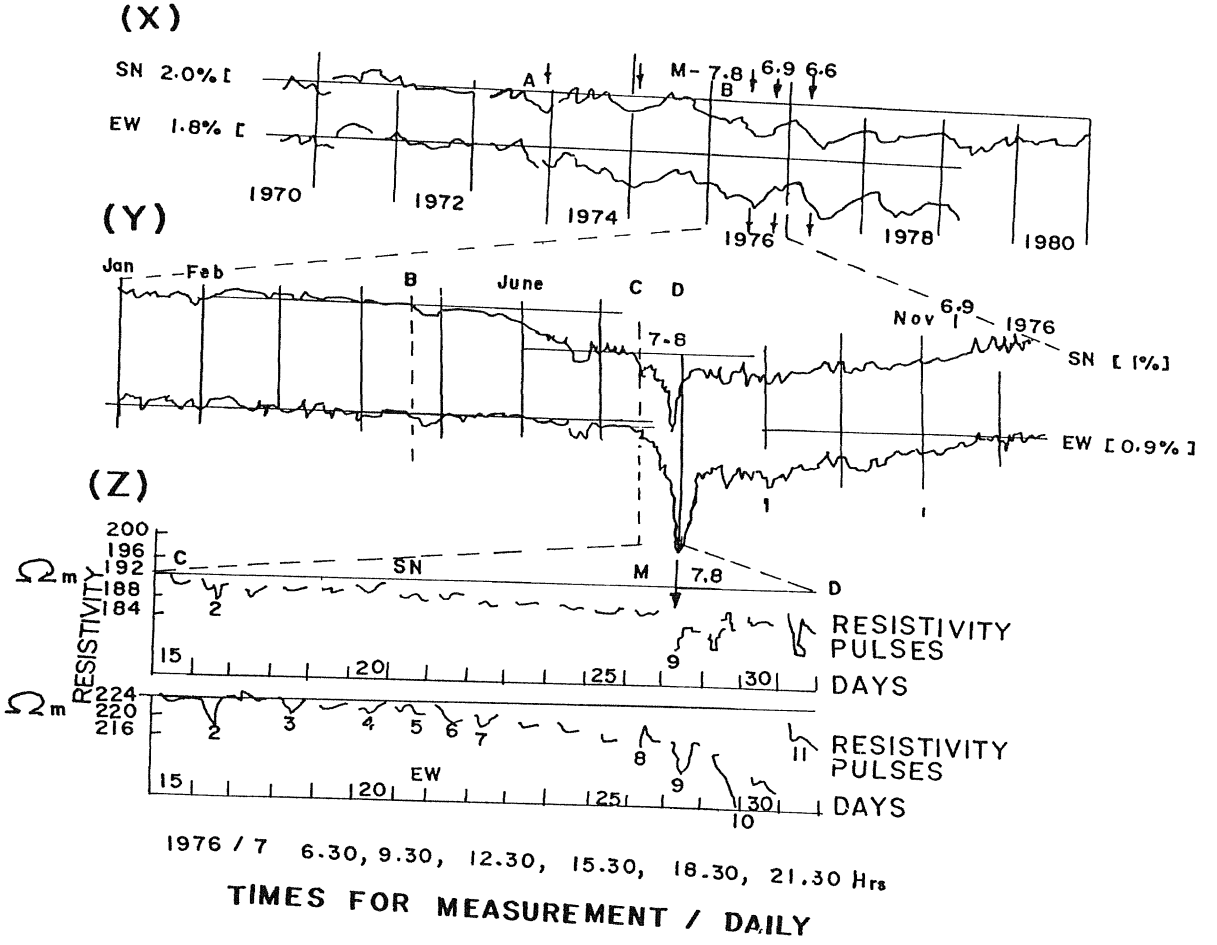

Fig 7–Temporal variation of earth resistivity at Changli station within epicentral zone before Tangshan earthquake. (X), (Y) and (Z) show variations of monthly, daily and resistivity pulses respectively. A to B - Medium term stage over 2 years B to C - Short term stage over a period of about 2 months. C to D - Imminent stage of earthquake The decrease of resistivity and large amplitude resistivity pulses indicated instant of impending earthquake

Georesistivity monitoring in Japan :

Continuous monitoring of electrical resistivities of rocks has been carried out by Yamazaki[3] and others in Japan using a very sensitive variometer since 14th May 1968. They have passed into ground alternating current having intensity of 100 ma at 250V and frequency 67 Hz. The current has been maintained at the odd frequency to avoid possible contamination by stray currents from commercial lines in Japan. The alternating current has been passed through a pair of outer electrodes in Wenner configuration of 4 electrodes while the inner pair of electrodes are used for measuring the potential difference. The system has been kept on tuffaceous rocks in a cave at a depth of 4.8 m below the ground surface, and electrode separation of 1.6 m has been used for measurements. The rate of resistivity change has been recorded continuously by a multi-channel plotting type recorder.

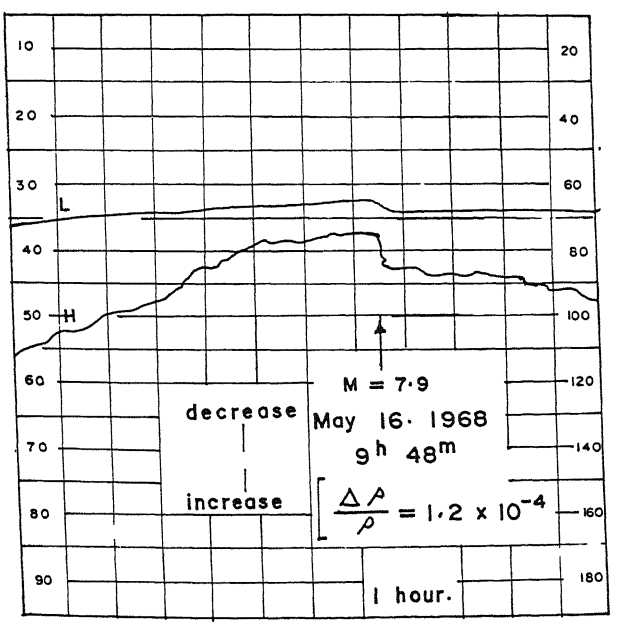

Fig. 8– Record by the Yamazaki variometer for co-seismic and precursory changes associated with a M 7.9 16th May 1968 earthquake in Japan. The epicenter is located at 800 km from the observation point. The step like change nearly coincides with the instant of earthquake (Yamazaki, 1977).

A rate of resistivity change of the order 10^{-4} has been observed corresponding to a strain value of the order 10^{-6} and hence with amplification factor of 10^{2}. They have observed more than 30 coseismic resistivity indications within 8 years period for earthquakes at epicentral distance varying from 60 to 1000 km. Fig. 8 shows a coseismic resistivity change for M 7 9 Tokachi-Oki earthquake on 16th May, 1968. The rate of change is 0.72×10^{-4} and about 300s are required to complete the change. The precursory resistivity change appears to start 4h preceding the main event. They have developed a method to determine the magnitude of the earthquake. They observed 12 increases and 18 decreases till 1977 in the trends of resistivities for the recorded events. This method can indicate the precursory changes hours in advance at teleseismic distance and intensive observation by a number of variometers can help in prediction of earthquakes.

Georesistivity monitoring near Shillong

The author and his colleagues carried out repetitive resistivity measurements on a hill in Shillong, Meghalaya as described under geoelectrical potentials in this paper. The measurements were started on 12-2-1980 with objectives to determine the tidal effects on rocks during the total solar eclipse on 16th February, 1980 and to study the georesistivity changes as related to earthquakes. The resistivities were measured using a potentiometer and accessories manufactured by Geological Survey of India powered by battery packs. Besides a Scintrex time domain 2.5 kW I.P unit powered by generator was used at the same site repeating observations passing currents at 400, 600 and 800 volts through a transmitter unit and measuring the potential difference by a receiver unit. The separation between the current electrodes along N 40^{0}W direction on the slope of the hillock was 380 m with potential electrodes separated by 40m ; and the current electrodes and potential electrodes along N20° E (strike direction of rocks) were separated by 120m and 20 m respectively. The measurements were continued for more than one year although the paper by Nayak *et. al.*[32] describes data upto August, 1980.

The resistivities decreased by about 25 percent in some cases and then increased to attain pre-anomaly level before earthquakes. Significant earthquakes were observed to occur when the resistivity values approached the normal level. As shown in Fig. 4, the resistivities decreased gradually and then rapidly from 12,800 Ωm to about 10,300 Ωm over a total period of 7 days starting from 1st March, 1980. An earthquake M 4.2

with its epicenter located approximately 55 km from the site occurred on 9th March, 1980 at a time when the resistivities were increasing. This trend was repeated for a few more events occurring at distance from 40 to 400 km. It was observed that the maximum change of the resistivity values is proportional to the hypocenter distance of earthquakes (Fig. 10a).

It was also observed that while the resistivity decreased at Shillong, the values increased for an array in a bowl like depression at a site about 80 km from shillong for a felt earthquake on 29th April, 1980.

Georesistivity monitoring in Maharastra

Nayak *et. al.*[22] took repetitive resistivity measurements at three sites across a prominent fault zone separating Gondwana rocks occurring in a depression from granite gneisses on a high ground all covered by basalts at Nagpur. The total spread lengths of 50m in Wenner configuration of electrodes were laid in the depression and on the high ground, whereas the spread length of 320m was laid near the edge of the inferred fault. The resistivities observed in July and August, 1991 showed increase of 54 percent (Fig. 9) in the depression, decrease of 7 percent on the fault edge and no change on the high ground. In Killari area of Maharastra, the apparent resistivities measured in the epicentral zone of M 6.3 disastrous earthquake of 30th September, 1993 showed significant changes before the medium magnitude and swarms of aftershocks.

The results of the above investigations suggest that the changes observed by repetitive resistivity measurements at sensitive sites can suggest the epicenter and time of earthquakes. Since the stations selected on the basis of their sensitivity can detect signals due to earthquake upto about 400 km, the number of permanent stations for systematic studies can be reduced without sacrificing the advantages of dozens of stations as in the case of Chinese techniques. Besides, the false signals can be discriminated monitoring the simultaneous increasing and decreasing trends in the pairs of configurations as suggested by the author.

Prediction of Earthquakes

The prediction of earthquake involves determination of three cardinal parameters such as epicenter, magnitude and time of the impending earthquake as accurately as possible at the earliest. Although, the procedure has been briefly described under the methodology and case histories, it is necessary to synthesize them.

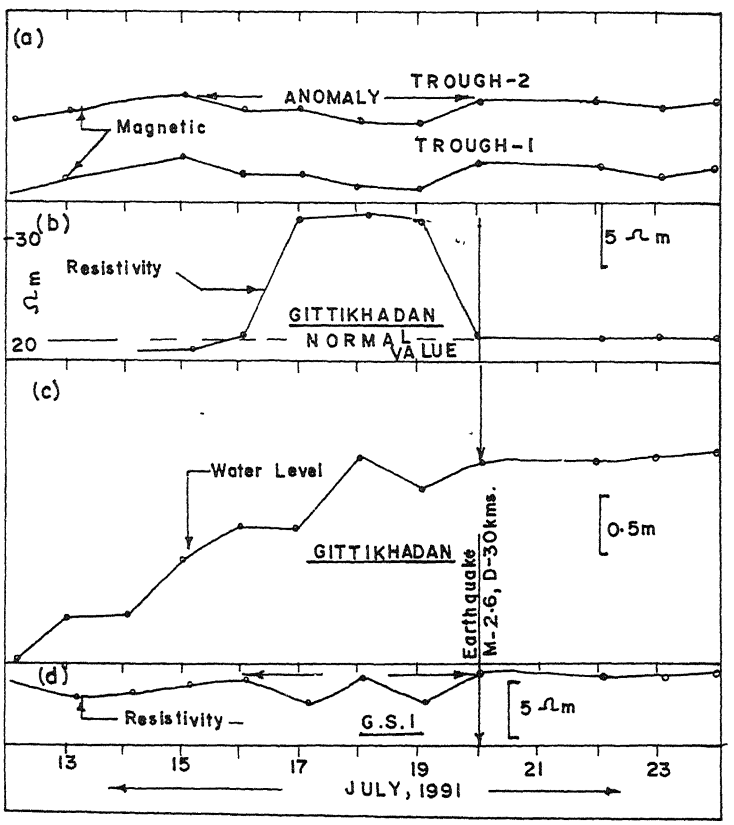

Fig. 9 (a)–Temporal variation of magnetic residuals between 11th and 20th July, 1991 at a site at Nagpur. (b) The apparent resistivities increased by 54% at Gittikhadan on the downthrow side of a fault, (d) The resistivities decreased by 7% on the flank of the fault zone

Forecasting epicenter : There are four different geoelectric techniques to forecast the epicenters of impending earthquakes (a) Based on the field data of strong earthquakes, the Chinese scientists have prepared a travel-time curve (Fig-10b) that shows the relationship between the duration of consistent anomaly at each station and its distance from the epicenter[2]. The epicentral distances from stations showing distinct precursors from the travel time curve can help determine the would be epicenter with accuracy of 100 km, (b) Contour map prepared on the basis of mean decrease as a percentage can also indicate the approximate location of the epicenter which will occupy the centre of maximum anomaly, (c) Nayak *et. al.*[8] have shown that the distance to the epicenter is related to the ratio of the magnitude of the anomaly to

the pre-anomaly value. In this method, fewer resistivity stations where the resistivities recover before the impending earthquake can indicate the epicenter (Fig. 10a). The relative geoelectrical signal densities at a number of stations can be compared to determine the epicenter with an accuracy of 100 km[4].

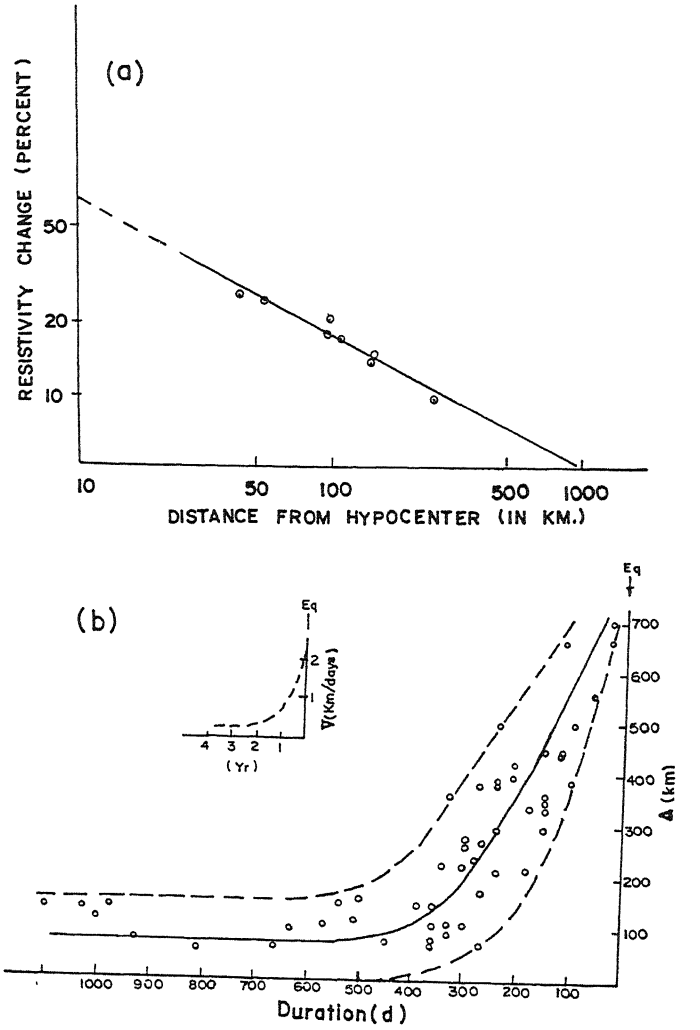

Fig. 10 (a) The relation between the maximum resistivity change near Shillong vs. distances of hypocenters of earthquake (Nayak *et al* 1983). (b) The travel time curve for the resistivity precursor front that can be used to determine the would be epicenter in the imminent stage of earthquake. (Zhao *et. al* 1994).

Comparing the techniques, the epicenter can be determined with reasonable accuracy combining the Chinese travel time curve and the graph described by Nayak *et al.*[8].

Determination of magnitude : The Chinese scientists have developed the following formulas on the basis of analysis of data collected for more than 50 earthquakes to forecast the magnitude of events.

$M = 0.50 + 2.50 \log T$

$M = 10.80 + 3.41 \log \triangle \rho x/\rho x$

$M = -1.34 + 3\ 40 \log \triangle m$

Where T is the duration time, $\triangle \rho x$ is the amplitude of the anomaly and ρx background resistivity at station near the epicenter, whereas $\triangle m$ is the maximum epicentral distance of the station exhibiting intermediate-term precursor with some limitations. The duration of the anomaly may be 2-3 years observed over 200-300 km for earthquake of magnitude M-7.

Varotsos and Alexopoulos[4] computed magnitude from the relationship between the product of relative signal intensity with the distance of the epicenter, but the procedure is rather cumbersome.

Foretelling time of earthquakes

The long term prediction involving decades are generally based on the calculation of return period, analysis of incidence of past earthquake, study of seismic risk zoning maps and mapping of the deep crustal conductors. They are useful for creating awareness regarding the incidence of earthquake. The intermediate, short and imminent stages involving periods of 2-3 years, 2-3 months and 2-3 weeks respectively are reflected in the slopes of the graphs depicting the magnitude of resistivity values against time. The rates of changes are discernible as in Fig. 7. At the short and imminent stages, SP anomalies must be integrated with the resistivity data characterised by anisotropy and recovery of anomalies at the farthest stations. At the imminent stage, continuous recording of resistivity indications may show pulses of the weakened crust correlatable to the frequency of crustal tides (Fig 7z). The amplitudes of the pulses may increase distorting the wave shapes and manifesting reversal phases. They must be integrated with triggering phenomena such as foreshocks with

impressions on the SP anomalies oil gushes in dry wells or water sprouts in tube wells.

The precursory changes observed by Nayak *et. al.*[8] may correspond to the intermediate, short term and recovery phenomena at the stations away from the epicentral zone described by the Chinese scientists. The transient changes observed by Varotsos and Alexopoulos[4] 6-114 h before earthquakes in Greece may be considered as a supplementary technique. It may be noted that the Greek scientists announced and issued telegraphs predicting earthquakes in Greece and out of 23 only 2 were missed. The precursory resistivity changes 0.5-6.8 hr preceding earthquakes by the sensitive Yamazaki variometers may also be useful[3].

Management of earthquake prediction

It is known that an earthquake does not kill people, but the buildings which should protect people collapse due to faulty constructions and kill people. Hence, the old buildings should be strengthened and the new buildings made earthquake resistant in all the cities in high seismic risk zones. Since it is not possible to strengthen all the old buildings, earthquake prediction programmes must be launched to avert the disasters witnessed in 1993 Latur, 1997 Jabalpur, 1999 Chamoli and 2001 Bhuj earthquake.

It has been shown in the paper that earthquake prediction programmes can be initiated employing the inexpensive technique using resistivity potentiometer. The seismic zoning map of India shows that Delhi, Kolkata and Mumbai are vulnerable to earthquakes. Out of them, case of Mumbai may be considered as an example. Earthquakes have been occurring around Koyna to the south of Mumbai and to some extent, west of Nasik to north of Mumbai since the nineteen sixties. The disastrous M 6.3 1993 Latur earthquake occurred to east of Koyna, Hence, the possibility of earthquake prone seismic gap in the Western Ghat hills to east of Mumbai cannot be ruled out. The presence of hot springs in the area suggest anomalous subsurface conditions. Located in Zone-II of the seismic zoning map, Mumbai is also associated with prominent high gravity anomalies. The positive isostatic anomaly may indicate deep crustal instability that warrants geoelectrical monitoring on priority basis to predict earthquakes.

Conclusions

It has been shown in this paper that the gradual accumulation of strain and its sudden release to cause earthquakes can be effectively indicated by monitoring the

spatial and temporal variation of geoelectric parameters of rocks. Careful analysis of the profile of earth resistivities and natural potentials can reveal the epicenter, magnitude and time of earthquakes that can not be done by any other method. While the Russian and Greek scientists have predicted the instant of earthquake depending on geopotential variations, the Chinese scientists have been predicting all the parameters integrating georesistivity and geopotential indications at a number of stations particularly in the vicinity of selected cities. The Japanese geophysicists also claim to have developed method to achieve these objectives employing sensitive Yamazaki variometers.

In India, the author has found that measurements at sensitive sites located on fault zones can enhance geoelectric signals due to strain accumulating in the crust within a range of 200-400 km from the site and thus a few stations would be needed for effective monitoring of parameters. Hence, it is suggested that monitoring of geoelectrical parameters near large cities should be undertaken to study the condition of crust in order to evaluate the earthquake risk using potentiometers at the earliest before it is too late for the next disastrous earthquake.

Acknowledgements

Encouraged by my friend Dr. P. Mohanty, Retd. Professor of JNU, New Delhi and Mr. J. K. Pattnaik of Self Education Trust, Krishnamurthy Foundation, Cuttack, the author prepared this paper with the hope that enterprising scientists may use the techniques to predict earthquakes to prevent reoccurrence of Gujarat type disasters. He thanks Dr. Y. Zhao and his wife Prof. F.Y. Qian for helping him. Thanks are due to Mrs. B. Nayak, wife of the author who supported him to prepare it.

References

1. Dmowska, R. (1977) *Geophys Surv.* **3** : 157
2. Zhao Y. & Qian, F. (1994) *Tectonophysics* **233** . 99.
3. Yamazaki, Y. (1977) *Geophysical* Survey **3** : 123.
4. Varotsos P. & Alexopoulos K (1984) *Tectonophysics* **110** :99
5 Barsukov. O.M. (1972) *Tectonophysics*, **14** : 273.
6. Sobolev, G.A. (1975) *Pure Appl Geophys* **113** : 229.
7. Mazzella, A. & Morrison, H.F. (1974) *Science* **185** : 855
8. Nayak, P.N., Saha, S.N., Dutta S., Rama Rao, M.S.V. & Sarkar, N.C. (1983) *Geoexploration* **21** : 137.

9 Fedotov, S A , Gusev, A.A & Boldyrev, S A. (1972) *Tectonophysics* **14** 279

10 Sobolev, G.A , Semercham A A , Salov, B G , Spetzler, H A , Sondergeld, C H , Badanov V N , Kol'tsov, A V , Los V F , Nasimov, R M , Ponomarev, A V , Stakhovskil, I R , Terent'ev V A & Turestkil I M (1983) *Izv Acad Sci Earth Phys* **18** 572

11 Ogilvy, A A , & Kuzmina, E N (1972) *Geophysics* **37 :** 839

12 Bogoslovsky, V A & Ogilvy, A A (1972), *Geophys Prosp* **20** 109

13. Oldham, R D (1899) *Mem G S I* **20**

14 Brace, W.F. & Orange, A S. (1968) *J Geophys Res* **73** 1433

15. Scholz, C H , Sykes L.R & Aggrawal Y P (1973) *Science* **181** 803

16 Rikitake, T. (1976) *Earthquake prediction,* Elsevier, Amsterdam

17 Zhao, Y , Qian F & Stopinski, W (1990) *Acta Geophysica Polonica* **38** · 229.

18. Park, S. (1995) *Internet.*

19. Myachkin, VI., Brace W F , Sobolev G A. & Dieterach J H (1972) *Pageoph* **113** : 169

20. Zhao Y., Zhengnan, L., Qian F., Baohua C., Haung, Y & Tiesheng, S (1996) *Jour Earthqauke, Procd Res.* **5** : 594

21. Gupta, H.K., Harinarayana, T., Kausalya, M., Mishra, D C , Indramohan, Purna Chandra Rao, M , Raju, P.S , Rastogi B.K., Reddy, P R & Sarkar D. (2001) *Jour of Geol Soc India* **57** 275.

22 Nayak, P.N., Das, A.K., Nand Lal, Sriram, B.V , Pal, T & Stayanarayan, K V (1992) *Seminar Vol.*, Ind Inst Geomag.

23. Nayak, P.N. (1981) *Geoexploration* **18** 311.

24. Zhao, Y., Zhao, B. & Qian, F. (1997) *Annali Di Geof* **11** 241

Editorial Board

EDITORIAL ADVISORY BOARD

Regd. No. R.N. 35621/78

CONTENTS

Published by Dr. V.P. Kamboj, General Secretary for the National Academy of Sciences, India, Allahabad and printed by National Graphics, Allahabad.
Managing Editor – Professor S.L. Srivastava